

DIFFUSION OF THALLIUM CHLORIDE INTO SINGLE
CRYSTALS AND BICRYSTALS OF POTASSIUM CHLORIDE

by

ROBERT JOSEPH TIERNAN

A.B. Boston College (1957)

M.S. Boston College (1959)

Submitted in partial fulfillment of the requirements

for the degree of

DOCTOR OF PHILOSOPHY

at the

Massachusetts Institute of Technology

(1969)

Signature of Author
Department of Metallurgy

Signature of Professor
in Charge of Research

Bernhardt J. Wuepisch

Signature of Chairman of
Departmental Committee on
Graduate Students

Phillip L. deBruyn



DIFFUSION OF THALLIUM CHLORIDE INTO SINGLE
CRYSTALS AND BICRYSTALS OF POTASSIUM CHLORIDE

by

ROBERT JOSEPH TIERNAN

SUBMITTED TO THE DEPARTMENT OF METALLURGY,
JANUARY 1969, IN PARTIAL FULFILLMENT OF THE
REQUIREMENTS FOR THE DEGREE OF DOCTOR OF PHILOSOPHY

ABSTRACT

The electron probe microanalyzer has been used to study the diffusion of thallium in single crystals and bicrystals of potassium chloride. Both vapor exchange and sandwich (thin film) boundary conditions were employed in the preparation of specimens for the study of volume diffusion. Only vapor exchange conditions were used in the study of grain boundary diffusion.

The volume diffusion data exhibited ranges of both intrinsic and extrinsic behavior. In the temperature range 232° - 480°C , the diffusion coefficient could be represented by

$$D = 9 \times 10^{-11} \exp - (0.25 \text{ eV/KT}) \text{ cm}^2/\text{sec}.$$

While in the temperature range 480° - 727°C , the data are described by

$$D = 6 \times 10^{-3} \exp - (1.42 \text{ eV/KT}) \text{ cm}^2/\text{sec}.$$

The extrinsic activation energy of 0.25 eV is assumed to represent the Δh for thallium ion migration. The derived Δh for

Schottky pair formation (twice the difference between the intrinsic and extrinsic activation energy) is 2.34 eV per pair. This value, and the energy for ion migration both agree well with theoretical estimates of these quantities.

Diffusion was studied in the temperature range 515C° - 700C° from grain boundaries prepared by a variety of techniques: pressure-sintered bicrystals, bicrystal Kyropoulos boules pulled from the melt, hot-pressed polycrystalline compacts, large grain polycrystalline material solidified from the melt, as-received bicrystals, and low angle and sub-grain boundaries in as-received single crystals. Enhanced diffusion along grain boundaries was not observed in solidified material or in the as-received single crystals, and was only occasionally noted in pressure sintered and as-received bicrystals. Enhanced diffusion was commonly noted along most (but not all) boundaries in hot pressed compacts and Kyropoulos bicrystals. In the latter specimens, values of $D' a$ (where D' is the grain boundary diffusion coefficient, and a is the grain-boundary half-width) were obtained by several methods, all of which were based on numerical integration of Whipple's exact solution. The values of $D' a$ obtained were in the range $3.1 \times 10^{-14} \text{ cm}^3/\text{sec}$ - $39.0 \times 10^{-14} \text{ cm}^3/\text{sec}$, and differed significantly from values obtained through Fisher's approximate solution.

The values obtained for $D' a$ were not reproducible. Attempts to determine the temperature dependence of $D' a$ and possible anisotropy within the plane of the boundary were therefore unsuccessful. The lack of reproducibility strongly suggests an extrinsic mechanism as the origin of the enhanced grain boundary diffusion. Bicrystals intentionally

synthesized in the presence of water vapor displayed an enormous increase in the degree of enhanced boundary diffusion. Attempts to reveal impurity segregation with the aid of ultraviolet and infrared absorption, and through electron microanalysis were not successful. The amount of impurity involved in the enhanced diffusion is therefore very small.

Thesis Supervisor: Bernhardt J. Wuensch
Title: Assistant Professor
of Ceramics

TABLE OF CONTENTS

	<u>Page</u>
ABSTRACT	ii
LIST OF FIGURES	vi
LIST OF TABLES	xi
ACKNOWLEDGEMENT	xii
I. INTRODUCTION	1
II. THEORY	2
III. MATHEMATICS OF DIFFUSION	11
A. Volume Diffusion	11
1. Sandwich Couple	11
2. Vapor Exchange Couple	13
3. Validity of Boundary Condition Assumptions	15
B. Grain Boundary Diffusion	18
IV. LITERATURE REVIEW	33
A. Single Crystals (no intentional impurities added)	33
1. Self Diffusion	33
2. Cationic Impurity Diffusion	35
B. Ionic Conductivity	37
C. Grain Boundary Diffusion	38
V. CONCLUSIONS FROM LITERATURE REVIEW	51
A. Volume Diffusion and Conductivity Results	51
B. Grain Boundary and Dislocation Results	51
VI. RESEARCH OBJECTIVE	54
VII. EXPERIMENTAL PROCEDURE	57
A. Preparation of Standard Composites	57
B. Sample Preparation for Volume Diffusion Runs	58
C. Preparation of Polycrystalline Pellets	60
D. Preparation of Bicrystals	64
1. Hot Wire Technique	64
2. Pressure Sintered Technique	66
3. Kyropoulos Technique	67
4. Harshaw Bicrystals	75
5. Harshaw Mosaics	75
6. Polycrystalline Pieces from the Melt in the Kyropoulos Oven	75

	Page
E. Diffusion Annealings	75
1. Polycrystalline Specimens and Single Crystal Specimens	75
a. Vapor Exchange Couples	75
b. Thin Film Couples	77
2. Bicrystals	77
F. Preparation for Analysis	81
1. Standards	81
2. Single Crystals and Polycrystals	81
3. Bicrystals	83
G. Analysis of Concentration - The Electron Microprobe .	83
1. Standards	92
2. Single Crystals	99
3. Polycrystalline Pellets and Harshaw Mosaic Crystals	100
4. Bicrystal	100
VIII. RESULTS	104
A. Volume Diffusion Anneals	104
B. Polycrystalline Diffusion Anneals	116
C. Harshaw Mosaics	116
D. Bicrystals	118
IX. COMMENTS ON BICRYSTAL DIFFUSION RESULTS	131
X. IMPURITY ANALYSIS OF GRAIN BOUNDARIES	133
XI. CONCLUSIONS	144
A. Volume Diffusion Work	144
B. Grain Boundary Diffusion Work	144
XII. SUGGESTIONS FOR FUTURE WORK	146
REFERENCES	148
AUTOBIOGRAPHICAL SKETCH	152

LIST OF FIGURES

<u>Number</u>	<u>Title</u>	<u>Page</u>
1	Atom moving one jump distance " Δx " in one dimension.	3
2	Free energy of an atom as a function of the distance x in a one dimensional crystal.	4
3	Typical plot of the natural logarithm of the diffusion coefficient versus the inverse of temperature for cation (anion) diffusion into a host crystal with aliovalent impurities.	10
4	"Sandwich Couple"	12
5	"Vapor Exchange Couple"	12
6	Three dimensional diagram arising from the solution of the vapor exchange couple diffusion equation.	16
7A	Sandwich couple with coordinate system for verifying the mathematical assumptions.	17
7B	Vapor exchange couple with coordinate system for verifying the mathematical assumptions.	17
8	Coordinate system for Fisher's mathematical analysis of grain boundary diffusion.	19
9	Coordinate system for Whipple's mathematical analysis of grain boundary diffusion.	22
10	Isoconcentration contours ⁹ derived from the numerical solution of equation (46).	24
11	Plot of the inverse of the isoconcentration slopes at the grain boundary edge ($\xi=0$) as a function of β^9 .	25
12	Plot of the angles that the isoconcentration contours make at $\xi=0$ with the grain boundary slab as a function of β^{10} .	27
13	Plot of the natural logarithm of the concentration at $\xi=0$ as a function of reduced penetration η for various values of β .	28
14	Plot of the natural logarithm of $\tilde{\phi} = \int_{-\infty}^{\infty} C_2(\xi\eta)d\xi$ as a function of reduced penetration η for various values of β .	29

<u>Number</u>	<u>Title</u>	<u>Page</u>
15	Plot of the least square slopes of the $LN\bar{\phi}$ and LNC versus η curves of figures 13 and 14 as a function ^p of β .	30
16	Laue back reflection of a typical Harshaw cube used for volume diffusion runs.	59
17	RF Press (induction heating): for pressing and sintering polycrystalline compacts and bicrystals	61
18A	RF pressed pellet of KCl (100x).	62
18B	Pellet, RF pressed in dry nitrogen and held for two days at 712C° (50x).	62
19	Apparatus for fabricating bicrystals.	65
20A	Four sketches of the appearance of anomalous grain boundaries in pressure sintered bicrystals.	68
20B	Grain boundary in a pressure sintered bicrystal (B-7).	69
20C	Grain boundary in a pressure sintered bicrystal (B-8).	69
21	Kyrcopoulos oven and crystal pulling apparatus.	70
22	Preparation steps for pulling a bicrystal from the melt.	71
23	Preparation steps for pulling a bicrystal with "symmetrical tile seeds" $\pm 10^\circ$ about the (100).	73
24	Typical bicrystal boule grown with a symmetrical seed.	74
25	Apparatus for a typical vapor exchange couple diffusion anneal.	76
26	Temperature controlled ovens used for the diffusion anneals.	78
27	Preparing a KCl single crystal for a "sandwich couple" and a diffusion anneal.	79
28	Apparatus for a bicrystal diffusion anneal.	80
29	Preparing a sample subjected to a diffusion anneal for the electron probe.	82
30	Illustration of how two orthogonal planes containing the grain boundary are analyzed with the electron probe for thallium.	84

<u>Number</u>	<u>Title</u>	<u>Page</u>
31	Schematic diagram of the essential parts of the electron probe microanalyzer.	85
32	Picture of probe main assembly.	86
33	Complete electron probe microanalyzer assembly.	88
34	Brass cannister sample holder of electron probe.	90
35	Hand scan of a standard with the electron probe.	94
36	Plot of $\text{Log } I_c$, $\text{Log } I_{B1}$ and $\text{Log } I_{B2}$ versus $\text{Log } w$.	97
37	Polycrystalline sample subjected to a diffusion anneal (vapor exchange couple).	101
38	Typical photomicrograph of a bicrystal subjected to a diffusion anneal (vapor exchange couple) in figure 29A,B.	102
39	Plot of weight fraction of thallium chloride versus penetration in microns for the case of anomalous behavior in the vicinity of the surface of a vapor exchange diffusion couple.	105
40	Plot of the inverse complementary error function of C/C_0 versus penetration for the concentration-penetration curve of figure 39.	106
41	Plot of the natural logarithm of the complementary error function versus penetration.	108
42	A typical plot of the inverse complementary error function C/C_0 versus penetration in microns ($T=688C^\circ$, $t=2.58 \times 10^{-4}$ seconds) for a vapor exchange couple.	109
43	A typical plot of the natural logarithm of the weight fraction of thallium chloride versus the square of the penetration for the sandwich couple.	110
44	Plot of the natural logarithm of the volume diffusion coefficient versus $1000/TK^\circ$.	113
45	Preferential diffusion in one of the grain boundaries of a polycrystalline pellet (200x).	117
46	Typical family of counts which occur when the bicrystal face orthogonal to the exposed face is scanned with the probe along a "constant η " trajectory.	119

<u>Number</u>	<u>Title</u>	<u>Page</u>
47	Isoconcentration contours and tabulated parameters that lead to an evaluation of β .	120
48	Plot of the natural logarithm of the peak values in figure 46 versus penetration "y".	122
49	Plot of the natural logarithm of the peak concentration (similar to figure 48) versus penetration; displaying a break in the slope at large penetrations.	127
50	Plot of the natural logarithm of $D'a$ (cm^3/sec) versus $1000/T$ for the bicrystals of table nine.	129
51A	Optical micrograph of the grain boundary surface of Kyropoulos bicrystal number one 500x.	134
51B	Scanning electron micrograph of the central part of the same grain boundary surface 6500x.	134
52	Scanning electron micrograph of the grain boundary surface of Kyropoulos bicrystal number two 2600x.	135
53	Scanning electron micrographs of the grain boundary of Kyropoulos bicrystal number four (A) 2400x (B) 24000x.	136
54	Optical micrographs of the thallium diffusion contours in a (A) "clean" (50x) and a (B) "wet" (100x) pressure sintered bicrystal. Temperature of diffusion anneal 515C° .	141
55	Optical micrographs of the thallium diffusion contours in a (A) "clean" (50x) and a (B) "wet" (100x) pressure sintered bicrystal. Temperature of diffusion anneal 545C° .	142
56	Optical micrographs of the thallium diffusion contours in a (A) "clean" (50x) and a (B) "wet" (100x) pressure sintered bicrystal. Temperature of diffusion anneal 595C° .	143

LIST OF TABLES

<u>Number</u>	<u>Title</u>	<u>Page</u>
1	Comparison of the slopes obtained from figure 15 with those obtained by Fisher for fixed values of β .	32
2	Collected data on quantities of physical interest obtained from diffusion of cations in the alkali halides	39
3	Collected data on quantities of physical interest obtained from conductivity experiments on pure and doped alkali halides.	41
4	Collection of data on diffusion permeability ($D^1 a$).	49
5	List of ionic polarizabilities.	55
6	Experimental data on the standards. Column headings are explained on pages 93 and 95.	96
7	Exact listing of the data points of figure 44, along with the times of the diffusion anneals.	112
8	Listing of the quantities of physical interest derived from diffusion data of this work and that of others.	115
9	Collected data on quantities of physical interest derived from preferential grain boundary diffusion analysis.	123
10	Comparison of the β 's obtained by different methods. The β 's in column one have been averaged over all the isoconcentration contours.	126
11	Impurity analysis of bulk crystals pulled from the melt.	138

ACKNOWLEDGEMENT

I would like to thank Professor William D. Kingery for extending a research assistantship to me, and the Ford Foundation for their loans, both of which enabled me to pursue the doctorate program at M.I.T.

I would like to thank Professor Bernhardt J. Wuensch for his suggestion of the problem and his continuous advice on both the experimental procedure and the final presentation of this work.

My deepest appreciation goes to my wife Lorette who, although unfamiliar with the finer problems of scientific work, was very patient and understanding throughout it all. Without her extra work both of a monetary and non-monetary nature all of this would have been impossible. I thank also her mother and my parents for their financial help.

I would like to thank Professor Robert Ogilvie and Professor Tom Ziebold for allowing me to use the electron probe microanalyzers, the vacuum systems, their fine optical systems, and their X-ray machines. I would also like to thank them for their advice on the use of all of this equipment, most especially the probe.

I would like to thank Joe Adario who took the scanning electron microscope pictures and Steve Duerr who gave of his time to help me with the analysis of oxygen segregation at the grain boundaries using the M.I.T. probe.

I would like to thank all the people in Professor Smakula's section who were of assistance in fabricating the Kyropoulos bicrystals. I would like to thank most especially Professor Smakula himself for the

valuable talks I had with him, and Janis Kelrajs for his very informative talks and his carrying out of the ultraviolet and infrared analysis of my crystals.

I would like to thank Professor Kenneth Russell for allowing me to use his diffusion ovens.

I would like to thank the technicians Pat Kearney, Al Frekker, Fred Wilson and all the people in the ceramics department with whom I discussed any aspect of my problems and from whom I obtained assistance.

My thanks also goes to Don Fellows and John Mara who did the fine drafting of pictures for the thesis presentation.



I. INTRODUCTION

Solid state diffusion plays an important role in many mass transfer phenomena. Reaction rates, uniformity of components throughout the bulk of a crystal, recrystallization, ionic conductivity, sintering, and mechanical properties such as creep, to mention a few, are determined by the rates of diffusion of one or several atomic species through the material.

There is experimental evidence to suggest that appreciable transfer of matter may take place by way of enhanced diffusion along grain boundaries and dislocations. This enhancement may occur to such an extent as to cause the above phenomena to be exclusively controlled by diffusion along such microstructural features. The materials in which the above phenomena are of practical concern are almost always of a polycrystalline or mosaic nature, and have significant dislocation densities. It is therefore of utmost importance to understand the origins and magnitudes of grain boundary diffusion in order to predict the materials and circumstances for which this mechanism may be the dominant means of mass transport.

II. THEORY

An expression for the diffusion coefficient may be obtained by comparing Fick's first law with an expression for the net transfer of atoms in a crystal across an imaginary plane.¹

Referring to figure one, the number of atoms, n , jumping from a plane at $x_0 - \frac{\Delta x}{2}$ to a plane at $x_0 + \frac{\Delta x}{2}$ per square centimeter per second is expressed by:

$$n(x_0 - \frac{\Delta x}{2}) = g \nu_0 C(x_0 - \frac{\Delta x}{2}) p_V p_J \frac{\Delta x}{2} \quad (1)$$

ν_0 is the number of vibrations per second of the atom and, when multiplied by a geometric factor "g", gives the number of times per second that the atom moves in the direction of the plane at $x_0 + \frac{\Delta x}{2}$. p_V is the probability that there will be a position available at $x_0 + \frac{\Delta x}{2}$ for the jumping atom. p_J is the probability of a jump. It will be assumed that g , p_V and p_J are constant throughout the crystal. Since the atoms in a crystal have a distribution of vibration frequencies ν_0 is not truly a constant. The distribution however is very complex and has been determined for only a few crystals. The spread is not large and a value of 10^{13} cycles per second is typical.

In order for an atom to go from a position on the $x_0 - \frac{\Delta x}{2}$ plane to a position on the $x_0 + \frac{\Delta x}{2}$ plane, it must move into close interaction with atoms neighboring both sites. As indicated in figure 2, there will initially be a repulsive force tending to push the atom back to its original site. This force will increase up to a maximum at a position (referred to as a saddle point) somewhere between $x_0 - \frac{\Delta x}{2}$ and $x_0 + \frac{\Delta x}{2}$. The atom will then be repelled into the new position. By letting g_0

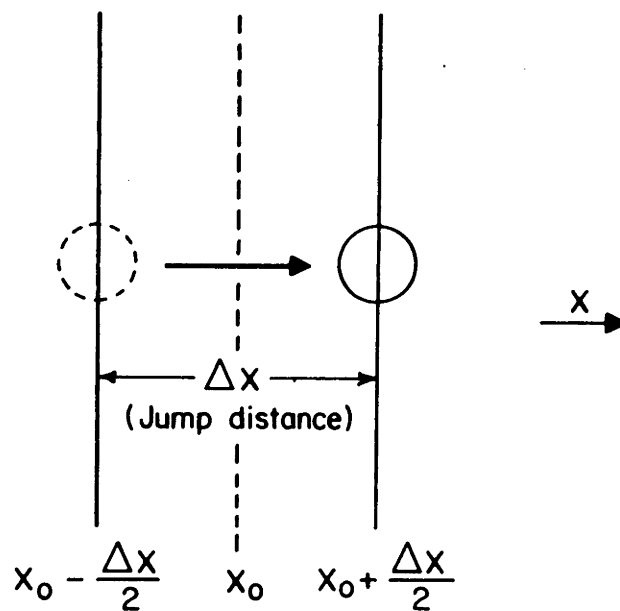


Figure 1 - Atom moving one jump distance " Δx " in one dimension.
Atom was initially at $x_0 - \frac{\Delta x}{2}$.

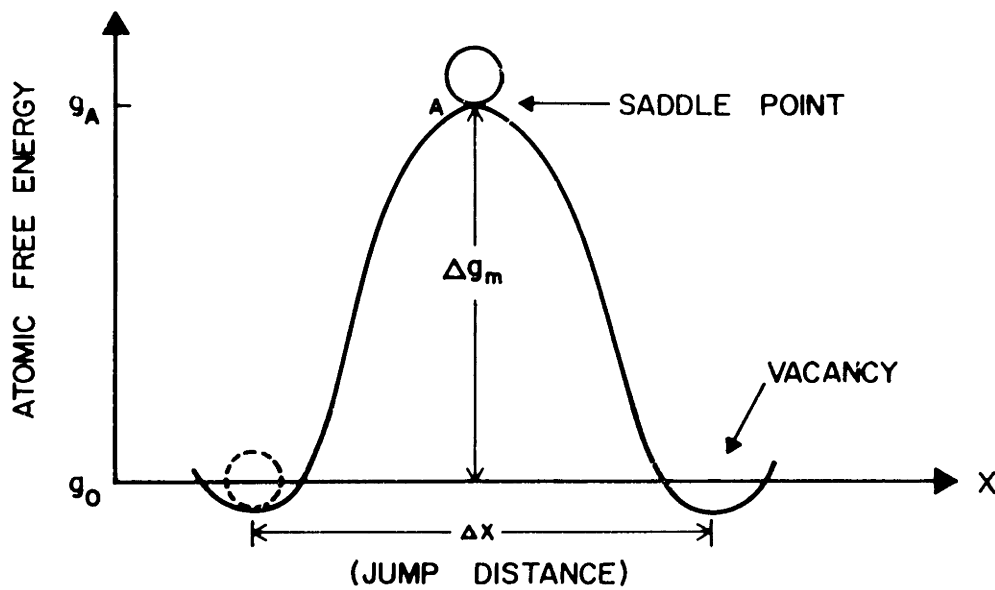


Figure 2 - Free energy of an atom as a function of the distance x in a one dimensional crystal as it jumps from its original site to a nearest neighbor vacant site. $g_A - g_0$ is referred to as Δg_m , the free energy barrier to motion for a jumping atom.

be the atomic energy at the positions $x_0 - \frac{\Delta x}{2}$ and $x_0 + \frac{\Delta x}{2}$, and g_A the atomic free energy at the saddle point, $g_A - g_0$ will be the barrier to motion (henceforth labelled Δg_m). The energy distribution of the atoms in a crystal obeys Boltzmann statistics, and hence the fraction which may jump from a saddle point to a neighboring site is equal to $e^{-\Delta g_m/kT}$. This will be the expression for p_j in (1).

The number of atoms jumping from the plane at $x_0 + \frac{\Delta x}{2}$ back to the plane at $x_0 - \frac{\Delta x}{2}$ per square centimeter per second is, in similar fashion, given by:

$$m(x_0 + \frac{\Delta x}{2}) = g v_0 c(x_0 + \frac{\Delta x}{2}) p_v e^{-\Delta g_m/kT} \frac{\Delta x}{2} \quad (2)$$

The net number of atoms crossing the imaginary plane at x_0 per square centimeter per second is given by the difference between (1) and (2).

Letting $m(x_0 - \frac{\Delta x}{2}) - m(x_0 + \frac{\Delta x}{2})$ equal J we obtain:

$$J = g v_0 p_v e^{-\Delta g_m/kT} \left[c(x_0 - \frac{\Delta x}{2}) - c(x_0 + \frac{\Delta x}{2}) \right] \frac{\Delta x}{2} \quad (3)$$

Since we are interested in concentration variations over, at the least, one micron increments, and since the jump distance in all crystals is of the order of about $1/10000$ of a micron, we can make use of the definition of the derivative of a function:

$$\frac{\partial c}{\partial x} = \lim_{\Delta x \rightarrow 0} \frac{[c(x_0 + \frac{\Delta x}{2}) - c(x_0 - \frac{\Delta x}{2})]}{\Delta x} = \frac{c(x_0 + \frac{\Delta x}{2}) - c(x_0 - \frac{\Delta x}{2})}{\Delta x} \quad (4)$$

where the true infinitesimal Δx is replaced by the jump distance Δx above. Putting (3) in a different form:

$$J = -g v_0 p_v e^{-\Delta g_m/kT} \frac{(\Delta x)^2}{2} \left(\frac{\partial c}{\partial x} \right) \quad (5)$$

Fick's Law states:

$$J = -D \frac{2C}{2x} \quad (6)$$

Where J is the net number of atoms crossing a unit area per second in the + x direction, c is the number of atoms per cubic centimeter and D is a proportionality constant referred to as the diffusion coefficient for transfer of this type of atom.

By comparing (5) and (6) the expression for D can be extracted:

$$D = g V_0 (\Delta x)^2 / 2 \left[p_v e^{-\Delta g_m / kT} \right] \text{ cm}^2/\text{sec} \quad (7)$$

The form of the p_v term will depend on the particular crystal. There are two predominant ways that atoms may migrate in a crystal.^{1,2} One is the interstitial mechanism whereby the diffusing species moves completely by way of normally unoccupied interstitial sites between the host atoms. The other is the vacancy mechanism whereby the atom moves by way of a vacant lattice site. The mechanism for a particular crystal will depend on the host structure as well as the diffusing atom.

At high temperature, one of two types of "defects" may predominate in a crystal. One is the Frenkel defect whereby an atom in a regular site moves to an interstitial position, thus creating a vacancy and an interstitial atom. At high enough temperatures these move independently of one another. For this type of defect the atoms may move by way of interstitial sites, by way of vacancy sites, or by a combination of both mechanisms.

On the other hand, Schottky defects form when vacancies are created at the surface, at grain boundaries, at dislocations or other strained regions and diffuse into the bulk.

In alkali halide crystals³ of the NaCl structure type we have two types of atoms, one with a negative charge and one with a positive charge. The bonding is almost purely ionic and, to maintain charge neutrality, the vacancies must be created in pairs. In these crystals the free energy change Δg_f associated with the defect production is much less than that of Frenkel defect production. The reason for this is the tremendous strain energy associated with the displacement of an ion from an octahedral site (all of which are occupied in the NaCl-type structure) to a smaller tetrahedral site.

Referring therefore to the dominating reaction for defect production in the alkali halides



For which the free energy change is expressed as:

$$\Delta g = \Delta g_f^0 + kT \ln \frac{V_K V_A}{B} \quad \text{ergs/pair} \quad (9)$$

At steady state, when $\Delta' g = 0$:

$$V_K V_A = B e^{-\Delta g_f^0 / kT} \quad (10)$$

Where Δg_f^0 is the free energy change associated with the formation of a Schottky pair (assumed to be independent of where the pair was formed), B is a constant related to the standard state of vacancies in a crystal (usually determined experimentally), and V_K and V_A are the mole fraction of the cation and anion vacancies.

The cation vacancy concentration V_K , is the probability of a neighboring cation site being vacant. Similarly, V_A is the probability of a neighboring anion site being vacant one jump distance away.

Substituting for p_V in (7) we obtain:

$$D = \frac{g V_0 (\Delta x)^2 B^{1/2}}{2} e^{-\Delta g_f^0 / 2kT - \Delta g_m / kT} \text{ cm}^2/\text{sec} \quad (11)$$

Using the fact that $\Delta g = \Delta h - T\Delta A$, (11) becomes

$$D = \frac{g V_0 (\Delta x)^2 B^{1/2}}{2} e^{1/k \left(\frac{\Delta \Delta_f^0}{2} + \frac{\Delta \Delta_m}{1} \right)} \left[e^{-\frac{1}{kT} (\frac{\Delta h_f^0}{2} + \Delta h_m)} \right] \text{ cm}^2/\text{sec} \quad (12)$$

The expression outside the brackets is usually combined and defined as D_0 . A plot of LND versus $\frac{1}{T}$ will thus yield a straight line whose slope will be $1/k \left[\frac{\Delta h_f^0}{2} + \Delta h_m \right]$.

In typical crystals there are impurities aside from the diffusing species. These impurities may be of different valency than the host ions. To preserve charge neutrality therefore, cation or anion vacancies must be formed.

Letting C be the aliovalent impurity mole fraction, (10) takes on the form

$$V_A (V_A + C) = e^{-\Delta g_f^0 / kT} \quad (13)$$

or

$$V_K (V_K + C) = e^{-\Delta g_f^0 / kT} \quad (14)$$

depending on whether C has created cation or anion vacancies by reason of the charge neutrality condition. Solving (13) and (14) for V_A and V_K one obtains:

$$V_A = -\frac{C}{2} + \frac{1}{2} \left[4 e^{-\Delta g_f^0 / kT} + C^2 \right]^{1/2} \quad (15)$$

$$\bar{V}_k = -\frac{C}{2} + \frac{1}{2} \left[4 e^{-\frac{\Delta G_f^0}{kT}} + C^2 \right]^{\frac{1}{2}} \quad (16)$$

(15) or (16) would then be substituted in (7) for p_V depending on whether D was the anion or cation diffusion coefficient.

For the case represented by equation (15), the fraction of vacant sites for the diffusion of a cation species is $C + e^{-\frac{\Delta G_f^0}{2kT}}$. If this is substituted in (7) for p_V , a plot of LND as a function of $\frac{1}{T}$ would exhibit a break at low temperatures as indicated in figure three. A similar break would occur in the LND versus $\frac{1}{T}$ plot for anion diffusion when the aliovalent impurities have created anion vacancies. The difference between the high and low temperature slope is $\frac{\Delta h_f^0}{2}$.

Extrapolating the low temperature line to $\frac{1}{T}$ equals zero yields a low temperature D_0 which, when divided by the high temperature D_0 , gives an approximate expression for the aliovalent impurity mole fraction, since B and $e^{-\frac{\Delta G_f^0}{2kT}}$ are usually of the order of unity.

There are other more complex effects which may show their influence. An example would be a case in which the host crystal has a few of each type of aliovalent impurity. The other would be the case of diffusion of an aliovalent ion which takes a vacancy with it from the surface into the bulk in either an associated or unassociated manner. This results in concentration dependent diffusion coefficients.

Other effects that may produce curvature in the LND versus curves are association between vacancy pairs, association between vacancies and aliovalent ions, dislocations and grain boundaries.

In conclusion, much can be learned from the temperature dependence of diffusion coefficients.

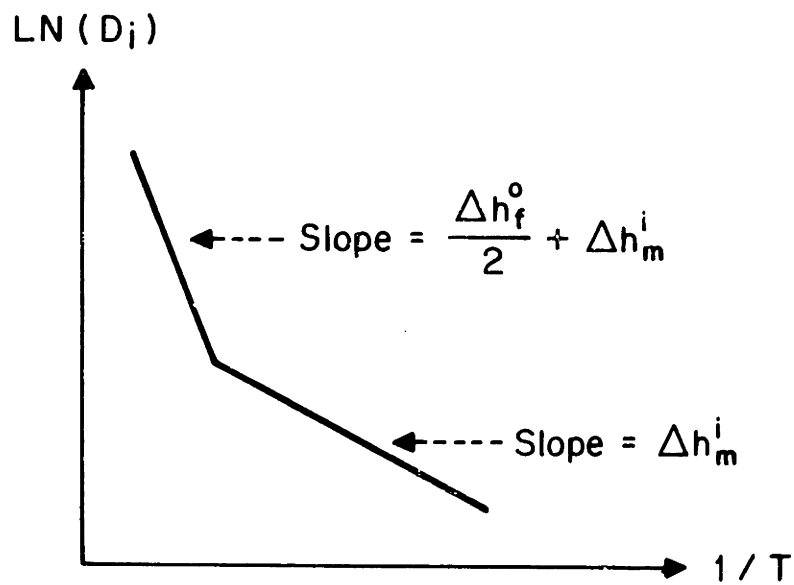


Figure 3 - Typical plot of the natural logarithm of the diffusion coefficient versus the inverse of temperature for cation (anion) diffusion into a host crystal with aliovalent impurities that have created cation (anion) vacancies by their presence.

III. MATHEMATICS OF DIFFUSION

A. Volume Diffusion

Methods for obtaining D from experimental data are suggested by the solution of the diffusion equation for various experimentally realizable boundary conditions.

1. Sandwich Couple

Figure four is a "sandwich couple" in which the diffusant is present as an initial thin film enclosed between two slabs of the host material. If the contact area of the slabs is large enough, the gradient of the concentration within the contact plane is zero over a large area near the center. One therefore essentially has a one dimensional problem.

For a concentration independent diffusion coefficient

$$\frac{\partial c}{\partial t} = D \frac{\partial^2 c}{\partial y^2} \quad (17)$$

where D is the diffusion coefficient expressed in (7).

The solution of (17) is subject to the following conditions.

$$c(\infty) = \infty \quad (18)$$

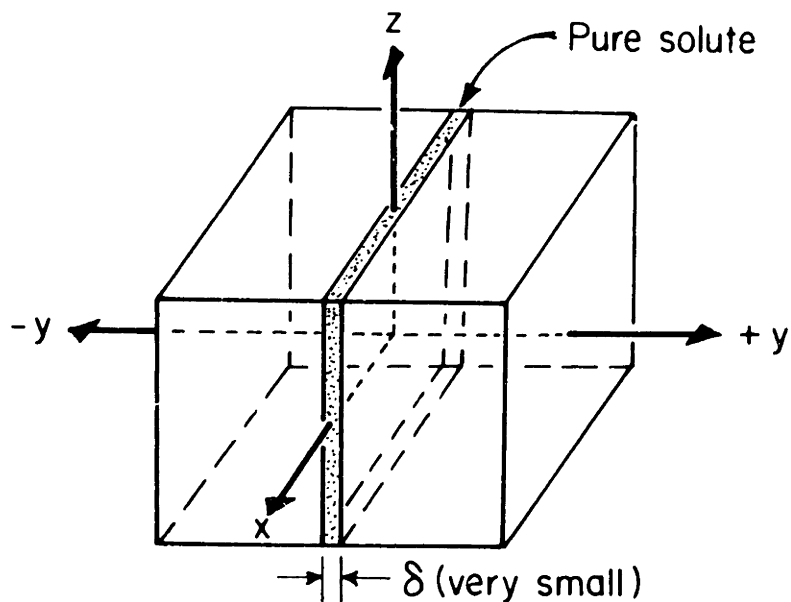
$$c(y_0) = 0 \quad |y| > \delta/2 \quad (19)$$

$$\int_{-\infty}^{\infty} c(y,t) \delta y = c_0 \delta \quad (20)$$

where δ approaches zero as C approaches infinity in such a way as to make (20) finite.

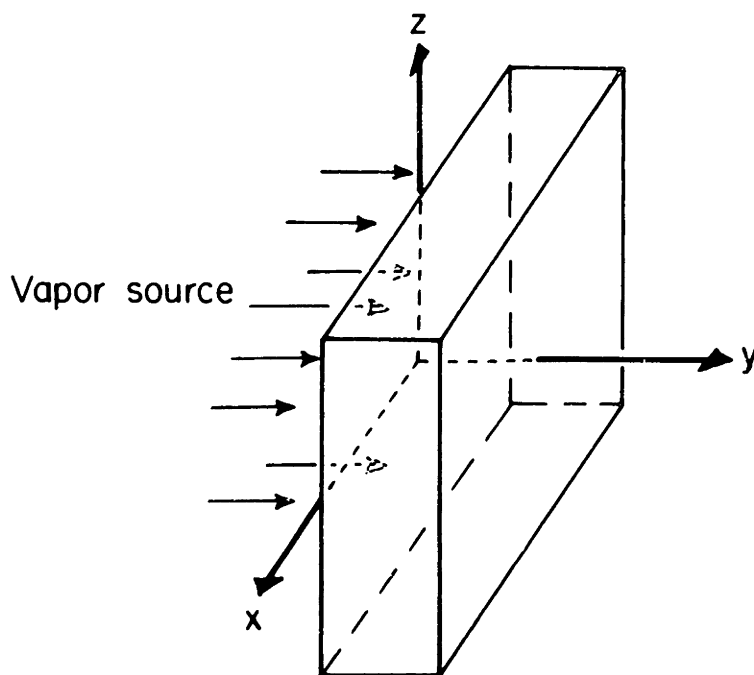
A trial solution of (17) is:

$$c(y,t) = \frac{A}{\sqrt{t}} e^{-y^2/4Dt} \quad (21)$$



THIN FILM (sandwich couple)

Figure 4 - "Sandwich Couple". Diffusant (in shaded region of width δ) is sandwiched between two single crystals.



VAPOR EXCHANGE COUPLE

Figure 5 - "Vapor Exchange Couple". Constant vapor pressure at diffusant is maintained at the $y = 0$ face.

where A is a constant. From (20) $C_0\delta = 2A\sqrt{\pi D}$ so that:

$$C(y,t) = \frac{C_0\delta}{2\sqrt{\pi Dt}} e^{-y^2/4Dt} \quad (22)$$

Therefore:

$$\ln C = \ln \left(\frac{C_0\delta}{2\sqrt{\pi Dt}} \right) - \frac{y^2}{4Dt} \quad (23)$$

By experimentally obtaining concentration as a function of penetration after a diffusion time of t_0 seconds, and by plotting LNC as a function of y^2 , one obtains a straight line whose slope is $1/4Dt_0$.

2. Vapor Exchange Couple

If by some means the host material is exposed to a constant vapor pressure of the diffusant as shown in figure five, the conditions on (17) are different, namely:

$$C = C_0 \quad \text{at} \quad y = 0 \quad \text{for} \quad t > 0 \quad (24)$$

$$C = C_0 \quad \text{for} \quad y = 0, \quad C = 0 \quad \text{for} \quad y > 0 \quad \text{at} \quad t = 0 \quad (25)$$

A Laplace transform⁴ can be performed on (17), eliminating the time variable, and allowing one to work in the semi infinite space $y \geq 0$. [It should be pointed out that (21) could have been obtained by a Laplace transform rather than guessing at a solution of (17).]

By definition, the Laplace transform of a function is:

$$\mathcal{L}\{C(y,t)\} \equiv \int_0^{\infty} C(y,t) e^{-pt} dt \equiv \hat{C}(p,y) \quad (26)$$

By multiplying both sides of (17) by $\exp(-pt)$, integrating t from zero to infinity, and making use of (25) and (26) we get:

$$\frac{d^2 \hat{C}}{dy^2} - \frac{p}{D} \hat{C} = 0 \quad (27)$$

$$\hat{c}(py) = A e^{-\sqrt{p/D} y} + B e^{\sqrt{p/D} y} \quad (28)$$

Converting (24) into a Laplace transformed boundary condition, and imposing it on (28) one obtains:

$$C_0 \int_0^{\infty} e^{-pt} dt = A + B \quad (29)$$

$$\frac{C_0}{p} = A + B \quad (30)$$

$\hat{c}(yp)$ must approach zero as y approaches infinity in order to obtain a bounded solution, since "Real p " also must be greater than zero in order that \hat{c} be defined. This requires B to be zero. This results in:

$$\hat{c}(yp) = \frac{C_0}{p} e^{-\sqrt{p/D} y} \quad (31)$$

From the Laplace inversion formula:

$$c(y,t) = \frac{1}{2\pi i} \int_{\substack{p_0+i\infty \\ p_0-i\infty}}^{\substack{p_0+i\infty \\ p_0-i\infty}} \hat{c}(py) e^{pt} dp \quad (32)$$

and from Carslaw and Jaeger,⁵ the contour integration of this latter expression is

$$c(y,t) = \frac{C_0}{2} \operatorname{erfc} \frac{y}{2\sqrt{Dt}} \quad (33)$$

where "erfc" is the complementary error function defined by:

$$\operatorname{erfc} \xi = \frac{2}{\sqrt{\pi}} \int_{\xi}^{\infty} e^{-\lambda^2} d\lambda \quad (34)$$

To obtain a value of D from an experimentally determined concentration gradient in this case, C_0 , the concentration of diffusant at the interface between solid and vapor would be divided into all the

experimentally measured concentrations. Let the ratio of C to C_0 be defined as β . The inverse complementary error function of these ratios, when plotted as a function of the penetration y will be a straight line whose slope is $1/2\sqrt{Dt}$, as indicated by figure six.

3. Validity of Boundary Condition Assumptions

Both the "sandwich couple" and "vapor exchange couple" solutions are valid if a one dimensional problem is assumed. Referring to figures 7a and 7b one sees that the decrease in concentration with z near the "xy" surfaces at $z = \pm L/2$ and the decrease with x near the "yz" surfaces at $x = \pm L/2$ have a dependence on " ξ " of the form.²

$$C(x, y, z, t) = \bar{C}(y, t) \left[\operatorname{erfc} \frac{\xi}{2\sqrt{Dt}} \right] \quad (35)$$

Where $\bar{C}(y, t)$ is $C_0 \delta / 4Dt e^{-y^2/4Dt}$ for the sandwich couple solution or $C_0/2 \operatorname{erfc} y/2\sqrt{Dt}$ for the vapor exchange couple, and $\xi = x - L/2$ or $z - L/2$.

A tabulation of the value of error functions shows that, for $\xi \leq -6\sqrt{Dt}$ the second term in (35) is greater than or equal to 1.99997. Thus, guided by this criterion, the diffusion samples can be chosen with dimensions significantly larger than $|6\sqrt{Dt}|$ so that (22) and (33) are valid.

The verification of (20) for the sandwich couple assumes a very thin layer of diffusant (solute) on the $y = 0$ surface and no loss of material to the surroundings. " δ " may be considered small enough to meet the assumed mathematical conditions if the total penetration of diffusant in the course of the experiment is much larger than $|\delta/2|$. The verification of the second part (namely no loss of material to the surroundings) cannot easily be shown analytically but a qualitative approach should suffice. Referring to figure 7a, one sees that the

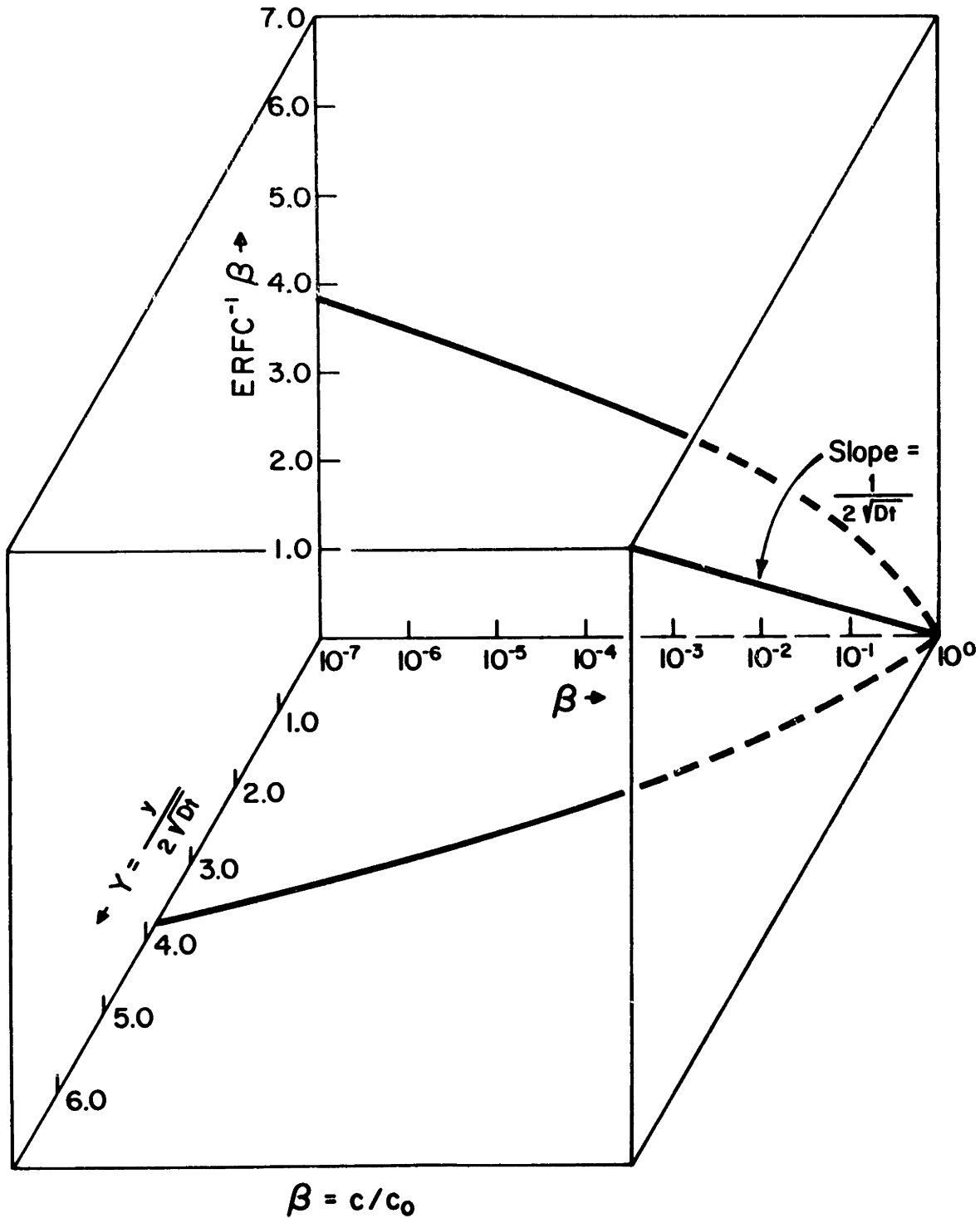
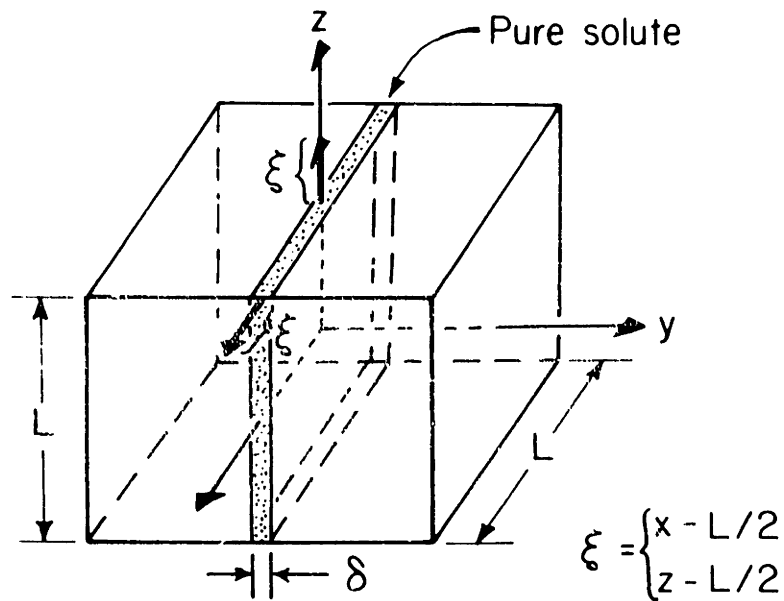
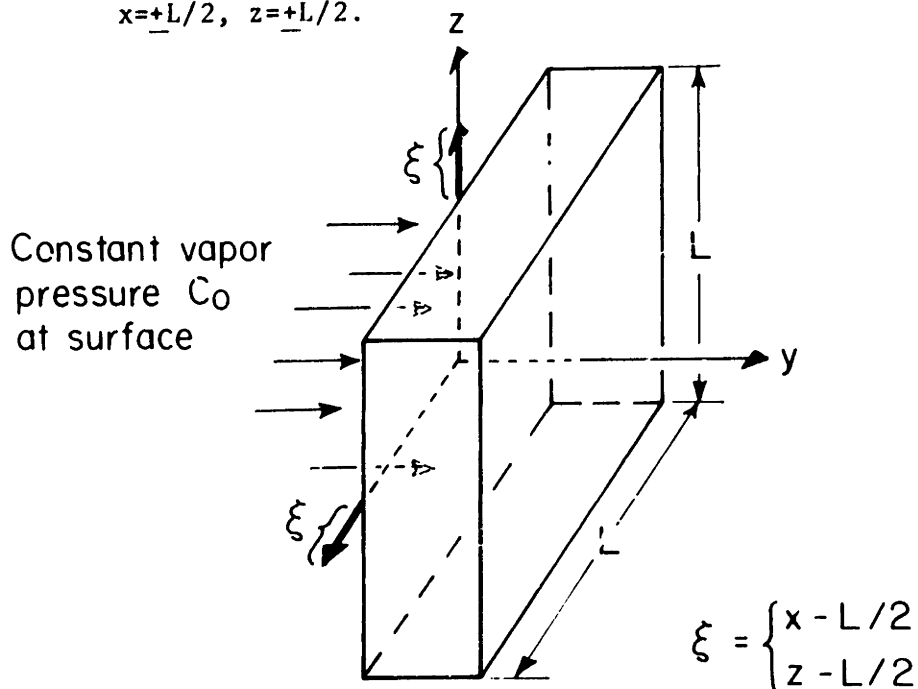


Figure 6 - Three dimensional diagram showing the functional forms of the important quantities arising from equation (33).



THIN FILM (sandwich couple)

Figure 7A - Sandwich couple with coordinate system at the center of the cube. Cube is of length L on each edge. ξ is defined as the distance away from the boundary planes at $x=+L/2$, $z=+L/2$.



VAPOR EXCHANGE COUPLE

Figure 7B - Vapor exchange couple with coordinate system at the center of the face exposed to the diffusant vapor. ξ is defined as the distance away from the boundary planes at $x=+L/2$, $z=+L/2$.

solute will diffuse very rapidly along the surfaces at $z = \pm L/2$ and $x = \pm L/2$ relative to the speed with which it will move in the underlying bulk layers. By eliminating surface loss by evaporation, (by putting the diffusion couple in a sealed tube containing a sufficient amount of solute to maintain the equilibrium vapor pressure at the diffusion temperature) one can actually keep the solute flowing inward rather than outward. This inward flow will alter the concentration near the faces but this extraneous penetration will also have an error function behavior similar to "[]" in (35) and so it can be neglected if the crystal dimensions are large relative to $|\delta\sqrt{Dt}|$.

B. Grain Boundary Diffusion

J. C. Fisher in 1951⁶ derived the first analytic expression for concentration as a function of penetration when grain boundary diffusion was present, figure eight. Fisher assumed that the grain boundary could be imagined as a slab, of uniform width $2a$, of uniform diffusivity D' , and extending to infinity in the z direction. The crystal was assumed infinite in the x and z directions. The initial conditions were the same as for the vapor exchange couple in section III.A.2.

Assuming a concentration-independent diffusion coefficient, he then set up two differential equations. One applied to the grain boundary region, and the other to the region outside the grain boundary.

$$\text{Region I} \quad \frac{\partial c'}{\partial t} = D' \left(\frac{\partial^2 c'}{\partial x^2} + \frac{\partial^2 c'}{\partial y^2} \right) \quad (36)$$

$$\text{Region II} \quad \frac{\partial c}{\partial t} = D \left(\frac{\partial^2 c}{\partial x^2} + \frac{\partial^2 c}{\partial y^2} \right) \quad (37)$$

The $\left(\frac{\partial^2 c}{\partial y^2} \right)$ term in (37) was neglected on the assumption that it was small at even slight distances into the bulk. The differential equations

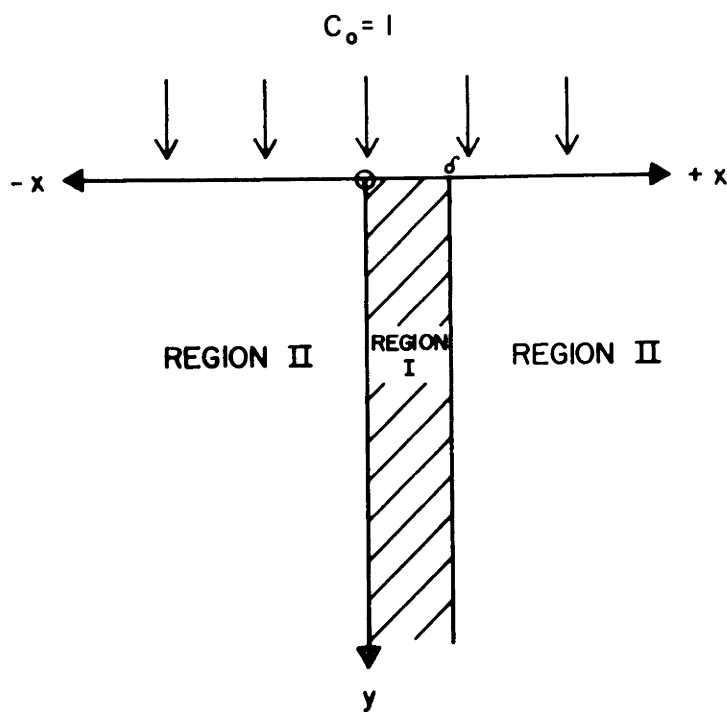


Figure 8 - Coordinate system for Fisher's mathematical analysis of grain boundary and volume diffusion in a semi infinite medium. Grain boundary slab is infinite in the $+x$ and $-z$ directions and of width δ (henceforth referred to as $2a$).

of (36) and (37) were converted into difference equations and then solved numerically for Δx and Δy increments of 8×10^{-3} microns, and selected values of D'/D , δ and time. The numerical results indicated that the C of region one rapidly becomes independent of time. Hence $(\frac{\partial C}{\partial t})$ in (36) may be set to zero. With these assumptions, the revised forms of (36) and (37) are solved for C yielding:

$$C(x, y, t) = \left\{ e^{-\frac{\sqrt{2} y}{\sqrt{\frac{2aD'}{D} (\pi Dt)^{1/4}}} } \operatorname{erfc} \frac{x}{2\sqrt{Dt}} \right\} \quad (38)$$

Therefore

$$\ln C = -\frac{y}{\sqrt{\frac{D'a}{D} (\pi Dt)^{1/4}}} + \ln \left[\operatorname{erfc} \frac{x}{2\sqrt{Dt}} \right] \quad (39)$$

From (39) we see that a plot of $\ln C$ versus y (for any x) yields a straight line from whose slope one may obtain $D'a$. Note that we could have a polycrystalline sample represented ideally by many high diffusivity planes and, if the distance between them is greater than about $\sqrt{4Dt}$,

$$\langle C(y, t) \rangle = \frac{1}{2L} \sum_{l=1}^K \int_{-L}^L C(x, y, t) dx \cong \frac{K}{2L} e^{-\frac{y}{\sqrt{\frac{D'a}{D} (\pi Dt)^{1/4}}} } \int_{-L}^L \operatorname{erfc} \frac{x}{2\sqrt{Dt}} dx \quad (40)$$

where L is the average distance about a given grain boundary over which C is significant and K is the total number of grain boundary planes emanating from the surface at $y = 0$. $\ln(C)$ versus y is again linear with the same slope as (39).

Whipple in 1954⁷ solved (36) and (37) exactly (a more detailed treatment of his analysis is carried out by F. J. Milford and C. C. Maneri⁸). Referring to figure nine and equations (36) and (37), C in region I (henceforth referred to as C_I) is expanded in a power series in x , under the assumption that a is very small compared to experimental penetrations in

the x direction. Making use of the boundary conditions at $x = a$:

$$\begin{aligned} \textcircled{a} C_I(ayt) &= C_{II}(ayt) & \textcircled{b} D' \left(\frac{\partial C_I}{\partial x} \right)_a &= D \left(\frac{\partial C_{II}}{\partial x} \right)_a \\ \textcircled{c} \left(\frac{\partial C_I}{\partial t} \right)_a &= \left(\frac{\partial C_{II}}{\partial t} \right)_a & \textcircled{d} \left(\frac{\partial^2 C_I}{\partial y^2} \right)_a &= \left(\frac{\partial^2 C_{II}}{\partial y^2} \right)_a \end{aligned} \quad (41)$$

one obtains, when terms involving x to the second or higher power are dropped, a differential equation boundary condition for C_{II} .

Equation (37) is then solved for C_{II} by a Fourier-Laplace transform:

$$\Psi(x, \mu, \lambda) = \int_0^\infty e^{-\lambda t} dt \int_0^\infty \sin \mu y C(x, y, t) dy \quad (42)$$

where λ and μ are in general, complex quantities. The solution of the transformed equation is composed of two parts, defined as Ψ_1 , and Ψ_2 . At this point Whipple makes a transformation to new variables:

$$\begin{aligned} \textcircled{a} \xi &= \frac{x-a}{\sqrt{Dt}} & \textcircled{b} \eta &= \frac{y}{\sqrt{Dt}} & \textcircled{c} \Delta &= D'/D \\ \textcircled{d} \alpha &= \frac{a}{\sqrt{Dt}} & \textcircled{e} \beta &= \frac{(D'/D - 1)a}{\sqrt{Dt}} \end{aligned} \quad (43)$$

The Fourier-Laplace inversion formula, when applied to Ψ_1 , and Ψ_2 , respectively, yields:

$$C_1(\eta) = \frac{1}{\pi^2 i} \int_0^\infty \sin \mu \eta \mu d\mu \int_{\gamma-i\infty}^{\gamma+i\infty} \frac{e^\lambda}{\mu^2 + \lambda} \frac{d\lambda}{\lambda} \quad (44)$$

$$C_2(\xi, \eta) = \frac{\Delta - 1}{\pi^2 i} \int_0^\infty \sin \mu \eta \mu d\mu \int_{\gamma-i\infty}^{\gamma+i\infty} \frac{e^{(\lambda - \sqrt{\mu^2 + \lambda}) \xi}}{(\mu^2 + \lambda) \left(\mu^2 \Delta + \frac{1}{\alpha} \sqrt{\mu^2 + \lambda} + \lambda \right)} \frac{d\lambda}{\lambda} \quad (45)$$

The second integral in (44) can be evaluated by the calculus of residues and Cauchy's integral formula since it has only two simple poles at $\lambda = \pm \mu^2$. This evaluation then provides C_1 in an integral form which

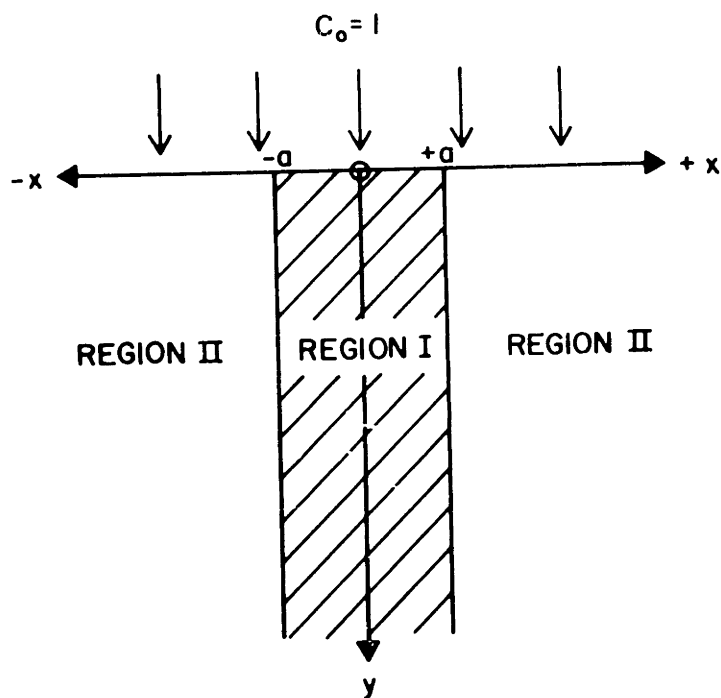


Figure 9 - Coordinate system for Whipple's mathematical analysis of grain boundary and volume diffusion in a semi infinite material with a slab of high diffusivity of width $2a$ extending to infinity in the $+z$ and $-z$ directions.

may be shown from standard integral tables to be $\operatorname{erfc} \eta/2$. We see from this that the first contribution to C at a point in the crystal is just that part that diffuses through the bulk from the surface. The expression for C_2 however is the one of interest since it involves " β " and hence depends on the value of $D'\alpha/D$. C_2 cannot be evaluated as readily as C_1 because of a branch point in "complex λ " space at $\lambda = -\mu^2$. This requires a special type path on the second integral in order to apply Cauchy's integral formula. Use of this special path is justified by the fact that the integrand is analytic everywhere within the closure of the path and approaches zero on the outer bounds of the path. The final expression for C_2 then comes out to be:

$$C_2(\xi, \eta) = \frac{\eta}{2\sqrt{\pi}} \int_1^{\Delta} \sigma^{-3/2} e^{-\eta^2/4\sigma} \operatorname{erfc} \left[\frac{1}{2} \sqrt{\frac{\Delta-1}{\Delta-\sigma}} \left(\xi + \frac{\sigma-1}{\beta} \right) \right] d\sigma \quad (46)$$

This expression may be evaluated numerically. Alternatively it may be expressed in analytic form for large values of the error function argument and large η , by the method of steepest descents. Since the latter approach assumes very large values of Δ and large η values without being too specific as to what these "large" values should be, the numerical approach will be used in this analysis. If C_2 is set equal to a constant, (46) can be solved numerically⁹ for various values of ξ and η . From this, ξ (or η) may be obtained as a function of η (or ξ) for each value of C_2 . This provides isoconcentration contours in the neighborhood of the grain boundary. An example for $\beta = 5.0$ is illustrated in figure ten. A series of such plots for various β 's can be used to plot $\left(\Delta\eta/\Delta\xi \right)_{\xi=0}$ as a function of β for various isoconcentration contours. This is illustrated in figure eleven.

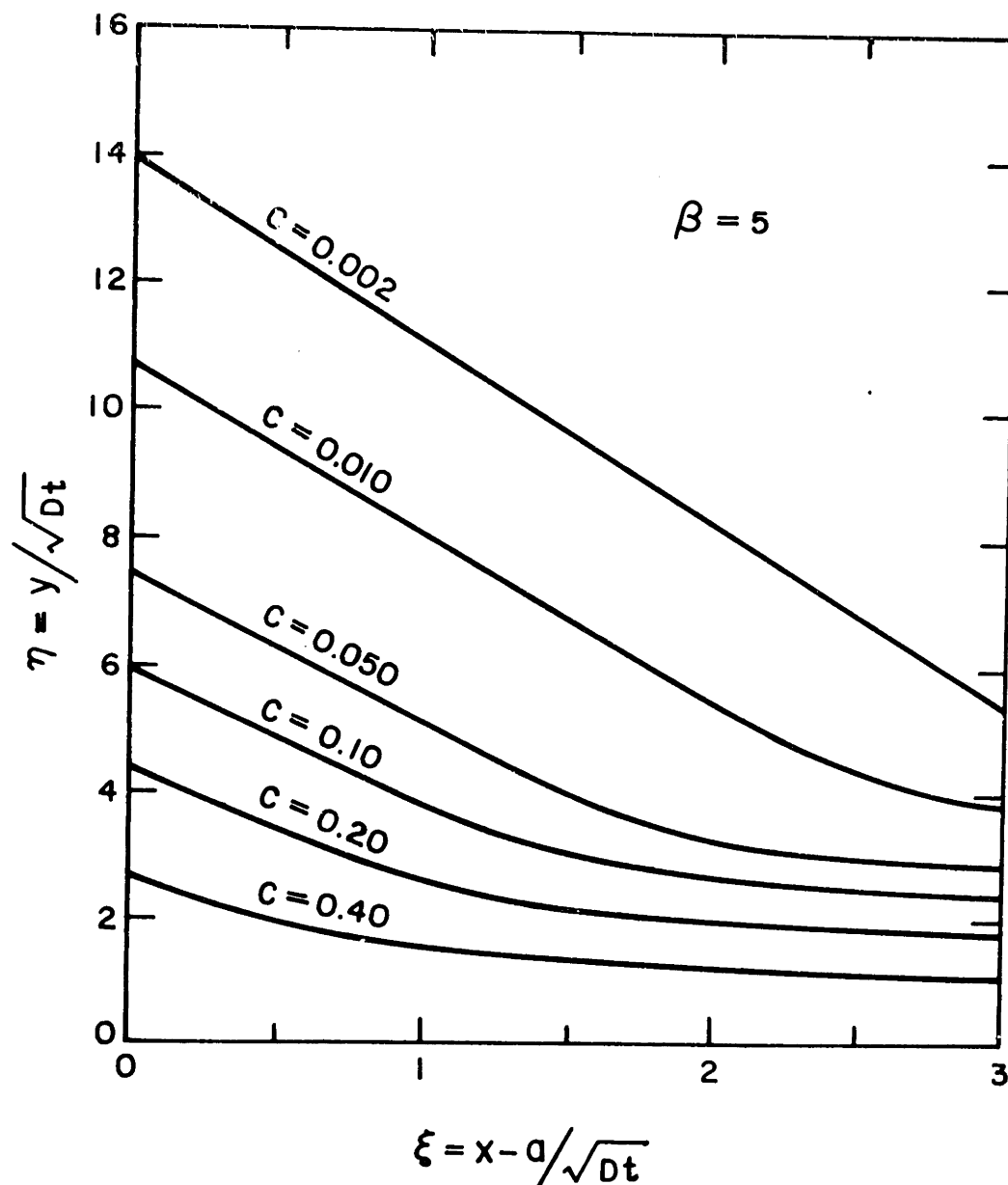


Figure 10 - Isoconcentration contours⁹ derived from the numerical solution of equation (46). η is the reduced penetration y/\sqrt{Dt} parallel to the grain boundary. ξ is the reduced penetration $x - a/\sqrt{Dt}$ perpendicular to the grain boundary for $\beta = 5$ [$\beta \equiv \frac{D}{D'} \frac{a}{\sqrt{Dt}}$].

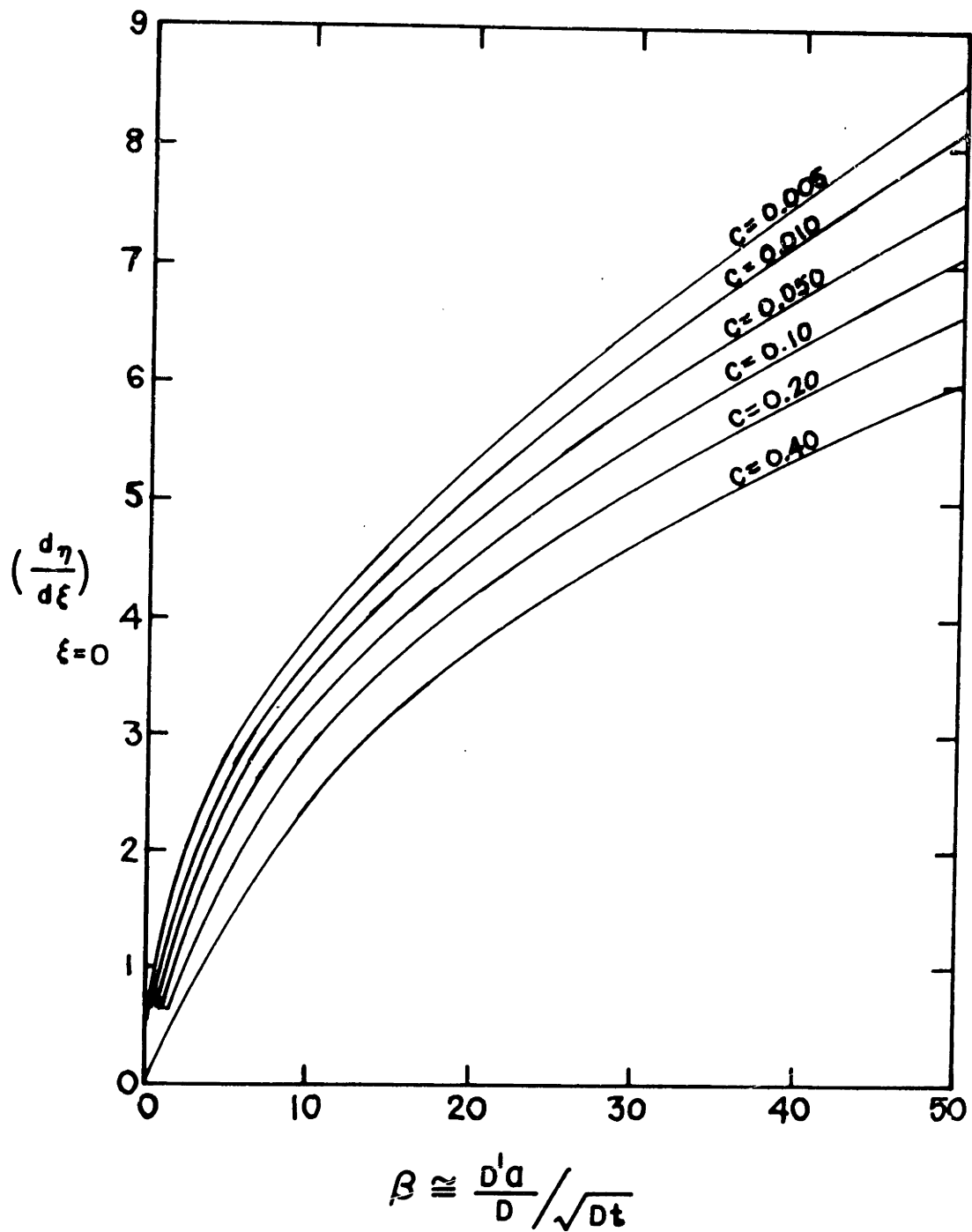


Figure 11 - Plot of the inverse of the isoconcentration slopes at the grain boundary edge ($\xi = 0$) as a function of β .⁹

Figure twelve is taken from the work of Karstensen and Whipple.¹⁰ ϕ is the inverse of $(\Delta\eta/\Delta\xi)_{\xi=0}$. Since the slope of an isoconcentration contour may be experimentally obtained, exact values of β may be computed by means of figures eleven and twelve. Hence D'a (assuming that one knows the bulk diffusion coefficient D through some other measurement) may be obtained from experiment.

Other quantities that may be experimentally measured are the average grain boundary concentration and, analogous to equation (40), the average concentration over a complete section at a given value of η ($\eta = y/\sqrt{Dt}$).

In figures thirteen and fourteen are plotted the natural logarithms of the concentration at $\xi = 0$ (approximately equal to average grain boundary concentration) labelled C_p , and the natural logarithm of the average concentration over a complete section at a given η , labelled $\bar{\Phi}$, as a function of η for various values of β . The variation of $\bar{\Phi}$ and C_p were also evaluated numerically by the same method⁹ as were the isoconcentration contours. To obtain an exact value of β using these last two techniques, absolute values of η , C_p and $\bar{\Phi}$ are required. This is not too feasible from an experimental standpoint. Therefore, the least square slopes of the curves in figures thirteen and fourteen in the range of η values below 18 have been plotted as a function of β in figure fifteen. The least square slopes do not depend on absolute measurements and hence figure fifteen is of practical value in obtaining the value of β .

For purposes of comparison (39) may be expressed in terms of η and β at $x = 0$ yielding:

$$\ln c(0\eta) = -\frac{\eta}{\pi^{1/4}\beta^{1/2}} = \ln C_p \quad (47)$$

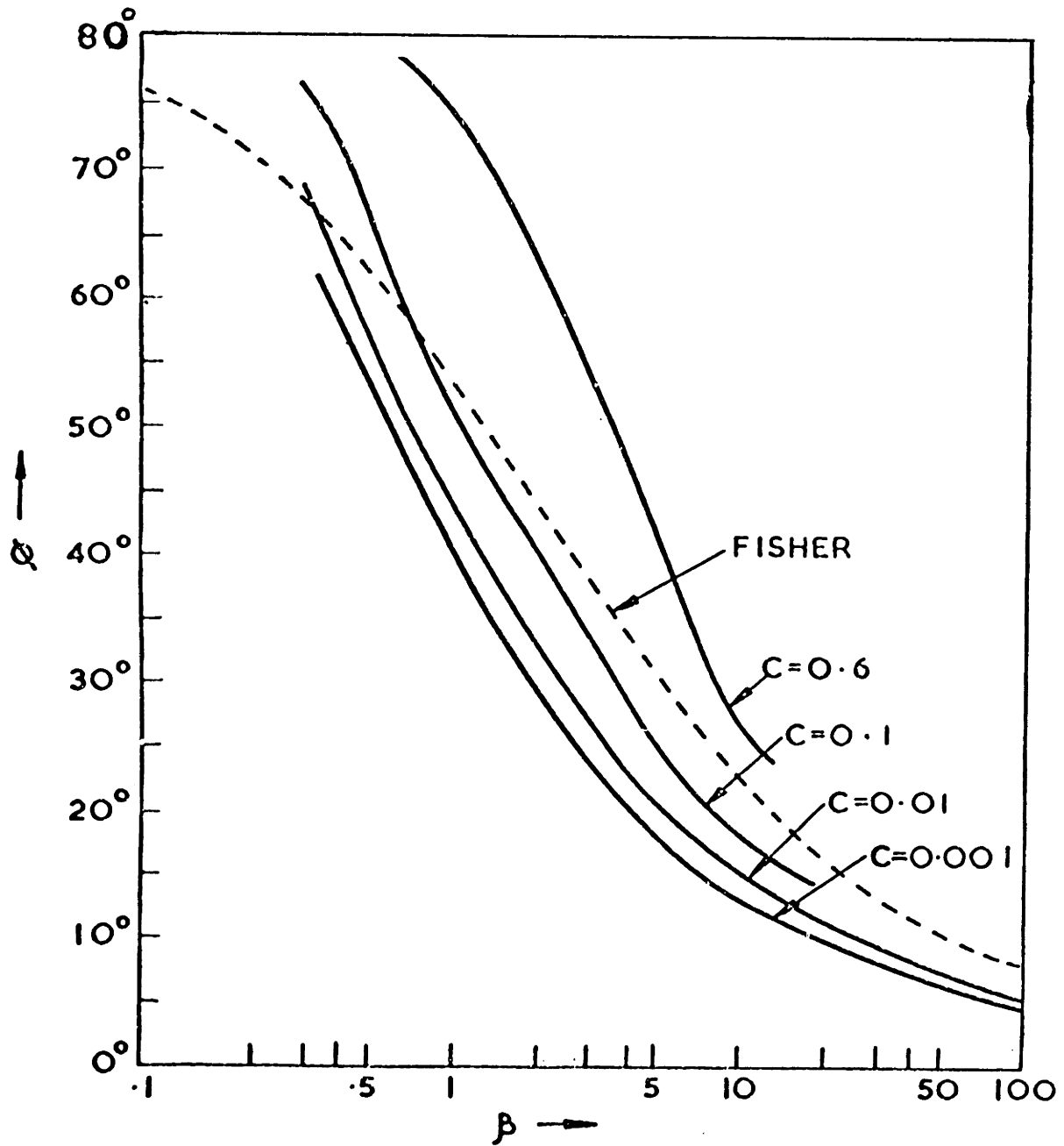


Figure 12 - Plot of the angles that the isoconcentration contours make at $\xi = 0$ with the grain boundary plot as a function of β .¹⁰ Included is the Fisher result derived from equation (39).

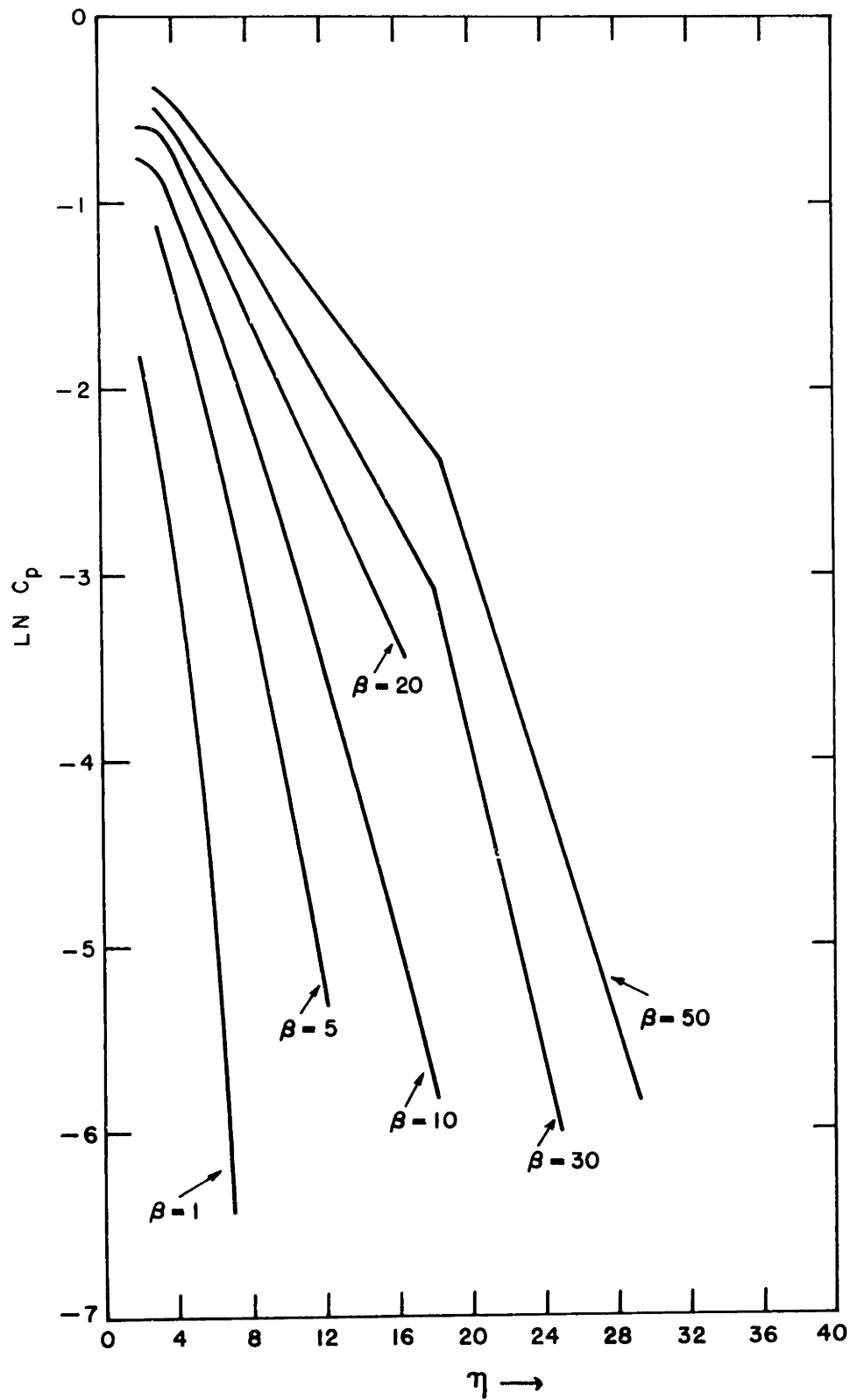


Figure 13 - Plot of the natural logarithm of the concentration at $\xi = 0$ as a function of reduced penetration $y/\sqrt{Dt} = \eta$, for various values of β .

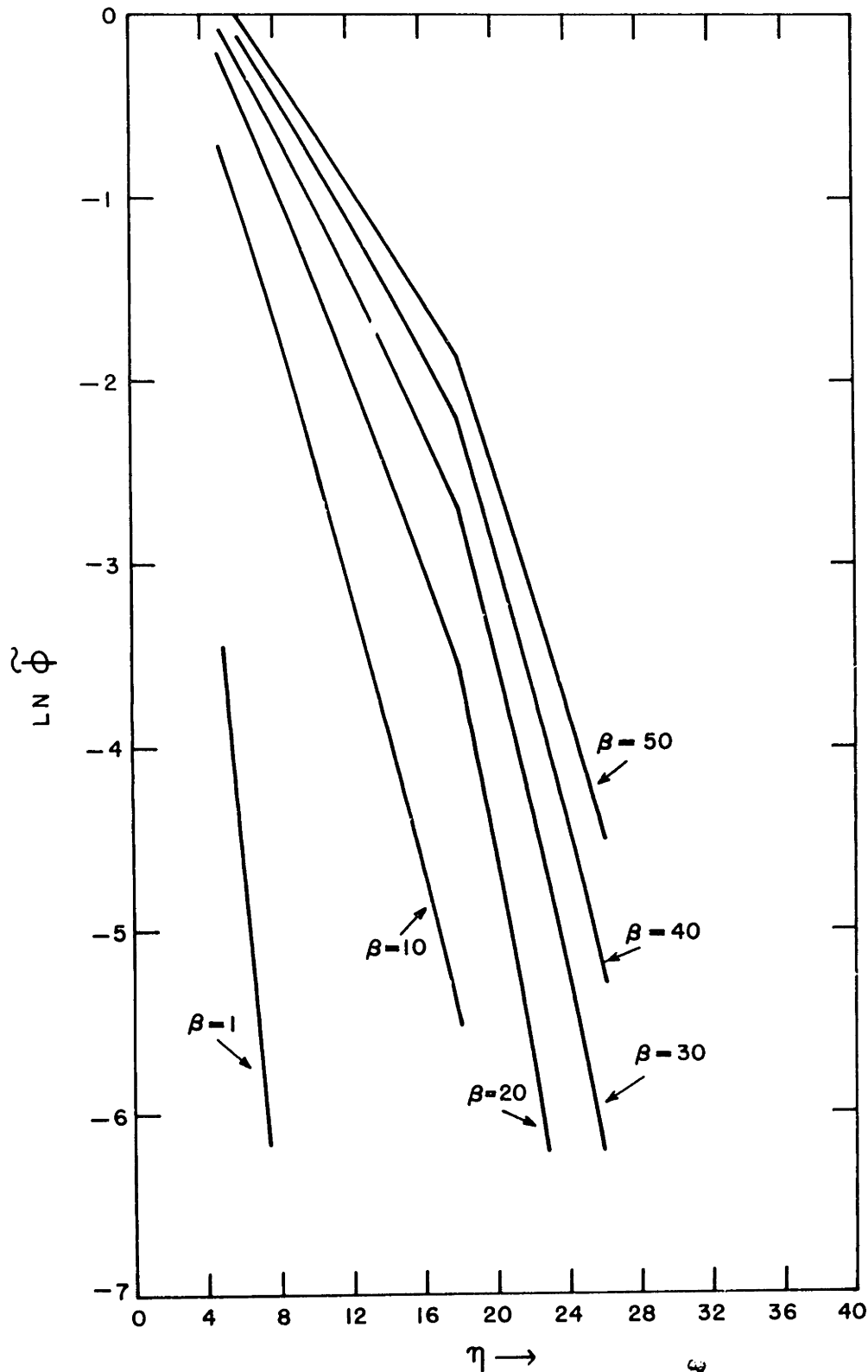


Figure 14 - Plot of the natural logarithm of $\tilde{\phi} = \int_0^{\infty} C_2(\xi\eta) d\xi$ as a function of reduced penetration $\eta = y/\sqrt{Dt}$ for various values of β . C_2 is from equation (46) and $\tilde{\phi}$ is obtained by numerical integration of C_2 .

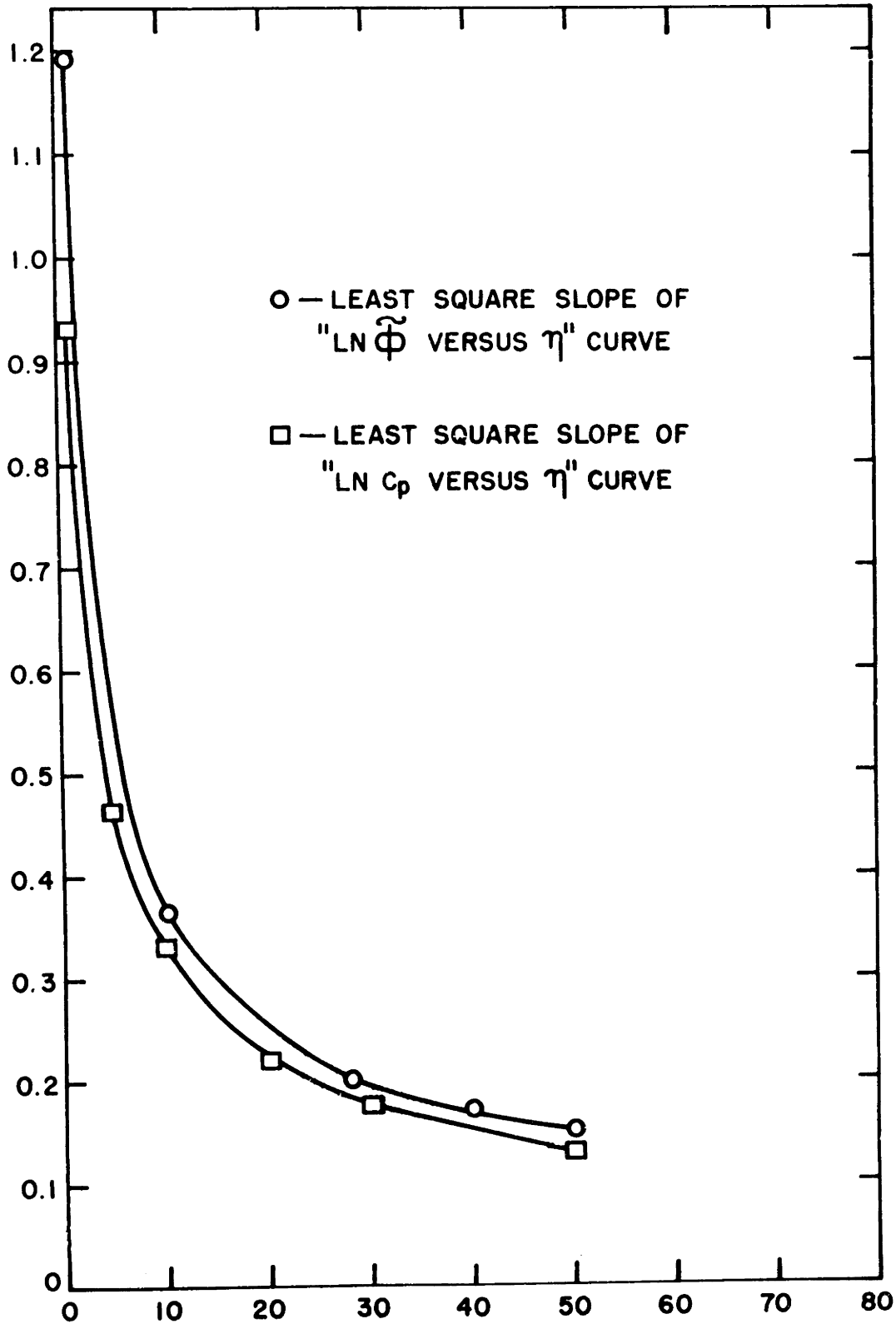


Figure 15 - Plot of the least square β slopes of the LN $\tilde{\phi}$ [labelled by the open circles ○] and LNC_p [labelled by the open squares □] versus η curves of figures 13 and 14 as a function of $\beta \cong \frac{D_1 a}{D} / \sqrt{Dt}$. The range of the η values is $0 \leq \eta \leq 18$.

The β 's obtained by equating $1/\eta^4 \beta^{1/2}$ to the experimentally measured least square slopes will only be approximate whereas the β 's obtained from figure fifteen are exact. Table one shows a comparison of the least square slopes obtained by the two curves in figure fifteen, and the Fisher equation (47) for various fixed values of β . The greater discrepancy is between the least square slopes of $\text{LN } \tilde{\phi}$ versus η and the slopes obtained by using Fisher's equation (47).

It is important to note that, in all the curves obtained by numerical analysis of (46) the contribution to C at a point $(\xi \eta)$ resulting from the C_1 term in (44) is neglected. Hence, for meaningful results an experimental analysis must be performed at large enough η that bulk contributions can be neglected. Alternatively the concentration analysis for large ξ values and fixed η can be subtracted from the concentration values in the vicinity of the grain boundary to get the true C_1 values.

If the grain boundary is not perpendicular to the $\eta = 0$ plane, and the concentration is evaluated far enough into the bulk, it may be assumed with a minimum of error that the $\eta = \text{constant}$ lines are perpendicular to the plane of the grain boundary.

In all cases it is assumed that D'/D is $\gg 1$. When this is done, β has the following temperature dependence:

$$\beta = \frac{a D'_0}{t^{1/2} D_0^{3/2}} e^{\frac{3/2 \Delta h - \Delta h'}{kT}} = \frac{a D'_0}{t^{1/2} D_0^{3/2}} e^{\frac{3\Delta h - 2\Delta h'}{2kT}} \quad (48)$$

Note from (48) that if Δh for grain boundary diffusion (referred to as $\Delta h'$) is less than the Δh of bulk migration, β will increase with decreasing temperature.

TABLE ONE

β	From Equ. 47 Fisher Slopes	Slopes of LN C_p from Fig. 15	Slopes of LN ϕ from Fig. 15
0.5	1.06	---	---
1.0	0.75	0.57 to 1.21	---
1.5	0.62	0.75 to 0.80	---
2.0	0.53	0.70	0.88 to 0.94
2.5	0.47	0.64	0.78 to 0.82
3.0	0.43	0.60	0.74
10.0	0.24	0.33	0.36
20.0	0.17	0.22	0.25

Table One: Comparison of the slopes obtained from figure 15 for C_p and $\tilde{\phi}$ with that obtained by Fisher ($\frac{1}{\pi^{1/4} \beta^{1/2}}$) for pre-determined values of β .

IV. LITERATURE REVIEW

A. Single Crystals (No Intentional Impurities Added)

1. Self Diffusion

Because of the vast amount of work on diffusion in single crystals, the review will be limited to alkali halides.

Mapother et al¹¹ conducted the first study of cation diffusion in single crystals of the alkali halides. They deposited five micron thick layers of radioactive Na (in the form of NaCl and NaBr) on host single crystals of NaCl and NaBr respectively and sealed them in glass ampules. Their diffusion runs spanned the temperature range 250°C to 720°C for NaCl, and 250°C to 700°C for NaBr. Thin sections of approximately equal thickness were cut from the samples in the direction of penetration, and their corresponding specific activities recorded. A plot of the logarithm of specific activity versus the square of penetration yielded a straight line whose slope, assuming the thin film solution was equated to $\frac{1}{4Dt}$. They observed intrinsic and extrinsic behavior for both crystals. From their NaCl work they obtained a value $\Delta h_{f/2} + \Delta h_m$ of 1.80 electron volts per ion and a D_0 of 3.1 cm²/sec for sodium diffusion and a Δh_m of 0.77 electron volts per ion and a D_0' of 1.6×10^{-6} cm²/sec. The $\Delta h_{f/2} + \Delta h_m$ and D_0 for diffusion of Na in NaBr were 1.53 electron volt per ion and 0.67 respectively. The data in the extrinsic range for NaBr had significant scatter, so that a value of Δh_m and D_0' were not calculated.

Arnikar and Chemla¹² have conducted self diffusion studies of potassium in KCl by depositing a radioactive thin film and using a sectioning type analysis similar to Mapother. Their measurements covered

the temperature range from 580C° to 750C°. No extrinsic behavior was observed. They obtained a $\Delta h_f/2 + \Delta h_m$ of 1.74 electron volt per ion and a D_0 of 3.0 cm²/sec for potassium self diffusion. They compare their data with that of J. F. Aschner¹³ who gets a corresponding $\Delta h_f/2 + \Delta h_m$ of 1.74 electron volt/ion and D_0 of 2.0 cm²/sec.

Laurent and Benard (1957) studied cation and anion self diffusion in the following single crystals: KI in the temperature range 460C° to 700C°, KBr in the temperature range 480C° to 720C°, KCl in the temperature range 520C° to 750C°, KF in the temperature range 580C° to 830C°, NaCl in the temperature range 600C° to 800C°, CsCl (NaCl structure) in the temperature range 465C° to 640C°, and CsCl (CsCl structure) in the temperature range 280C° to 465C°. They used radioactive thin film deposits and a sectioning technique. No extrinsic behavior was observed in any of the curves. Their results are shown in table two.

There are several other works^{15,16,17} on cationic self diffusion in the alkali halides. Their final results are listed in table two. The values of D_0 show no variation consistent with present theories. The temperature dependence of the diffusion coefficients however are linear enough to assume only one predominant transfer mechanism in the intrinsic region and one in the initial part of the extrinsic region. The difference between the intrinsic and extrinsic slopes also give estimated heats of formation that agree reasonably well with one another and with the few theoretical estimates (also listed in table two) of the heats of formation of Schottky pairs in alkali halides. This confirms the idea that cations move in the alkali halides by way of unassociated cation vacancies for a wide temperature range.

2. Cationic Impurity Diffusion

Chemla¹⁸ diffused radioactive cesium into NaCl in the temperature range 550C° to 750C°. No extrinsic behavior was observed. The $\Delta h_{f/2} + \Delta h_m$ for diffusion of cesium was 1.80 electron volt per ion and D_0 , which is stated to be about three times larger than the D_0 of Na in NaCl,¹¹ is about 9.0 cm²/sec.

In a later work¹⁹ he studied the diffusion of radioactive K, Rb and Ag in single crystals of NaCl in the temperature range 600C° to 750C° (using a "sandwich couple" as described in III.A.1.). The value obtained for $\Delta h_{f/2} + \Delta h_m$ was 1.90 electron volts per ion for all three cations. The values obtained for D_0 for cesium, potassium and rubidium were 67, 13, and 16 cm²/sec respectively. No extrinsic behavior was observed. The diffusion coefficient at a given temperature increased with increasing size of the alkali ions, and he associates this with an increasing oscillation frequency due to the increased repulsive potential for the larger size ions.

Arnikar and Chemla¹² carried out an investigation of sodium and cesium diffusion in KCl. Their self diffusion work for potassium has already been mentioned. This analysis also spanned the temperature range 570C° to 750C°. They obtained a $\Delta h_{f/2} + \Delta h_m$ of 1.75 electron volt/ion for sodium and 1.74 electron volt/ion for cesium with corresponding values of D_0 of 6.7 and 1.8 cm²/sec. Including their self diffusion results, they obtain a D (at fixed temperature) that decreases with increasing ionic radius. This is in direct opposition to their results for NaCl.

Glasner and Reisfeld²⁰ used a novel spectroscopic technique to investigate the diffusion of lead and thallium in single crystal KCl.

In this method the total amount of lead or thallium diffused into the tiny grains of KCl in a fine powder mixture of host and diffusant material is measured by making use of their characteristic absorptions in the ultra violet. By measuring the amount diffused in as a function of time a diffusion coefficient can be obtained.

The temperature span of their diffusion runs were very narrow: 150C° to 200C° for thallium diffusion and 300C° to 375C° for lead diffusion. The formula by which they obtain \underline{D} assumes a concentration-independent diffusion coefficient. This would not alter the thallium results because it is monovalent, but it yields an inaccurate value for D of lead. They obtain Δh 's of 1.09 electron volt per ion and 0.99 electron volt per ion for thallium and lead diffusion respectively and corresponding values of D_0^i of 7.14 and 4.4×10^{-3} cm²/sec.

Murin et al²¹ studied the diffusion of radioactive calcium in NaCl doped with 0.2 mole percent of CaCl₂, in the temperature range 350C° to 650C°. The diffusion coefficient was determined by the Boltzmann-Matano analysis,⁴ and was observed to have a concentration dependence; large in the high concentration region and falling off to a constant value over a fairly wide concentration range. This constant value, called D saturation, was plotted versus temperature to get a Δh of 0.96 electron volt per ion for calcium diffusion.

Other work^{22,23,24,25,26} in which divalent impurities were diffused into alkali halides, requiring the use of the Boltzmann-Matano analysis, and a plot of D saturation versus temperature are listed, along with the above mentioned works, in table two. Because the temperature dependence of D saturation has no intrinsic region, a heat of formation can not be extracted from the data. However it is

generally agreed that the concentration dependence of D follows quite well the formula of Lidiard.³ The expression was derived on the assumption of mass transfer by divalent impurity-cation vacancy complexes. The Δh_m obtained from the slope varies sufficiently from work to work (for a given divalent impurity) that no definite conclusions can be drawn about which predominant physical interactions between impurity, lattice, and defects control the value of Δh_m .

There are several other papers^{27,28,29,17} on monovalent impurity diffusion in the alkali halides. Their results and the results of those mentioned earlier are also in table two. All of this work bears out the hypothesis that monovalent impurities also move by way of unassociated cation vacancies. The difference in the slopes in the intrinsic and extrinsic region gives a value of Δh_f (heat of formation of a Schottky pair) which is as close to the theoretical values as those obtained from self diffusion data.

B. Ionic Conductivity

Conductivity experiments are useful for several reasons. They can quite easily be performed as a function of temperature yielding very many experimental points. Slopes may therefore be obtained more accurately and any slight curvature due to the effect of more than one process will readily be apparent.

From the Nernst-Einstein relationship¹:

$$D_i = \frac{\sigma t_i k T}{n_i z_i^2 e^2}$$

where t_i is the fraction of the total conductivity carried by species i , σ is the total conductivity, n_i is the number of atoms of type i per cubic centimeter, and z_i is the valence of the i 'th species (e , k , T are

electronic charge, Boltzmann constant and temperature respectively). Thus, for pure (as grown) samples, the slopes of the $\text{LN } \sigma$ versus $\frac{1}{T}$ curves can be compared with those from LND versus $\frac{1}{T}$ curves in order to verify (or disprove) the same mechanisms for both processes.

Many of the authors already mentioned, carried out conductivity measurements on their crystals in connection with diffusion runs. These crystals were "pure" in the sense that they contained only "as-grown" impurities. The intrinsic and extrinsic slopes showed good linearity and values which were in satisfactory agreement with their diffusion data. Their data, along with those of others who performed conductivity measurements alone on their crystals, are listed in table three.

The temperature dependence of conductivity for crystals doped with divalent impurities showed only extrinsic slopes (also labelled Δh_m in table three). The values of the slopes differ from author to author and, in general, from one type of divalent impurity to the next. Although the extrinsic region is one in which speculations should be carefully made, the prevalent idea as to how the ions are moving in this region seems to be, associated divalent impurities and cation vacancies. The data on conductivity in divalently doped alkali halides are also shown in table three.

C. Grain Boundary Diffusion

Studies concerned with the influence of grain boundaries and/or dislocations on mass transfer are not too extensive. This review will therefore cover both alkali halides and oxides. The behavior of boundaries

TABLE TWO Part 1

Host	Cation	$\Delta h_{\text{intr.}}^{(\text{ev})}$	D_0 cm ² /sec	$\Delta h_{\text{extr.}}^{(\text{ev})}$	D_0 cm ² /sec	$\Delta h_f^{(\text{ev})}$	Temp Range	T_{break}	Ref.
KCl	Na	1.75	6.7	---	---	---	570-750C°	---	12
KCl	K	1.74	3.0	---	---	---	570-750C°	---	12
KCl	Cs	1.74	1.8	---	---	---	570-750C°	---	12
KCl	K	1.88	3.8	0.59	---	2.54	570-750C°	---	13
KCl	K	1.47	4x15 ²	---	---	---	520-750C°	---	14
KCl	Cd	---	---	0.54	4.7x10 ⁵	---	350-500C°	---	24
KCl	Rb	2.04	26.8	---	---	---	597-750C°	---	17
KCl	Tl	---	---	1.09	7.14	---	150-200C°	---	20
KCl	Pb	---	---	0.99	4.41x10 ³	---	300-375C°	---	20
KCl	Tl	1.70	2.0	0.43	2x10 ⁸	2.54	253-740C°	560C°	29
KCl	Pb	---	---	0.73	1.02x10 ³	---	200-475C°	---	23
KBr	Tl	2.01	50	1.03	4.1x10 ⁵	1.96	330-680C°	497C°	28
KBr	Tl	1.98	47	---	---	---	520-700C°	---	27
KBr	K	1.94	---	---	---	---	300-700C°	---	15
KBr	K	1.25	10 ⁻²	---	---	---	480-720C°	---	14
NaCl	Na	1.80	3.1	0.77	1.6x10 ⁵	2.06	250-720C°	---	11
NaCl	Na	1.60	0.5	---	---	---	600-800C°	---	14
NaCl	Mn	---	---	0.66	---	---	450-750C°	---	22
NaCl	Cs	1.85	9	---	---	---	550-750C°	---	18
NaCl	K	1.90	13	---	---	---	600-750C°	---	19
NaCl	Rb	1.90	16	---	---	---	600-750C°	---	19
NaCl	Ag	1.90	123	---	---	---	600-750C°	---	19
NaCl	Cs	1.90	67	---	---	---	600-750C°	---	19

Table Two - Collected data on quantities of physical interest obtained from diffusion of cations in the alkali halides.

TABLE TWO Part 2

Host	Cation	$\Delta h_{intr.}^{(ev)}$	D_0 cm ² /sec	$\Delta h_{extr.}^{(ev)}$	D_0 cm ² /sec	$\Delta h_f^{(ev)}$	Temp Range	T_{break}	Ref.
NaCl	Pb	---	---	0.98	---	---	320-530C°	---	26
NaCl	Rb	2.11	205	---	---	---	600-750C°	---	17
NaCl	Zn	---	---	1.04	2×10^{-2}	---	560-770C°	---	25
NaCl	Zn	---	---	0.52	1.5×10^{-4}	---	560-770C°	---	25
+ ZnCl ₂	"	2.27	1300	---	---	---	640-790C° ^a	---	16
"	Cu	---	---	0.96	---	---	350-650C°	---	21
NaBr	Na	1.53	0.67	---	---	---	250-700C°	---	17
RbCl	Rb	1.99	33.3	---	---	---	600-780C°	---	17
KI	K	0.64	10^{-5}	---	---	---	460-700C°	---	14
CsCl ^a	Cs	1.38	0.1	---	---	---	465-640C°	---	14
CsCl ^b	Cs	0.69	10^{-5}	---	---	---	280-465C°	---	14
THEORY									
KCl	---	---	---	---	---	2.14	---	---	66
KCl	---	---	---	---	---	2.26	---	---	67
KCl	---	---	---	---	---	2.21	---	---	68
KCl	---	---	---	---	---	2.18	---	---	69
KCl	---	---	---	---	---	---	---	---	70
NaCl	---	---	---	---	---	1.93	---	---	66
NaCl	---	---	---	---	---	2.11	---	---	67
NaCl	---	---	---	---	---	2.12	---	---	68
NaCl	---	---	---	---	---	1.91	---	---	69

Table Two - Collected data on quantities of physical interest obtained from diffusion of cations in the alkali halides.

TABLE THREE

Host Crystal	$\Delta h_{\text{intr.}}^{(\text{ev})}$	D_0 cm ² /sec	$\Delta h_{\text{extr.}}^{(\text{ev})}$	D'_0 cm ² /sec	$\Delta h_{\text{f}}^{(\text{ev})}$	Temp Range	Ref.
RbCl	1.58	3.58×10^6	----	----	----	550-700C°	30
NaCl	1.89	14.0	0.83	2.5×10^{-6}	2.12	250-720C°	11
NaBr	1.68	5.98	0.84	1×10^{-5}	1.68	250-700C°	11
NaCl	----	----	0.71	----	----	450-750C°	22
NaCl+MnCl ₂	----	----	0.66	----	----	450-750C°	22
NaCl	1.90	----	----	----	----	600-750C°	19
NaCl	1.81	----	----	----	----	560-630C°	25
KBr	1.91	----	----	----	----	300-700C°	15
NaCl	1.86	----	0.85	----	2.02	250-700C°	31
NaCl+CdCl ₂	----	----	0.85	----	----	250-400C°	31
KBr	1.96	----	0.96	----	2.00	240-740C°	32
NaCl	1.72	----	0.87	----	1.70	283-730C°	33
KBr	----	----	0.65	----	----	60-720C°	34
NaCl	----	----	0.75-0.82	----	----	30-500C°	35
NaCl+Mg	----	----	0.80	----	----	30-500C°	35
NaCl+Mn	----	----	0.70	----	----	30-500C°	35
NaCl+Cd	----	----	0.79	----	----	30-500C°	35
NaCl+Sr	----	----	0.83	----	----	30-500C°	35
KBr	1.94	----	0.67	----	2.53	441-727C°	36
KCl	2.02	----	0.99	----	2.06	250-727C°	32
KCl+Ca	----	----	0.79	----	----	300-750C°	37
KCl+Sr	----	----	0.86	----	----	300-750C°	37
KCl+Ba	----	----	0.94	----	----	300-750C°	37
KCl	----	----	0.68	----	----	500-750C°	13
KCl	----	----	0.77	----	----	60-700C°	34
KCl	1.95	----	0.84	----	2.20	200-750C°	38
KCl	1.66	----	----	----	----	450-750C°	39

Table Three - Collected data on quantities of physical interest obtained from conductivity experiments on pure and doped alkali halides.

and dislocations in metals is far enough removed from that of the ionic materials that they will be neglected.

Laurent and Bernard⁴⁰ have studied the diffusion of radioactive Na^+ and Cl^- in polycrystalline sodium chloride using a sectioning technique and the thin film solution. They noticed no change in the diffusion of sodium as the size of the pellets was varied from 3000 microns to 50 microns grain size. There was a marked increase in the chlorine diffusion rate although the activation energy for diffusion did not vary with grain size. By autoradiograph techniques they were able to show that chlorine, bromine, iodine, and cesium were in much higher concentration at the grain boundaries than the bulk of the polycrystalline aggregates.

In a later paper⁴¹ the same two authors self-diffused radioactive cations and anions into polycrystalline potassium chloride, potassium iodide, potassium bromide, cesium chloride and sodium chloride. Using an autoradiographic technique they were able to observe preferential grain boundary diffusion of all the anions and cesium but no preferential diffusion of the other cations. The general conclusion they drew from both works was that the anions and cesium move preferentially along the grain boundaries because of their higher polarizabilities.

Roberts and Wheeler⁴² observed preferential diffusion of radioactive zinc oxide in polycrystalline zinc oxide pellets. Their plots of log concentration versus penetration were linear as predicted by Fisher (III.B.). Using an available bulk diffusion coefficient from another work they were able to obtain $2D'a$. A plot of $\text{LN}(2D'a)$ versus $\frac{1}{T}$ obeyed a relationship of the form $Ae^{-\frac{Q}{kT}}$. Their results are listed in table four. Their value of $\frac{D^{1/2}}{aD}$ had very large scatter at every

temperature being very sensitive to the oxygen or argon ambient pressure. $\frac{D^{1/2}}{aD'}$ decreased with decreasing oxygen pressure and they associated this with an increasing D' rather than a decreasing D (a was assumed to stay constant). These results, which suggest an extrinsic mechanism for preferential grain boundary diffusion are in conflict with an earlier result⁴³ on zinc oxide pellets where well sintered pellets showed no effect of preferential diffusion in the boundaries and the LND versus $\frac{1}{T}$ plot was quite linear with a slope slightly smaller than that obtained from pellets that were not sintered.

Barr et al⁴⁴ studied the diffusion of chlorine in single crystals of potassium chloride and sodium chloride with high dislocation densities. The magnitude of their D 's, as well as the slopes of the LND versus $\frac{1}{T}$ plots in the low temperature region varied for KCl depending on annealing times. The longer the annealing times, the lower were the D values. They associated this with preferential diffusion of chlorine along dislocations and sub grain boundaries.

The results on a given pretreated crystal did not vary even when it was used in a crushed form for the diffusion run. This latter effect was explained as a saturation on the part of the dislocations initially existing in the crystal, such that, introducing additional dislocations by crushing did not effectively increase the net transfer of diffusant from the surface to any point in the bulk. The anomalous feature of these results is that the concentration dependence on penetration obeys single crystal behavior (namely an error function behavior for their diffusion set up) and yet the predominant mass transfer occurs in the vicinity of these "high diffusivity" paths. A similar anomaly

occurs for Laurent and Benard's work since they obtain their D's from the thin film solution and yet their anion and cesium D's are not associated with bulk transfer. This is discussed in detail by Harrison⁴⁵ who shows that, in certain cases, the techniques used by Laurent, Benard, Barr et al are valid. Of course the D's they obtain are "average" D's in the sense that atom transfer from the surface to a given point requires many interactions with the bulk and preferential regions.

Oishi and Kingery⁴⁶ have measured diffusion coefficients of oxygen in polycrystalline aluminum oxide two order of magnitude higher than bulk values. The Δh was also smaller than that of bulk. They feel that this is the result of predominant mass transfer by way of grain boundaries.

Cabane and Beaumont⁴⁷ used a radiographic technique and compared logarithm of activity-versus-penetration squared curves for iodine and chlorine diffusion in potassium iodine, potassium chloride, and sodium chloride pressed polycrystalline pellets. Their results indicated that iodine diffuses much more readily by way of the grain boundaries than does chlorine.

Cabane⁴⁸ has studied the diffusion of iodine, chlorine, potassium, and sodium in polycrystals of potassium iodide and sodium chloride, and bicrystals of potassium iodide. No preferential diffusion of sodium or potassium was observed but preferential diffusion of chlorine and iodine definitely occurred. In his work on polycrystalline pellets he used a radiographic technique on "y=constant" sections and compared experimental fall off in concentration away from grain boundary with theoretical curves of Whipple to get " β ". In the bicrystals he compared " $C/C_0 = \text{constant}$ " values with theoretical curves

of Whipple and Karstensen to obtain the β 's. In the potassium iodide bicrystals $\frac{D'a}{D}$ is essentially independent of temperature from 350C° to 550C° indicating, since Dt was held constant, that the enthalpy of motion in the grain boundary is equal to the enthalpy of motion in bulk, i.e., 25 k.calories per mole. These bicrystals were lightly pressure sintered with no exceptional care taken to eliminate water. Further, the mismatch angle was very small.

In the transparent polycrystalline pieces $\frac{D'a}{D}$ decreased with increasing temperature and no preferential diffusion was detected at temperature above about 520C°. The Δh_{gb} for this case was much smaller (12 k calories per mole). In the more opaque type polycrystalline pellets preferential diffusion persisted up to the highest temperatures. Cabane associates the preferential diffusion in the transparent pieces with the higher polarizabilities of the chlorine and iodine relative to the Na and K. The preferential diffusion in the impure pellets is associated with water. If care is used to eliminate water, even the anions do not diffuse preferentially above about 520C°.

Wuensch and Vasilos,⁴⁹ using the electron microprobe, have detected preferential diffusion of Ni^{2+} in bicrystals of MgO for temperatures less than 1700C°. They also observed that the contours of " $\gamma = \text{constant}$ " lines ($\gamma = y/\sqrt{Dt}$) at high penetrations didn't approach a spike-like behavior at the grain boundary as is observed in metal bicrystals. Instead, they peaked over a range of several microns. In a later paper,⁵⁰ they showed that preferential diffusion of Ni^{2+} and Co^{2+} in MgO bicrystals was due to impurity segregation at the grain boundaries, and that when this was eliminated (by using more care in preparing the

bicrystals, or by performing the diffusion runs above 1300C°, preferential diffusion ceased. The impurities appeared, in electron micrographs, as a second phase precipitate at the grain boundaries which disappeared above 1300C° due to rapid solution of the impurities into the bulk.

Paladino et al⁵¹ have noticed anomolous behavior in the temperature dependence of the diffusion coefficient of oxygen in single crystals of strontium titanate (SrTiO₃) below 1200C°. D in this region depended on prior heat treatment and dislocation density, the higher the dislocation density the higher the D's and the $\Delta h'$.

Geguzin and Dobrovinskaya⁵² observed enhanced diffusion of Na in NaCl due to the presence of screw type and edge type dislocations in the temperature range 200C° to 540C°. They diffused radioactive sodium (thick film sandwiched between two NaCl crystals) into two crystals of different (known) dislocation densities. They assumed that the concentration versus penetration has a complementary error function behavior and thus obtained an effective D (labelled D*). Assuming that $D_V t$ (D_V is the bulk diffusion coefficient, and t is the time of the diffusion anneal) is much larger than L (average distance between dislocations) the expression derived by Hart⁵³ can be used to get $D_{disl} S$.

$$D_{disl} S = \frac{D_1^* - D_2^*}{P_1 - P_2} \text{ cm}^4 / \text{sec}$$

Where D_{disl} is the diffusion coefficient in the preferential region around the dislocation, S is the area of this preferential region assuming that this region takes on the form of a cylinder whose axis is

parallel to the dislocation. In terms of the quantity "a" introduced by Whipple, $S \cong \pi a^2$. By knowing p_1 and p_2 (the dislocation densities in the two crystals), and getting D_1^* and D_2^* from the slope of a plot of $\text{erfc}^{-1}C/C_0$ versus penetration, $D_d S$ can be obtained for both screw type and edge type dislocations.

An additional set of diffusion runs were conducted for the case $D_v t$ much smaller than L but much greater than S for which the Smoluchowski⁵⁴ formula is used to get $D_d S$:

$$D_d S = \frac{8A D_v}{\pi} \left(\frac{\partial}{\partial y} \ln C_d \right)^{-2}$$

C_d is the average concentration in the dislocation, y is the direction of penetration of the diffusant and A is an integral that, for the above assumptions, can be expressed in terms of the measurable parameters. Their results for $D_d S$ obtained by both methods are the same and are listed in table four.

The same authors⁵⁵ have studied the diffusion of thallium along edge and screw dislocations in KI and KCl single crystals and in bicrystals of the same. The temperature range of their investigation was 200°C to 540°C. Their analysis for $D_d S$ was the same as for NaCl and their results are in table four.

Their bicrystals had twin boundaries (misorientation angle 12° to 15°). In order to obtain β ($\beta = \frac{D'a}{D} / \sqrt{Dt}$) for their bicrystals, they used a microhardness technique (thallium solid solution strongly increases the hardness of potassium chloride and potassium iodide) to obtain isoconcentration contours. From these contours they obtained ϕ , the angle that a contour makes with the grain boundary. The Fisher data of figure twelve was then employed to obtain β . Their values of $D'a$

as a function of temperature for both KCl and KI bicrystals are shown in table four. From the data one sees that $\Delta h_{GB} < \Delta h_{edge\ disl} < \Delta h_{screw\ disl}$. They associated the reduced activation energy with the fact that cation vacancies do not have to be created at the grain boundaries and hence Δh_{GB} is just the Δh of motion.

Rhodes and Carter⁵⁶ have studied the self diffusion of Zr and Ca in calcia stabilized zirconia. They diffused the radioactive species and analyzed for concentration using a sectioning technique. The samples were obtained from pressure sintered pellets whose central regions were melted and recooled, yielding large grain crystallites and negligible porosity. Their LNC versus y^2 plots showed a deviation from linearity for penetrations that were not too large. The accompanying autoradiographs which were also taken at various penetration distances exhibited anomalously high diffusant concentrations at the grain boundaries. Similarly their plots of LNC versus y were not linear either, a result contrary to that predicted by the Fisher analysis.

Rhodes and Kingery⁵⁷ have observed preferential diffusion of Ti^{4+} and Sr^{2+} in "single" crystals of strontium titanate ($SrTiO_3$). This, despite the fact that the polarizabilities of the two cations differ by a factor of four. The fact that the diffusion coefficient of both cations depended on dislocation densities complements the fact that the LNC-versus-penetration squared curves of the two cations were anomalous. The authors postulate that impurities are not the only factor affecting preferential grain boundary diffusion since both cation and anion have now been known to diffuse preferentially along dislocations in $SrTiO_3$. Rhodes results for strontium are listed in table four.

TABLE FOUR

Type of Preferential Path	$D'a \text{ cm}^3/\text{sec}$	Temp Range C°	Material	Diffusant	Method of Obtaining D'a	Author
Grain Boundary	$2.5 \times 10^8 \exp(-3.02/kT)$	800-1400	ZnO	Zn	Fisher	42
Edge Disl.	$6.5 \times 10^{-14} / a \exp(-0.51/kT)$	200-540	KI	Tl	error function plus Hart (Smoluchowski)	55
Screw Disl.	$1.6 \times 10^{-13} / a \exp(-0.63/kT)$	200-540	KI	Tl	error function plus Hart (Smoluchowski)	55
Edge Disl.	$2.0 \times 10^{-12} / a \exp(-0.61/kT)$	200-540	NaCl	Na	error function plus Hart (Smoluchowski)	52
Screw Disl.	$2.5 \times 10^{-10} / a \exp(-1.1/kT)$	200-540	NaCl	N	error function plus Hart (Smoluchowski)	52
Edge Disl.	$4.3 \times 10^{-15} / a \exp(-0.44/kT)$	200-540	KCl	Tl	error function plus Hart (Smoluchowski)	55
Screw Disl.	$3.2 \times 10^{-14} / a \exp(-0.58/kT)$	200-540	KCl	Tl	error function plus Hart (Smoluchowski)	55
Edge Disl.	$4.8 \times 10^{-8} / L \exp(-4.92/kT)$	1500-1860	SrTiO ₃	Sr	Fisher	57
<u>Bicrystals</u>						
Grain Boundary	$1.1 \times 10^{-10} \exp(-0.38/kT)$	200-540	KCl	Tl	Fisher	55
Grain Boundary	$3.0 \times 10^{-9} \exp(-0.48/kT)$	200-540	KCl	Tl	Fisher	55

Table Four - Collection of data on diffusion permeability (D'a). 2a is the width of the grain boundary. The numerators in the parenthesis in column one (to the left) is in electron volts. L is the average distance between dislocations.

G. H. Frischat^{58,59} has observed preferential grain boundary diffusion of radioactive sodium and calcium in polycrystalline (grain sizes of 10A° to 20A°) $\text{Na}_2\text{O} \cdot 2\text{CaO} \cdot 3\text{SiO}_2$ over the temperature range 300C° to 900C° . D_{GB} (grain boundary diffusion coefficient) showed definite dependence on crystallite size distribution; the smaller the grain size the smaller the effect of preferential diffusion.

To quote an example of grain boundary effects on electrical conductivity, Geschwind and Machlin⁶⁰ have measured σ (conductivity) as a function of temperature in tilt and twist bicrystals of KCl. The temperature range of their measurements was 60C° to 227C° . Water polishing these crystals in preparation for an experiment caused the $\text{LN } \sigma$ versus $\frac{1}{T}$ curve to exhibit a low temperature slope significantly smaller than the typical bulk value. Above 100C° the slope was equal to the bulk value. On cooling down the slope maintained the bulk value down to the lowest temperature. When the crystals were prepared without coming in contact with the water no such anomalous low temperature slope was observed.

V. CONCLUSIONS FROM LITERATURE REVIEW

A. Volume Diffusion and Conductivity Results

The D_0 values obtained for both the extrinsic and intrinsic range vary considerably in the few experiments where they can be compared for the same diffusant and host crystal. Many of the diffusants for a given host crystal (with the exception of NaCl and KCl) have only been investigated by one author. Reproducibility of data in the intrinsic region is not good for the diffusion analysis but is quite good for the conductivity analysis. The Δh 's in the extrinsic regions for a given crystal scatter badly for the diffusion runs but seem to have only a small range of variation in the conductivity runs regardless of the dopant.

Conductivity experiments give more consistent results and should be used to get better values of Δh_{intr} , Δh_{extr} , D_0 and D_0' . However care should be used since associations between defects (where a foreign cation is also considered as a defect) can appreciably alter diffusion and conductivity experiments in different ways making a correlation between the D_0 's and Δh 's sometimes impossible.

Slopes in the extrinsic range vary widely due to the effect of strains, dislocations and impurities on mass transfer. The only chance for reproducible results in this range is to use samples of equal impurity content and defect concentration

B. Grain Boundary and Dislocation Results

Several problems have arisen concerning grain boundary diffusion work. The first problem concerns the physical mechanism for grain

boundary and dislocation preferential diffusion. On one side we have the work of Laurent and Benard who feel that the preferential diffusion is associated with a specific ions ability to polarize more easily in the saddle point region. Cabane, however, states that this might be the mechanism at low temperature, but at higher temperature it may be eliminated by keeping water from the grain boundaries. To support Cabane's impurity hypothesis, we have the opinion of Wuensch and Vasilos who have similarly repressed preferential diffusion of cations by making clean grain boundaries.

An article by J. H. Westbrook⁶¹ surveys the situation of impurity effects at grain boundaries in ceramic materials. He indicates the importance of precipitation effects in these regions. Wuensch and Vasilos similarly noted second phase precipitates in their MgO bicrystals that exhibited preferential diffusion. Frischat observes preferential diffusion in a material that is also susceptible to second phase precipitates as does Rhodes and Carter in calcia stabilized zirconia. The work of Roberts and Wheeler and Geschwind and Machlin give extra support to the idea of an impurity mechanism as the controlling factor in preferential grain boundary diffusion.

Barr et al seem to feel that there is preferential diffusion of anions at any rate, along internal dislocations and sub grain boundaries in clean single crystals. They attribute the curvature of their low temperature diffusion data to this.

In support of Barr, Geguzen, Paladino and Rhodes have definitely shown that, assuming an error function (or thin film type) behavior of concentration on penetration, anomalous diffusion results occur for

cations in crystals with artificially created dislocations and grain boundaries.

These works off hand seem to be involved with "clean" defects. Hence no second phase precipitation or impurities should be localized there.

VI. RESEARCH OBJECTIVE

This work will concern itself with the diffusion of thallium chloride into single crystals, polycrystals, and bicrystals of potassium chloride. Thallium chloride has been chosen because, as seen in table five, it has a high polarizability and hence, studying its diffusion will determine whether its high ability to be deformed will enhance its diffusion along grain boundaries. TlCl is also monovalent, and should exhibit concentration independent diffusion. It also has a relatively high solubility in KCl thus making the use of the electron probe (to be described in the next section) practical.

Careful bulk diffusion data over a wide temperature range will be carried out in order to obtain D_0 's and Δh 's that are as accurate as possible, thus making future analysis of alkali halide data more exact. These data will be further used to obtain values of aD' from the values of $\beta = (D'/D - 1)a/\sqrt{Dt}$ obtained in the grain boundary diffusion study.

Work will be undertaken on polycrystals and bicrystals of potassium chloride of a wide range of mismatch angles to determine whether thallium chloride diffuses preferentially. If such enhancement is observed, an attempt will be made to determine whether the effect is associated with an intrinsic (such as polarizability) or extrinsic (impurity) mechanism. Also, if consistent preferential diffusion prevails over a sufficiently wide temperature range, $\Delta h_{\text{grain boundary}}$ will be obtained as a function of the crystallographic orientation of the grains. The analysis for thallium concentration gradients will be performed

TABLE FIVE

<u>Ion</u>	<u>α (Polarizability) in units of 10^{-24} cm^3</u>	<u>Ion</u>	<u>α (Polarizability) in units of 10^{-24} cm^3</u>
Li	0.03	Cd	0.08
Na	0.41	Tl	5.20
K	1.33	Cu	0.20
Rb	1.98	Pb	4.90
Cs	3.34	O	0.5-3.2
Cu	1.60	S	4.8-5.9
Ag	2.40	F	0.64
Ca	1.10	Cl	2.96
Sr	1.60	Br	4.16
Ba	2.50	<u>T</u>	6.43
Zn	0.80		

Table Five - List of ionic polarizability from Tessman, Kahn, Shockley.⁶¹

using the electron microprobe (to be described in next section). This work will allow the investigation of individual grain boundaries of controlled orientation which in turn may be characterized for impurity content. Diffusion in two orthogonal directions within the grain boundary will be investigated to determine whether there is anisotropy of the preferential diffusion. Comparison of experimental data with Fisher's analysis and with the exact theoretical functions derived in section III.B. will be made to test their validity in real situations.

VII. EXPERIMENTAL PROCEDURE

A. Preparation of Standard Composites

Analysis for a particular element with the probe is done through excitation of the characteristic X-radiation of the element with a one micron diameter electron beam. The radiation is, in turn, counted in a manner similar to the radiation from radioactive materials. In order to convert these counts to weight fraction of the specific species present, counting rates must be obtained from standards of two phase mixtures of potassium chloride and thallium chloride in known composition. The potassium chloride employed was Baker analyzed reagent grade obtained from Baker Chemical Company, Phillipsburgh, New Jersey. This material was ground to submicron size with a small Trost Jet Mill. The thallium chloride powder, obtained from Alfa Inorganics, Beverly, Massachusetts, was obtained with rather fine size. It was therefore not put in the jet mill. The powders were weighed out with a Mettler macro analytical balance for thirteen standards (see table six). The powders were put in solution in deionized water. The water was heated in some cases to facilitate complete solution. The solution was dried by a fan while being continuously stirred. The powder was then scraped from the jar with a spatula and oven dried at 170C° to 200C° from one to two full days in flowing dry nitrogen. The powders were then pressed in a die at about 10,000 psi, ground on their sides with 400 mesh silicon carbide paper (to remove residue from the die), and then rinsed well in hot acetone and trichlorethylene to remove die oils and foreign particles. The samples were then ground with 600 mesh

silicon paper, placed in an ultra sonic cleaner with denatured alcohol for fifteen minutes to remove traces of the silicon carbide, and then polished on politex supreme cloth (Geoscience, Mount Vernon, New York) with 302 1/2 and 309W alumina. They were then put back in the ultra sonic cleaner with the denatured alcohol for ten to fifteen minutes and dried. The polish was not uniform but sufficiently large sections of good polish were obtained. The grain size ranged from seven microns to ninety microns. Small sections of each sample were then removed and assembled together in cold setting plastic mount. The same polishing procedure (starting with the 600 mesh silicon carbide) was then repeated. As a check, a section of two of the standards were sent to a chemical laboratory to be analyzed. The results of the analyses were within eight percent of their nominal concentrations (see table six).

B. Sample Preparation for Volume Diffusion Runs

The potassium chloride used for the sandwich (thin film) couples and vapor exchange couples was "optical grade" material from the Harshaw Chemical Company, Cleveland, Ohio. The oxygen content of the material was obtained using a Carey Model 14 ultra violet spectrophotometer through which the electronic excitation of oxygen (204 millimicrons) could be investigated. The oxygen was present to about seven parts per million and was probably adsorbed on the surfaces and in the form of OH^{-1} in the bulk. The as-received crystals were about one inch on an edge and contained considerable mosaic structure (see figure 16), with domain size of the order of millimeters and mismatch angles of a few degrees. The Harshaw company analyzes a section of each of its boules

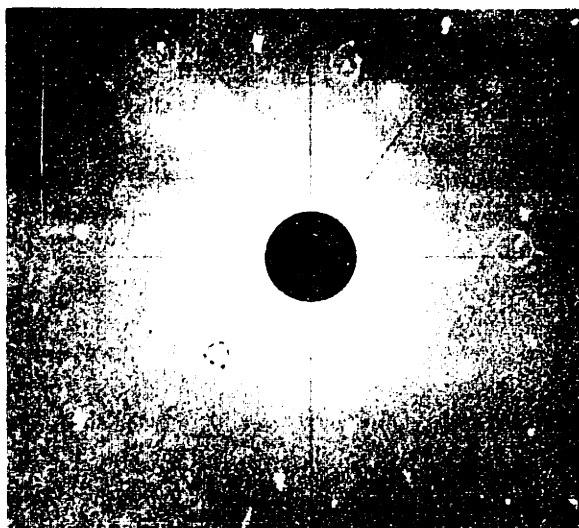


Figure 16 - Laue back reflection of a typical Harshaw cube used for volume diffusion runs and pressure sintered bicrystals. Film-to-sample distance is 3.0 cm. Typical mismatch angles are 3° to 4° .

for cation impurities. The boule used in this work for all the volume diffusion runs had company-estimated divalent impurity contents under six parts per million. The cations of highest concentration were calcium, silicon and magnesium.

For the vapor exchange couples, pieces of KCl, three to six millimeters thick and eight millimeters by eight millimeters in cross section were cut from the Harshaw cubes. They were then polished in the same manner as the standards with the addition of an extra light brushing on a politex cloth in which was embedded a very dilute mixture of 0.05 micron alumina and denatured alcohol. They were then rinsed well in alcohol and put in an oven at about 250C° for about twenty to forty minutes to dry.

For the sandwich couples, the samples were taken through the same steps as above. They were then put in a vacuum system and thallium chloride was vapor deposited, from a vycor crucible sitting in a spiral tungsten filament, at a pressure of 1×10^{-5} torr. The vycor crucible was initially outgassed in vacuum at 1000C° to remove impurities (specifically water and/or OH^{-1}).

A thin layer of KCl was then deposited over this by means of a separate crucible. The KCl was reagent grade Baker analyzed.

C. Preparation of Polycrystalline Pellets

Polycrystalline pellets were formed in three ways. In one case, reagent grade KCl was poured directly from the jar into an RF press (figure 17) and pressed at 2000 psi at 450C° for two hours. Grain size varied from twenty micron to greater than one hundred micron (figure 18A).

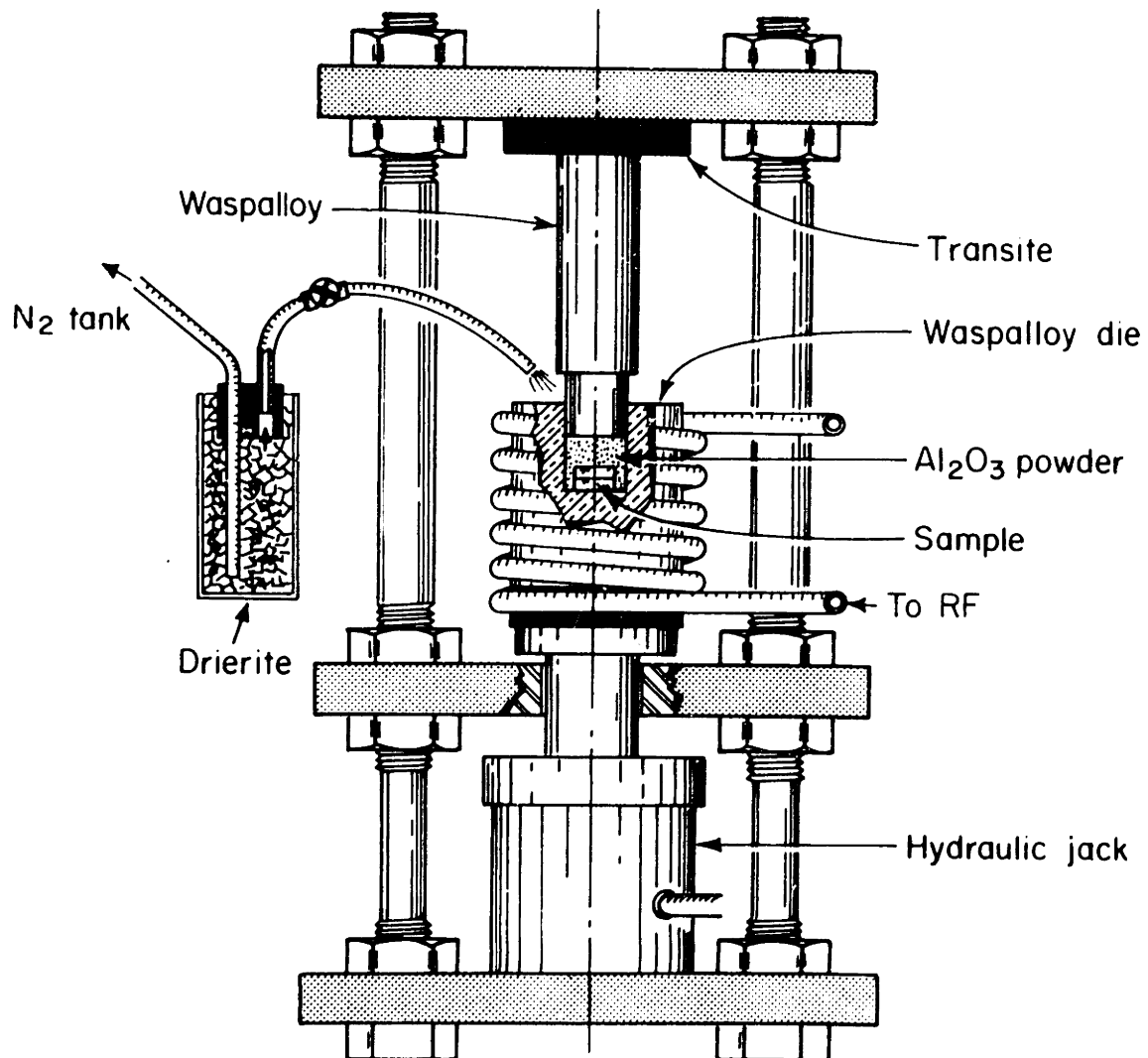


Figure 17 - RF press (induction heating) for pressing and sintering polycrystalline compacts and bicrystals.



Figure 18A - RF pressed pellet of KCl (100x).

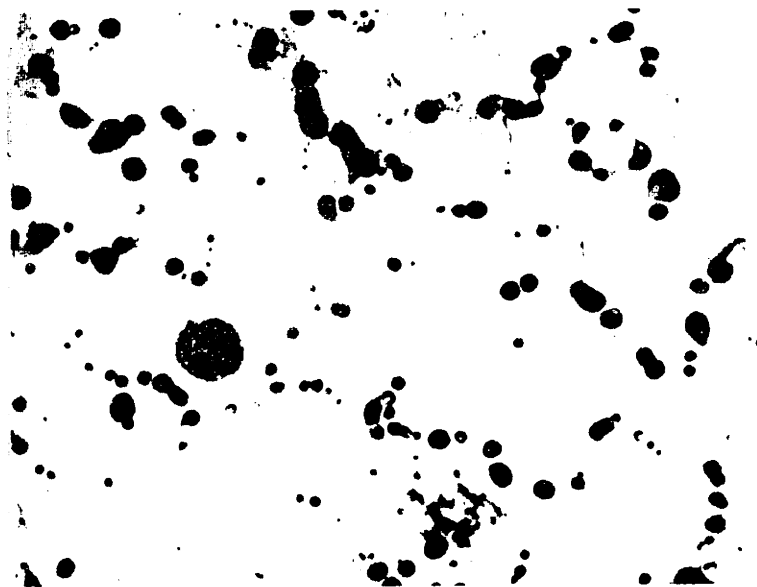


Figure 18B - Pellet, RF pressed in dry nitrogen and held for two days at 712C° (50x).

In the next method, in which extra precautions were taken to keep out water, reagent grade KCl was added in small amounts to the RF press over which pre purified, water-free nitrogen was flowing. The die was slowly brought up to 460C° while the quantities of powder were added over the course of two and one half hours. The nitrogen was then removed and the powder pressed at 440C° under a pressure of 2000 psi for two hours. The pressure was then released, and the temperature lowered in steps to reduce thermal shock. The pellets were much more transparent and took a much better polish. There was a slight amount of "fog" in local areas and the grains were of the order of several hundred micron with a few under one hundred micron.

The polishing procedure for the polycrystalline pellets and the bicrystals (to be mentioned in next sub section) was different.⁶³ After a grind on 600 mesh silicon carbide, the samples were ultra sonically cleaned in denatured alcohol for fifteen minutes. They were then water polished on a politex supreme cloth with a fifty percent ethanol-fifty percent distilled water solution followed by a rinse in a solution of twenty-five percent methanol, twenty-five percent distilled water and fifty percent ethanol. They were then dipped in pure ethanol, rinsed in anhydrous ether and air dried.

Etching⁶³ was also necessary to delineate the grain boundaries. The etchant was ten drops of a saturated solution of $ZnCl_2$ and glacial acetic for every twenty milliliters of pure glacial acetic, followed by a dip in pure acetic acid. They were then rinsed in ether and air dried. The time of etch varied from twenty seconds to two minutes and the etch was unheated.

A portion of this pellet was then placed in an oven at 712°C in air for two days to produce grain growth. The grains were in general larger than 1000 microns but still slightly "foggy." (See figure 18B.) The pores remained behind, some inside the grains and others at the boundaries. Some seemed to form the locus of an original boundary but, even with lengthy etching, no boundary was revealed.

Samples were cut from these pellets (about 5mm x 5mm and three millimeters thick) polished as described on page 63 and hot air dried.

D. Preparation of Bicrystals

1. Hot Wire Technique⁶⁴

As a first attempt at fabricating bicrystals, two well polished pieces of Harshaw crystal with differently oriented faces were mounted in a jig (figure 19) and lightly pressed together. The unit was heated to about 630°C in air (and in some cases dry nitrogen) and then current was passed through a platinum-ten percent rhodium wire. This wire was wrapped around the junction of the two crystals and extended out through the bottom of the oven.

To one end of the wire was mounted weights ranging (from run to run) from 200 grams to 300 grams. As the wire became hot, it moved through the junction. After passing through, the crystal was held at 650°C for about a day or more and then slowly cooled down. Several of these crystals broke at the grain boundaries. Others had regions of high porosity.

On the whole, the grain boundaries produced in this fashion exhibited very large amounts of light scattering when viewed in a

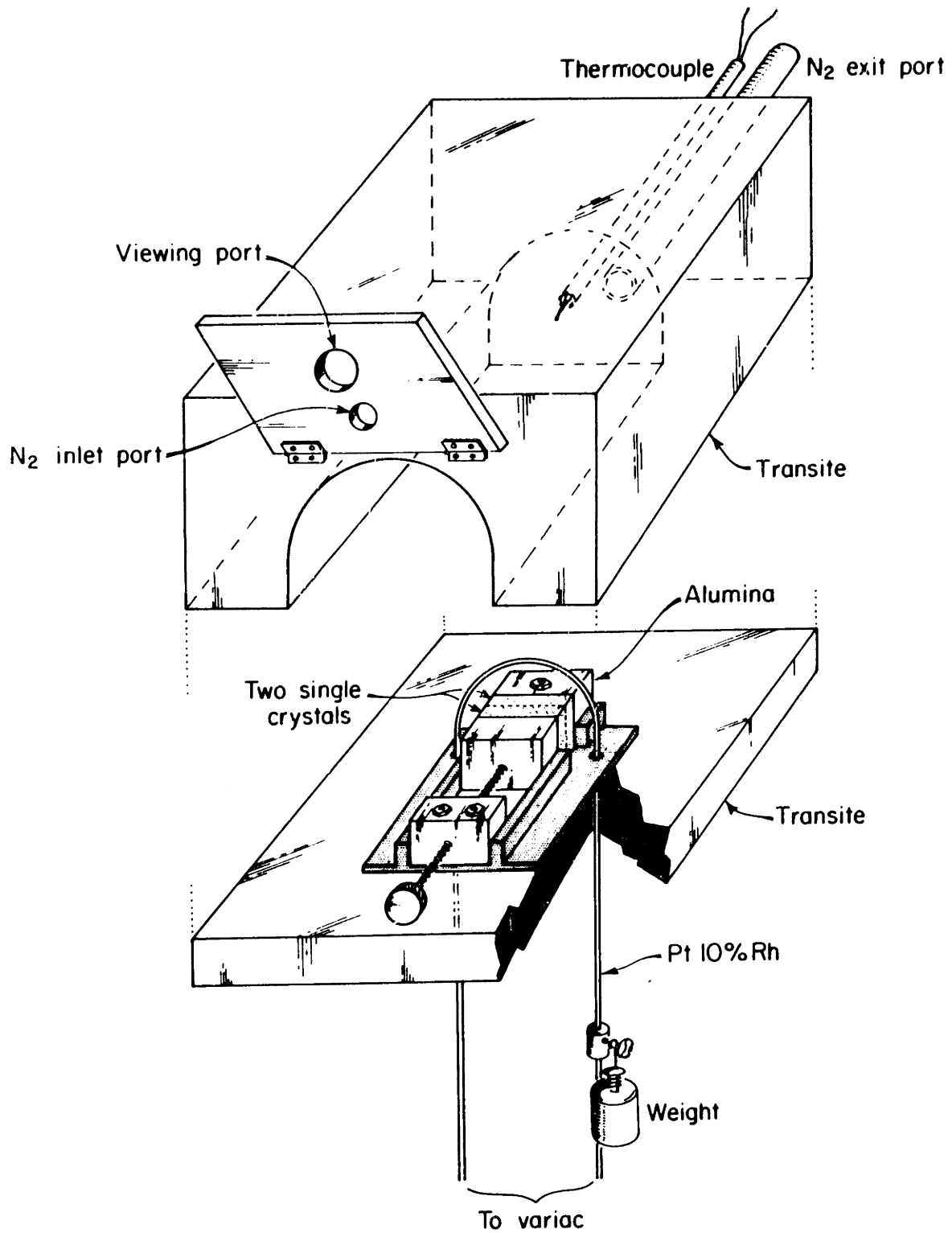


Figure 19 - Apparatus for fabricating bicrystals.

direction orthogonal to a parallel beam (less than a millimeter in diameter) of light passing parallel to the plane of the boundary.

2. Pressure Sintered Technique

As a second effort, two Harshaw crystals were cut along different crystallographic planes and highly polished. In order to form these bicrystals under water free conditions (since water has been associated with the preferential diffusion in alkali halides) one piece was put in an oven at about 300C° while the other piece was put in the die of the RF press. Prepurified, water-free nitrogen was flowed through a dessicator into the die close to the face of the crystal. The die was then brought up to 300C° to 350C° , and held there for one to three hours. At this point the piece from the other oven was quickly put in. The two were gently held by way of a long vycor rod, and two hundred mesh alumina (no pretreatment) was put around them and over them. The assembly was allowed to remain at 350C° for about one half to one hour. Then the nitrogen was stopped and the press activated to anywhere from 1500 psi to 2500 psi. The temperature was then brought up to about 450C° and held there for times that varied from three to five hours. The pressure was then released and the temperature lowered in discrete steps (to minimize thermal shock) for from forty-five to ninety minutes.

All the bicrystals formed in this way were ground, to remove surface regions, polished, and then put in a vycor tube (precleaned and torched to red heat) in a temperature controlled oven. The oven temperature was brought up to 670C° while the atmosphere in the tube was kept evacuated by a rough pump. The samples were maintained at this temperature for one and one half hours. The vacuum valve was then closed and

the system allowed to remain at 670C° for twenty hours. It was then controlled-cooled at 10C° per hour to less than 100C° .

The grain boundaries in some of the bicrystals had migrated to one side of the specimen. Others developed either polycrystallinity or heavy mosaic structure on one or both sides of the grain boundary.

Still others had grain boundaries that were normal to the surface near the surfaces of the bicrystal but broke up in the interior. Figure 20A shows some sketches of these irregular bicrystals.

The sections displaying straight grain boundaries, free from pores, were used for diffusion studies. A few bicrystals had grain boundaries so perfect that they were very difficult to observe even after lengthy etching and polishing procedures. They could be observed more easily by transmission optics due to a few infinitesimal pores in the boundaries. In general, the grain boundaries exhibited very few pores and there were, even in the worst cases, very large regions of planar, pore-free grain boundary (figures 20B and 20C). These crystals were cut and polished similar to the polycrystalline samples.

3 Kyropoulos Technique

Bicrystals were also pulled from the melt using the Kyropoulos technique (figure 21). The potassium chloride powder to be used was put in a vycor crucible, 75 millimeters in diameter and fourteen inches long, and placed in an oven at 300C° overnight. The first seeds to be employed consisted of two Harshaw single crystals of random crystallographic orientation twenty millimeters long and six millimeters by six millimeters in cross-section. They were polished and wrapped tightly together with platinum wire (figure 22). The system was evacuated and flushed with

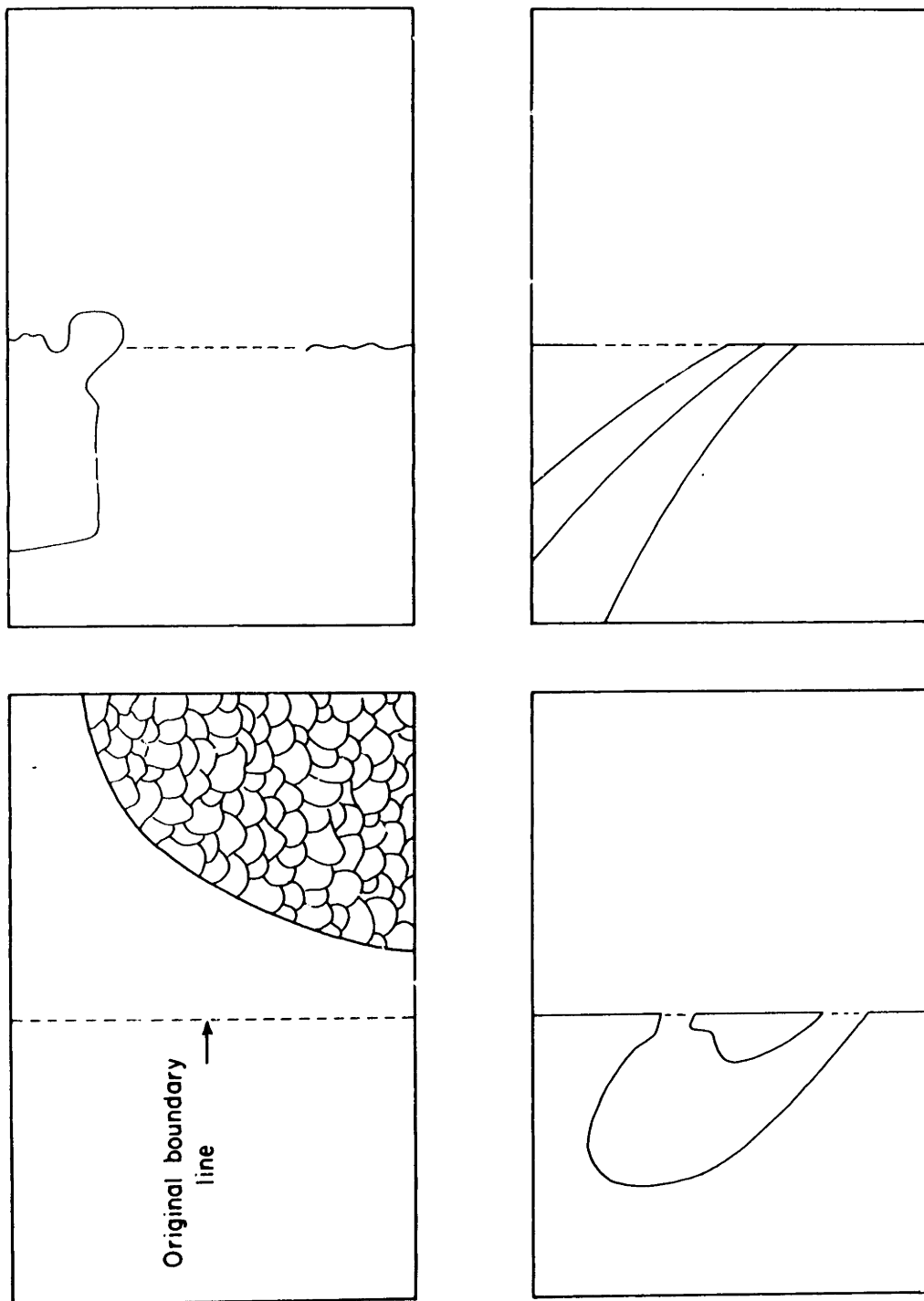


Figure 20A - Four sketches of the appearance of anomalous grain boundaries in pressure sintered bicrystals.



Figure 20B - Grain boundary in a pressure sintered bicrystal (B-7).

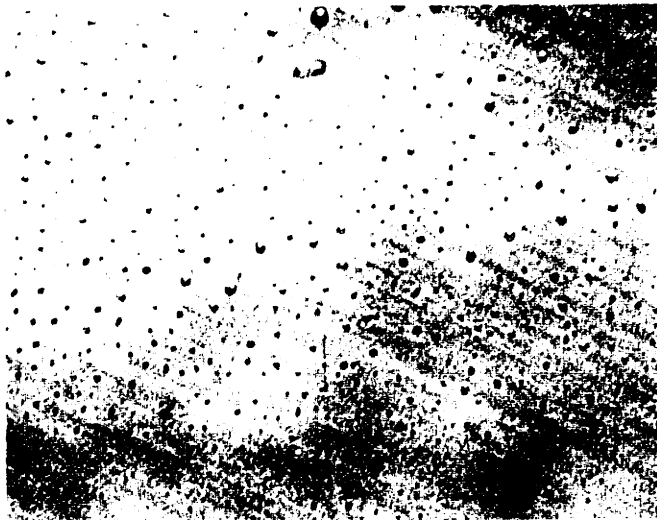


Figure 20C - Grain boundary in a pressure sintered bicrystal (B-8).

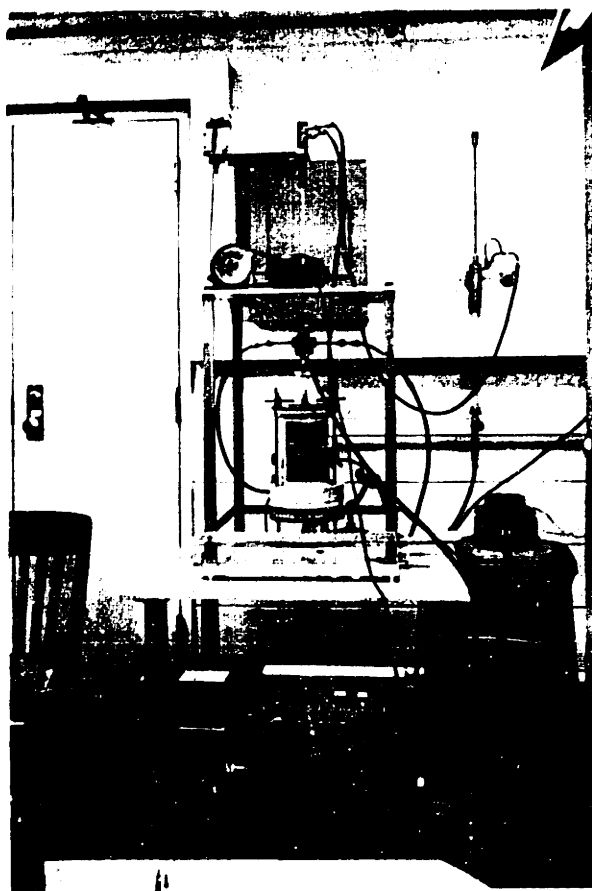


Figure 21 - Kyropoulos oven and crystal pulling apparatus.

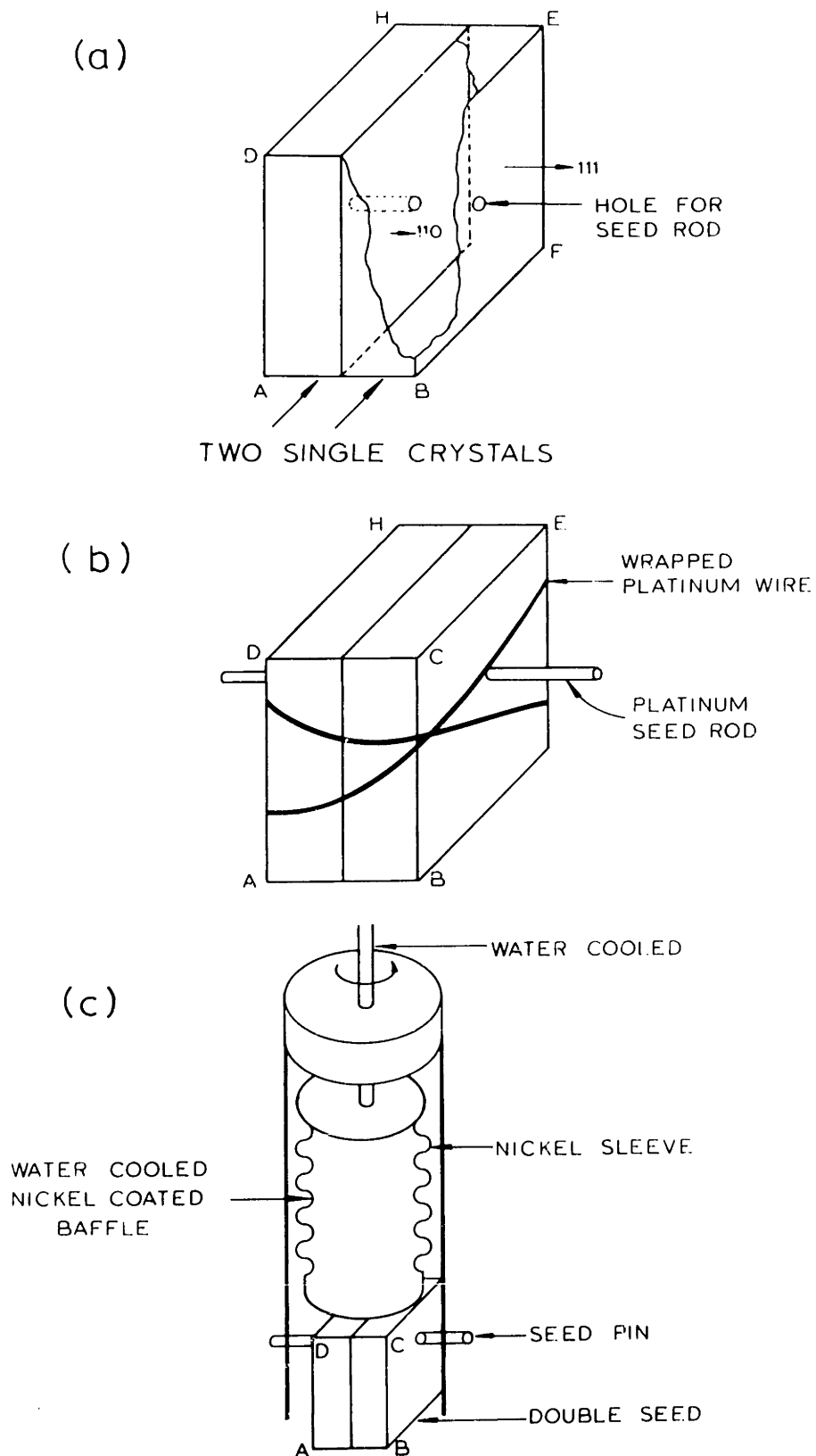


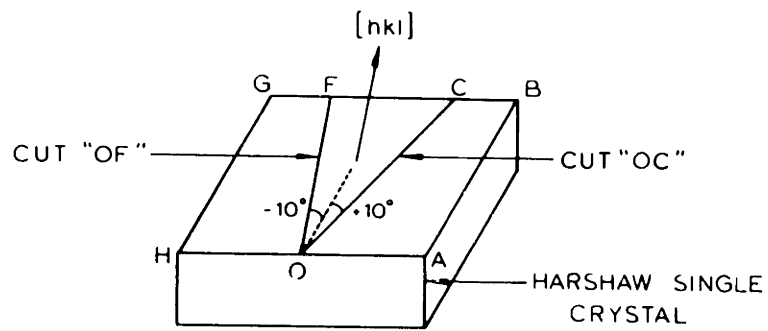
Figure 22 - Preparation steps for pulling a bicrystal from the melt.

nitrogen five times and then a steady (very slow) flow of nitrogen was maintained for the crystal pulling.

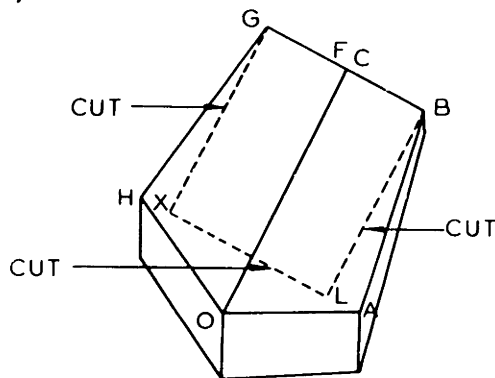
Pulling rates varied from three to five millimeters per hour and the double seed was continuously rotated. Steady state cooling rates of $4\text{C}^\circ/\text{hour}$ to $6\text{C}^\circ/\text{hour}$ were used until a sufficient boule developed. The boule was then pulled from the melt and the cooling rate increased to $10\text{C}^\circ/\text{hour}$ down to 100C° .

The grain boundaries did not remain normal to the growth interface but quickly curved and passed out of the boule. Only in one case was there sufficient grain boundary to obtain several samples, but in this case, the relative orientation of the grains was not the same from sample to sample. The remaining Kyropoulos bicrystals were prepared with the use of "symmetrical tilt seeds" (see figure 23). These were seeds whose adjacent faces (faces in contact in figure 22A) were related to each other by a rotation of plus or minus a certain angle from the (100) face. In general these yielded bicrystals with more useable grain boundaries but, even in this procedure, the boundaries were continuously curved and ultimately grew out of the boule (figure 24). There was really no way of cutting samples from these batches (all cuttings of bicrystals were done with a string saw with a 5 mil steel wire) with grain boundaries that remained perpendicular to the face to be exposed to the thallium vapor. In general, with careful cutting, the grain boundary was within a few degrees of being perpendicular to the exposed faces.

(a)



(b)



(c)

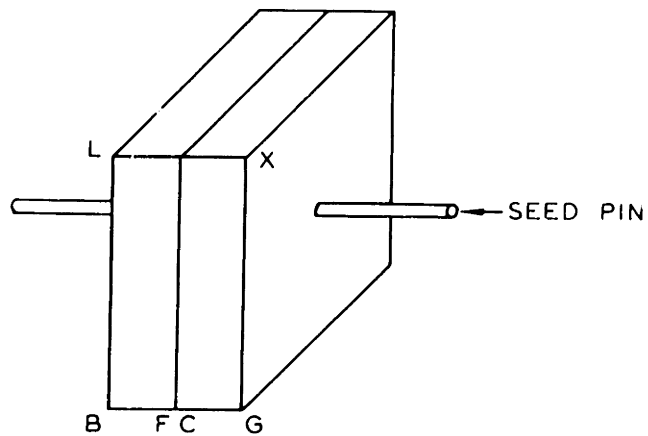


Figure 23 - Preparation steps for pulling a bicrystal with "symmetrical tilt seeds" $\pm 10^\circ$ about the (100).

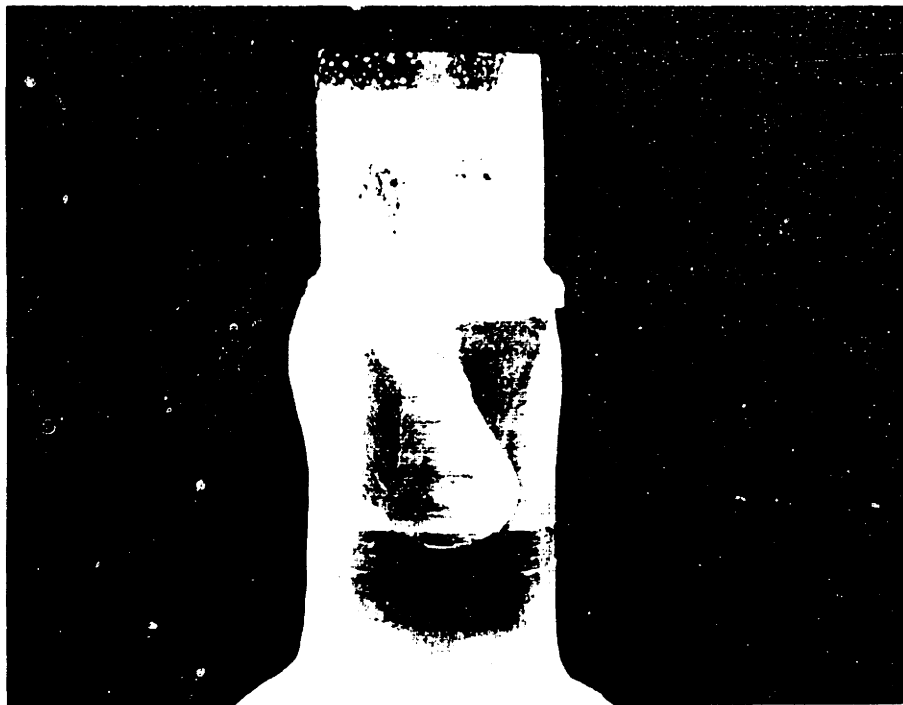


Figure 24 - Typical bicrystal boule grown with a symmetrical seed.

4. Harshaw Bicrystals

Some of the scrap pieces ("optical grade") obtained from Harshaw had grain boundaries that occurred during growth. Upon polishing and etching, these grain boundaries were found to be free of pores along their entire length with no mosaic and/or recrystallization in either grain. It was possible to cut samples from these crystals with the string saw, such that grain boundaries were very close to being orthogonal to two external faces.

5. Harshaw Mosaics

The complete batch of samples from Harshaw had heavy mosaic structure (as explained in section VII.B.). These were also used in the grain boundary diffusion studies.

6. Polycrystalline Pieces from the Melt in the Kyropoulos Oven

The solidified melts had polycrystalline sections of millimeter grain size. These were also cut to size and polished for diffusion runs.

E. Diffusion Annealings

1. Polycrystalline Specimens and Single-Crystal Specimens

a. Vapor Exchange Couples

Vycor crucibles were used to hold the thallium chloride powder. These were inserted into holes drilled in small pieces of firebrick (figure 25). A platinum ten percent rhodium thermocouple was held firmly against the sample; the steatite casing being ground so that it could be firmly held to the firebrick and against the sample by means of a chromel alumel wire.

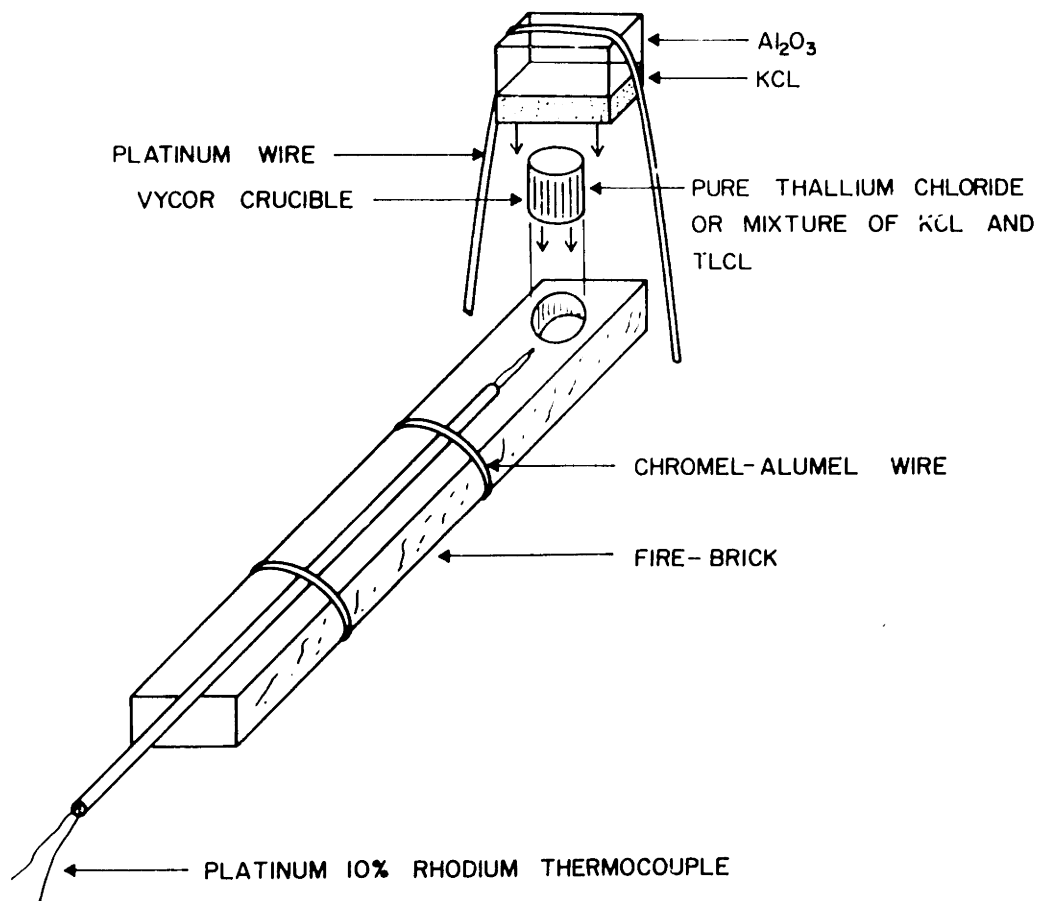


Figure 25 - Apparatus for a typical vapor exchange couple diffusion anneal.

The diffusion annealings were performed in twenty-four inch long, one and one half to two inch diameter mullite tubing ovens with controllers (figure 26). Firebrick "stops" were inserted so that the samples were inserted the same distance in each run. The controllers kept temperature fluctuation within \pm two degrees. There was no time delay in either insertion of the samples or in their removal. "Time zero" was measured as thirty minutes from the time of "insertion" for the entire temperature range, since the thermocouples indicated temperatures within four percent of the equilibrium temperature as early as twenty minutes from "insertion." Diffusion times were long enough to neglect the amount of thallium chloride diffusion during the warm up period. At diffusion anneal temperatures above 680C° , a mixture of thallium chloride and potassium chloride were used in the vycor crucible to prevent sample loss by melting.

b. Thin Film Couples

The samples on which thin films of TlCl had been evaporated were sandwiched between two pieces of potassium chloride and wrapped with platinum wire. They were then placed inside a vycor tube, opened at one end and sealed off at the other, and firmly held against a "stop" (section where the tubing was tapered to a small neck) by means of a platinum ten percent rhodium thermocouple (figure 27). The sealed end contained pure thallium chloride powder.

2. Bicrystals

All the bicrystals were set up as vapor exchange couples. They were allowed to remain in an oven at about 250C° for one half an hour before being loaded into a prefired vycor tubing. This tubing (figure 28) was sealed at one end. Pure thallium chloride or a mixture

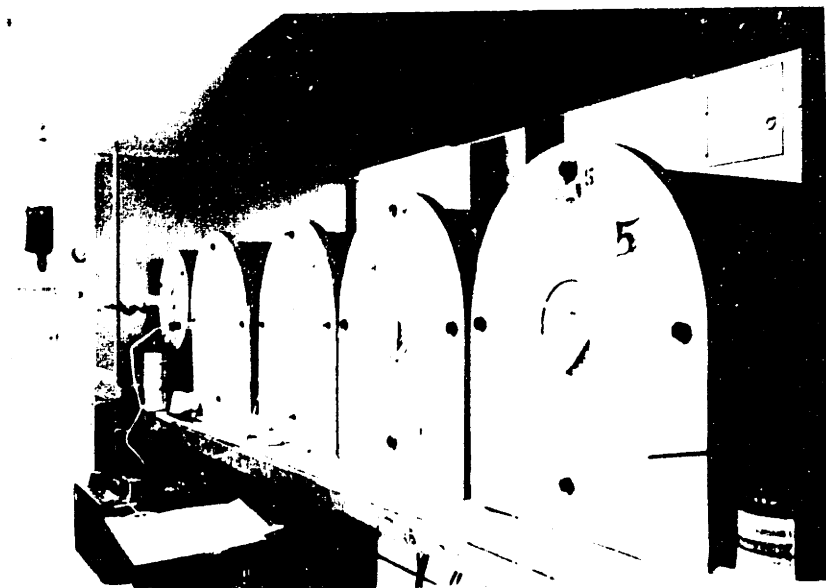


Figure 26 - Temperature controlled ovens used for the diffusion anneals.

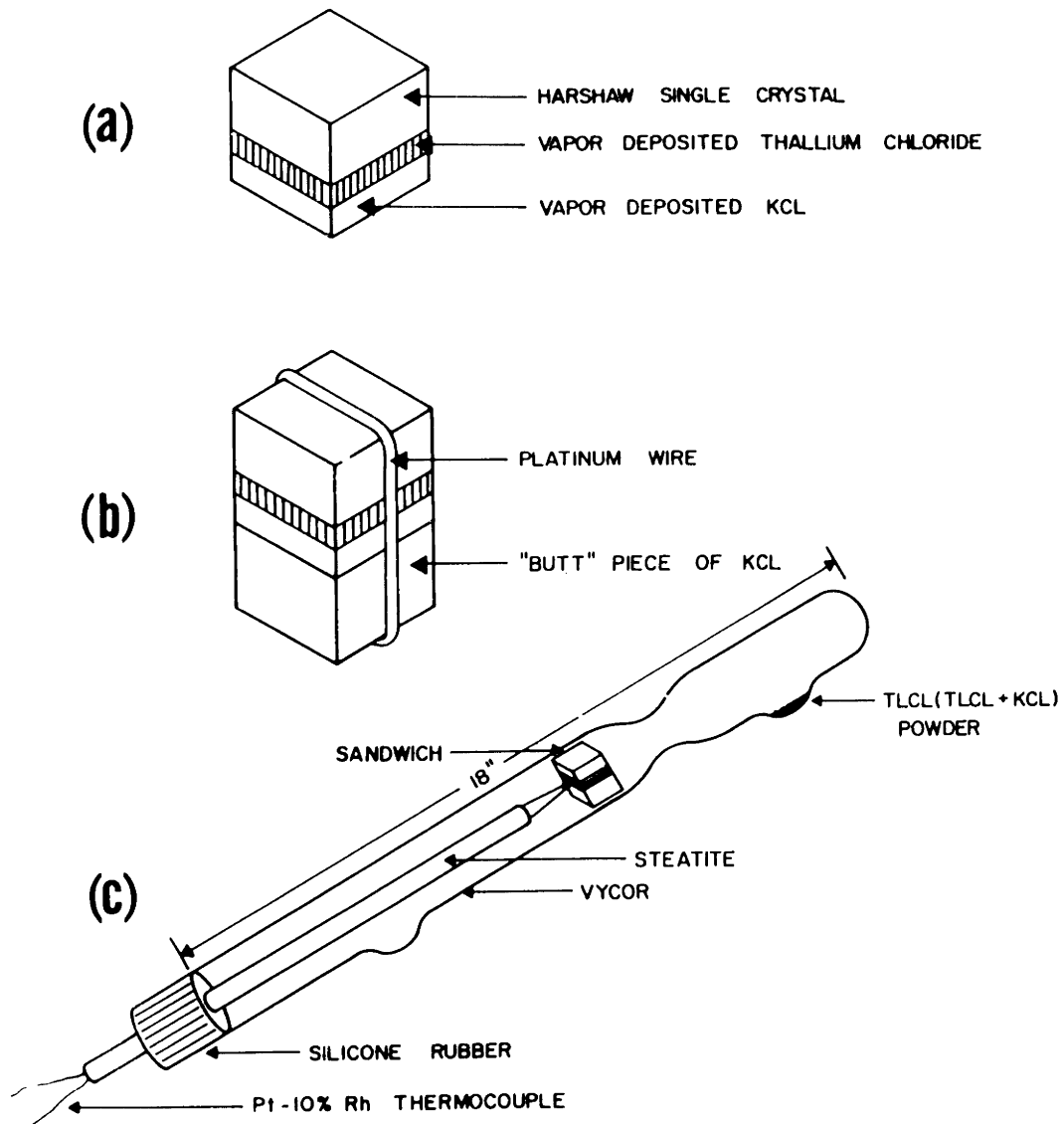


Figure 27 - a, b: Preparing a KCl single crystal for a "sandwich couple".
 c: Preparing a diffusion anneal with the sandwich couple.

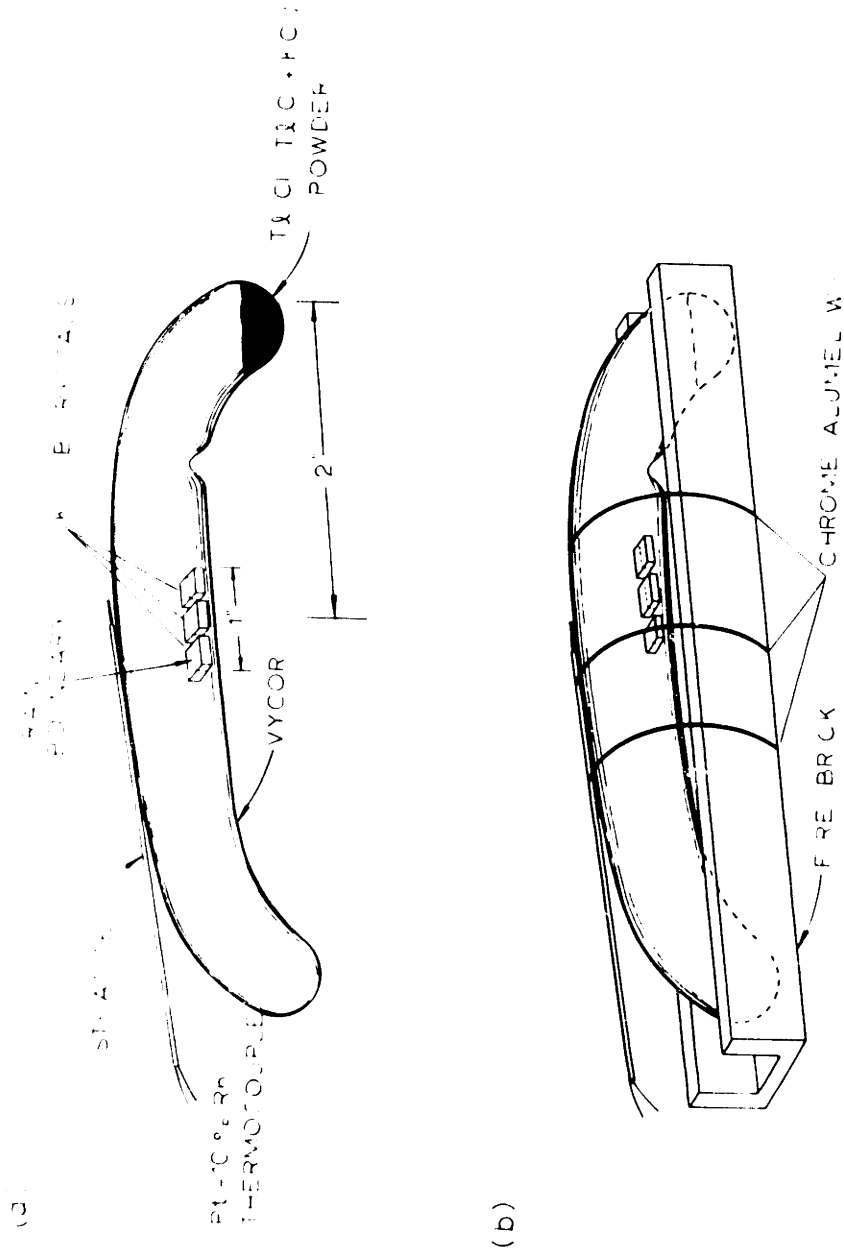


Figure 28 - Apparatus for a bicrystal diffusion anneal.

of thallium chloride and potassium chloride was placed at this end. Several samples were loaded at one time but their dimensions were such that they never spanned more than one inch lengthwise along the length of the tubing. The tube was quickly sealed off, inserted in a firebrick, mounted with a thermocouple, and placed in the oven.

F Preparation for Analysis

1. Standards

Standards were carbon coated in an atmosphere evacuated to $1-3 \times 10^{-5}$ torr. The source to sample distance was about six inches. The purpose of the coatings, employed for all diffusion samples that were analyzed with the electron probe, was to provide a conducting path for the current of the incident electron beam, thus preventing charge build up.

2. Single Crystals and Polycrystals

When the diffusion runs were completed, the samples were cut with a string saw along a direction perpendicular to the face exposed to the thallium chloride. The specimen was then sandwiched between two extraneous pieces of potassium chloride (to prevent rounding off at the edges of the diffusion sample) and set in bakelite (figure 29). Bakelite was preferred over the cold setting plastics because of its lower outgassing rate during bombardment with the electron beam of the probe.

The bakelite and sample were then ground on 360 mesh and 600 mesh silicon carbide and polished with 0.05 micron alumina. As a final polish, the sample was lightly brushed on a politex cloth embedded with a very dilute alcohol-0.05 alumina solution. The sample was then rinsed in anhydrous ether and hot air dried. It was then carbon coated.

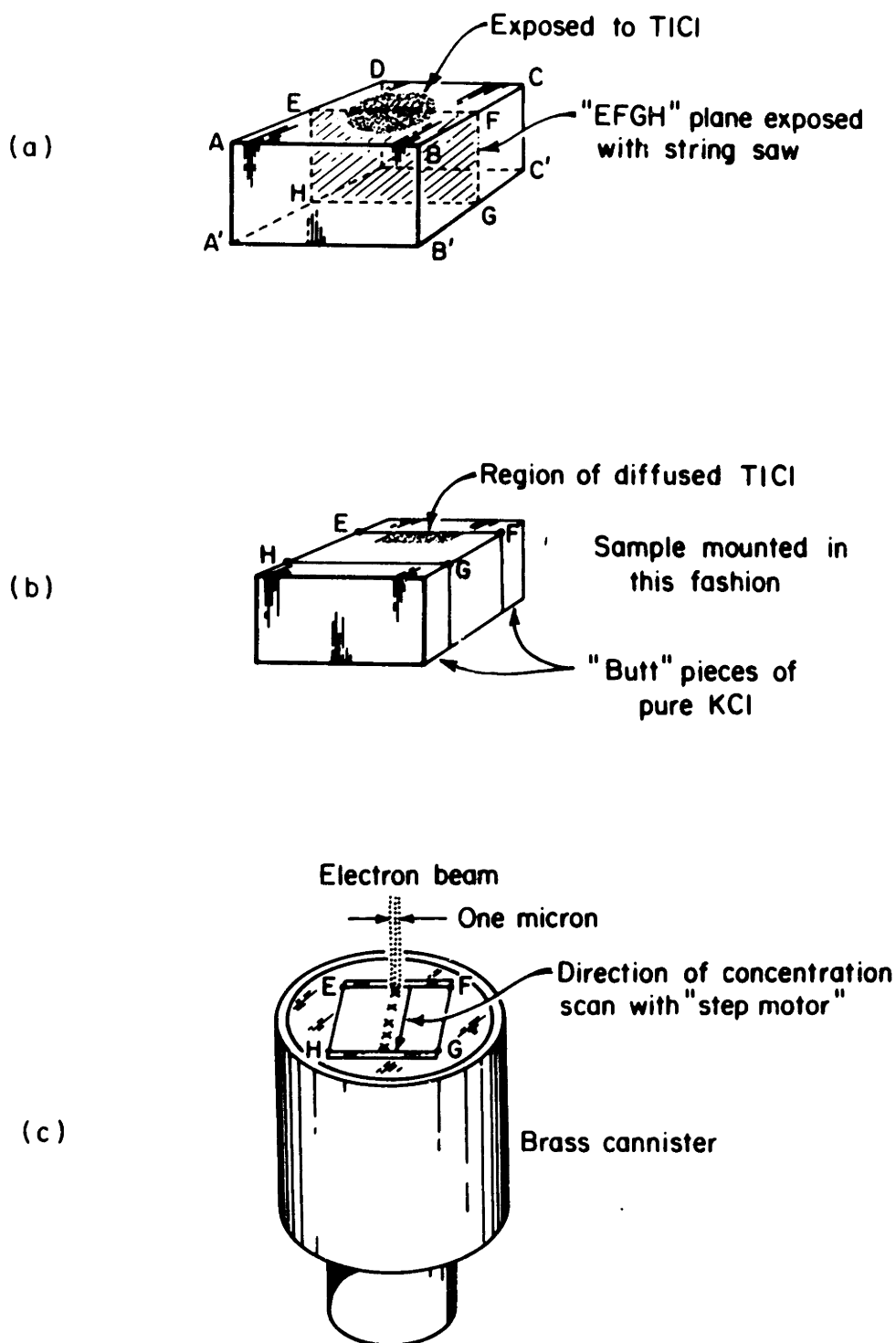


Figure 29 - Preparing a sample subjected to a diffusion anneal for the electron probe.
 a - cutting procedure, b - mounting procedure,
 c - scanning technique.

3. Bicrystals

The bicrystals could not be removed from the diffusion ovens as fast as the single crystals because of the mechanical stresses introduced with the large thallium atoms in the grain boundaries. Some of the Harshaw and Kyropoulos bicrystals broke due to this fact. Because of this, fifteen to thirty minutes were allowed for taking these samples out of the ovens. Also, it was beneficial to use potassium chloride with the thallium chloride (as a source material) from 640C° to 700C°.

The bicrystals were analyzed with the electron probe on two orthogonal planes, each of which was normal to the grain boundary. The cutting and mounting procedure is indicated in figure 30. Probe analysis was first carried out on the face in 30B and then (after recutting and recoating with carbon) on the face in 30C.

G. Analysis of Concentration - The Electron Micro-Probe

An Applied Research Laboratories (Glendale, California) electron probe microanalyzer was used to detect the thallium chloride. Basically (see figures 31 and 32), the probe is an instrument which accelerates electrons from a hot filament toward the sample to be investigated. There are two main lenses. The one closest to the filament, called the condenser lens, collects the electrons diverging from the filament and focuses them on the image plane of a second lens. This lens, called the objective lens, causes further demagnification. The condenser lens controls the intensity of the electron beam hitting the sample, while the objective lens controls the beam diameter on the sample. The minimum spot size is determined not only by the objective lens setting but also by the condenser lens setting. The lower limit is about one micron.

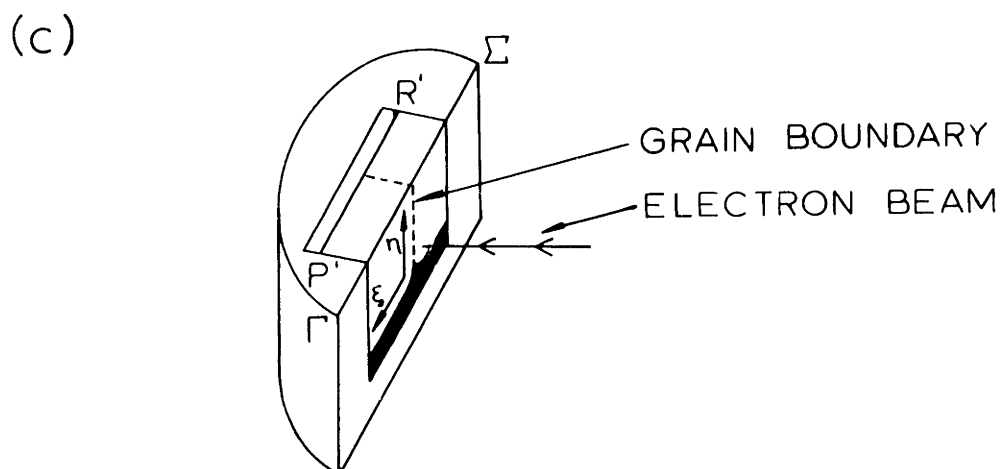
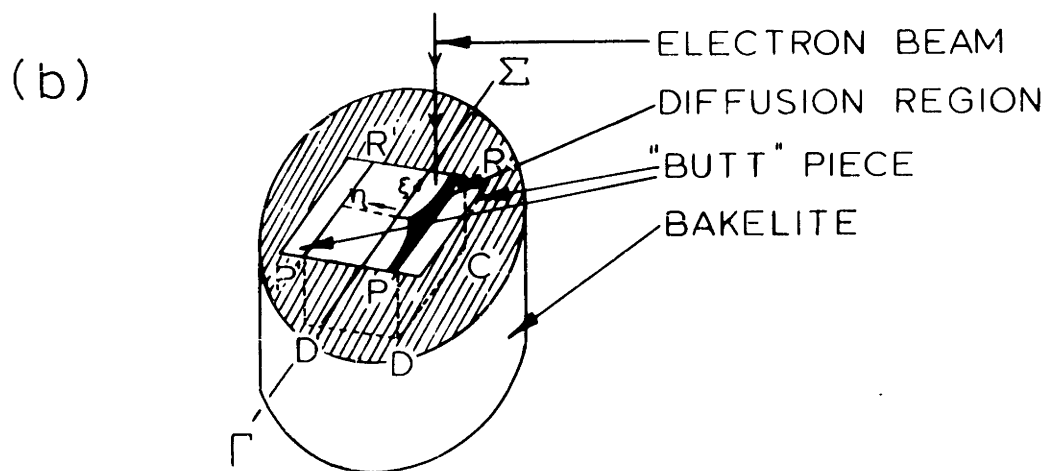
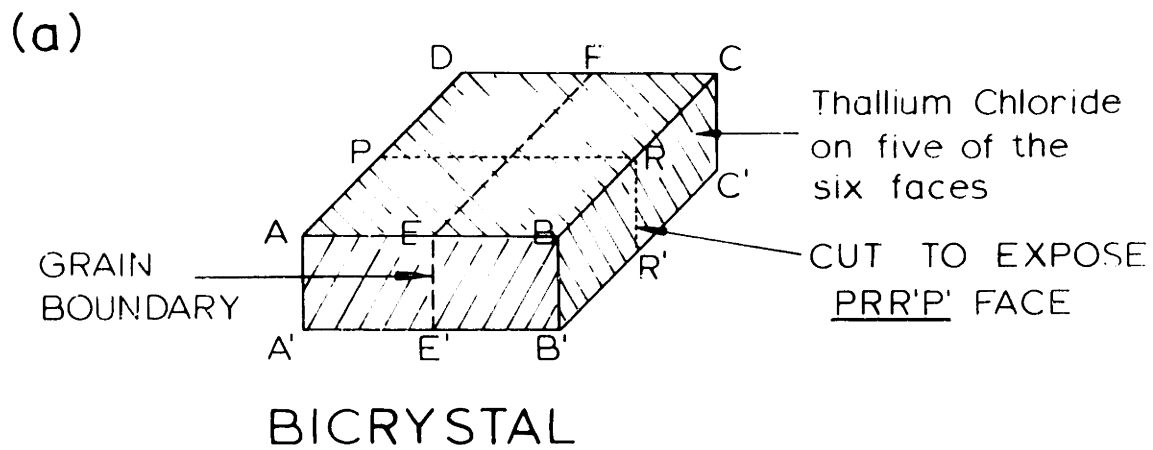


Figure 30 - Illustration of how two orthogonal planes containing the grain boundary are analyzed with the electron probe for thallium. (a) cutting procedure for exposing one plane containing the grain boundary. (b) scanning of this plane. (c) cutting and scanning technique for the plane orthogonal to the first plane.

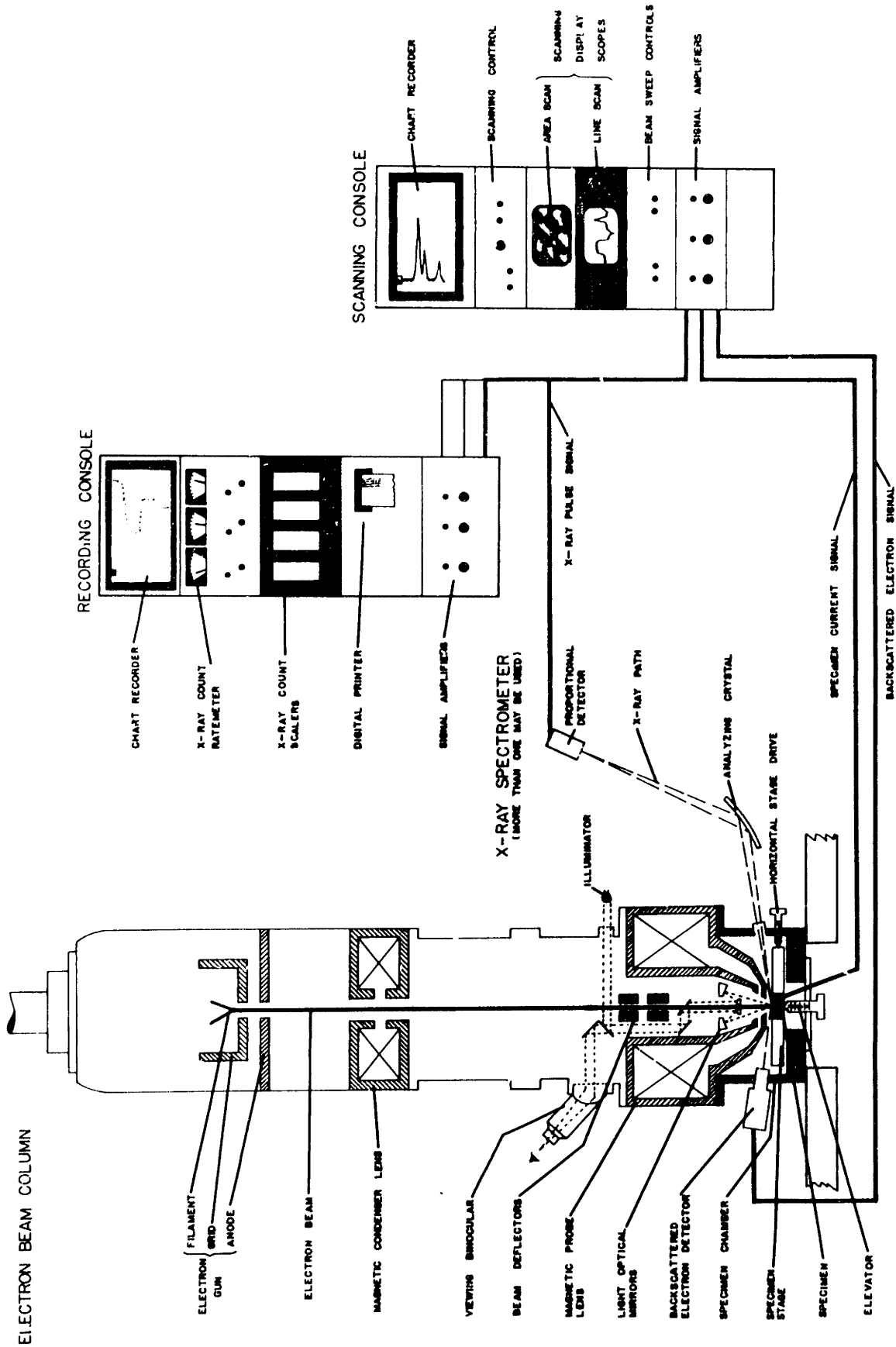
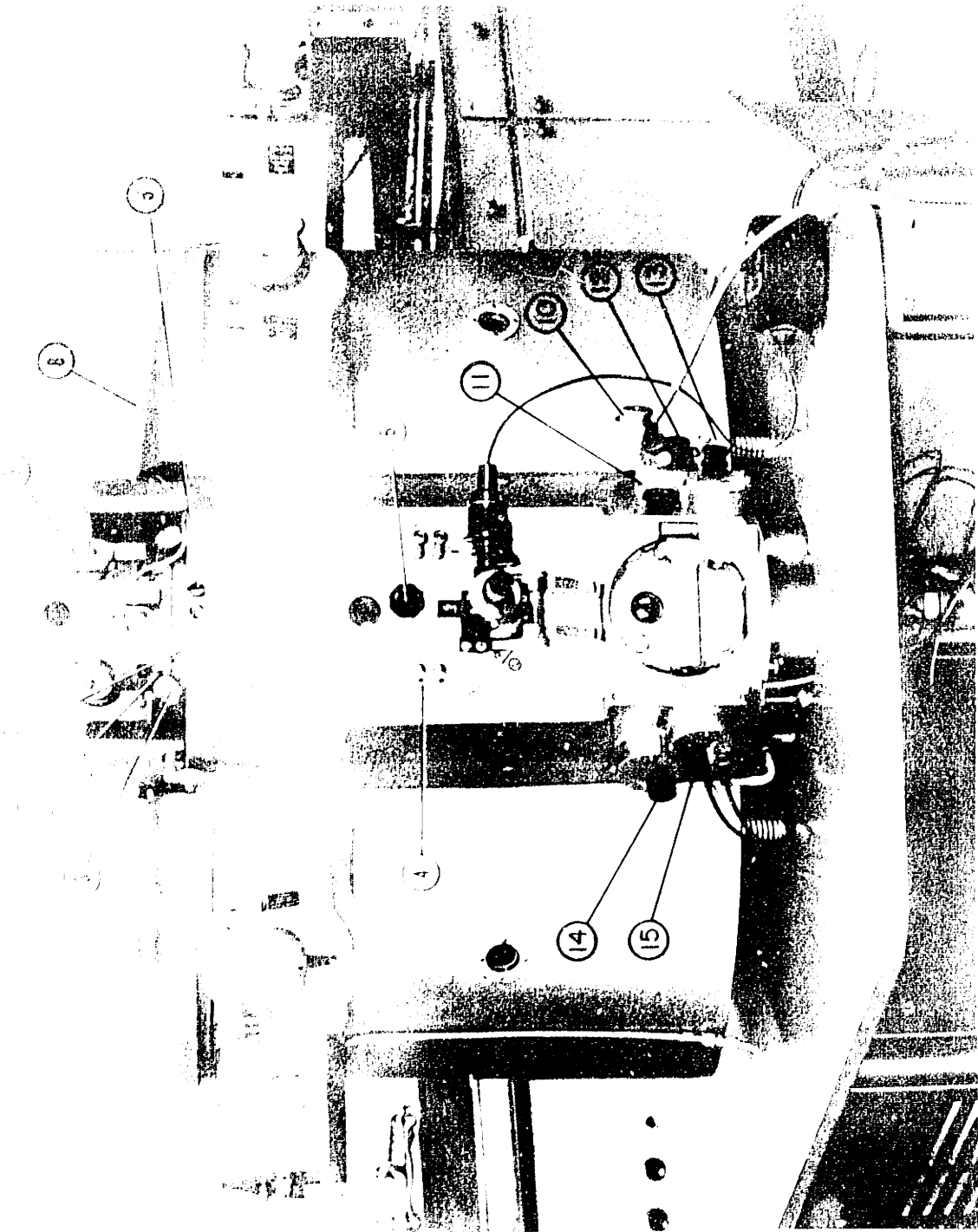


Figure 31 - Schematic diagram of the essential parts of the electron probe microanalyzer.



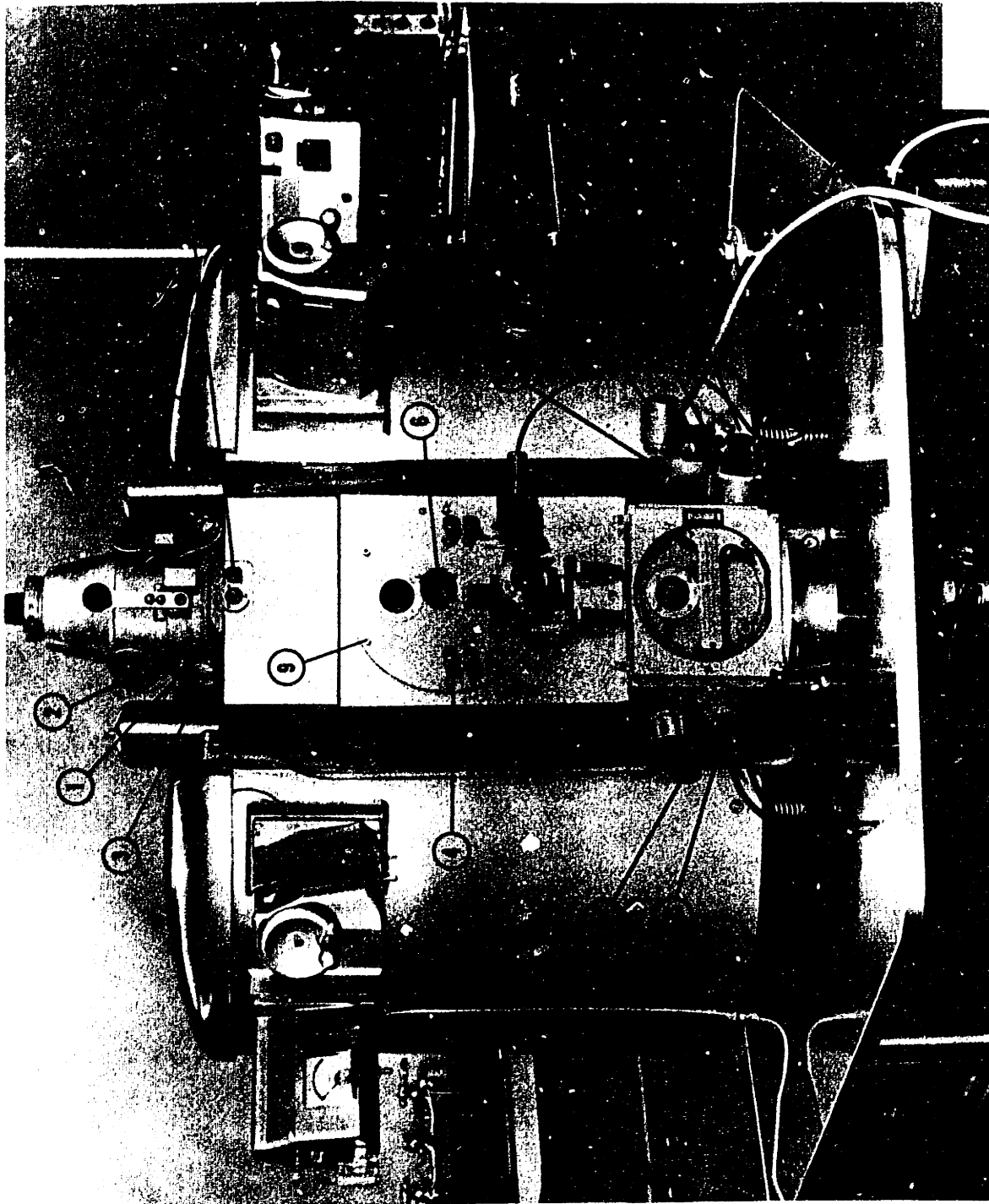


Figure 32A - Picture of probe main assembly.

INTENTIONAL DUPLICATE EXPOSURE

1. Not required
2. Electron gun translation
3. Gun and condenser translation
4. Aperture translation
5. Fluorescent screen - beam stop
6. Fluorescent screen - lower stop
7. Filament translator
8. Cover
9. Plate of optical assembly
10. Step scanning mount - steps in one to ten micron increments depending on setting
11. "Lazy susan" (multiple sample holder) rotator
12. X drive
13. Individual sample rotation
14. Elevator (for optical focusing)
15. Y drive

Figure 32B - Explanation of the essential parts on the main assembly.

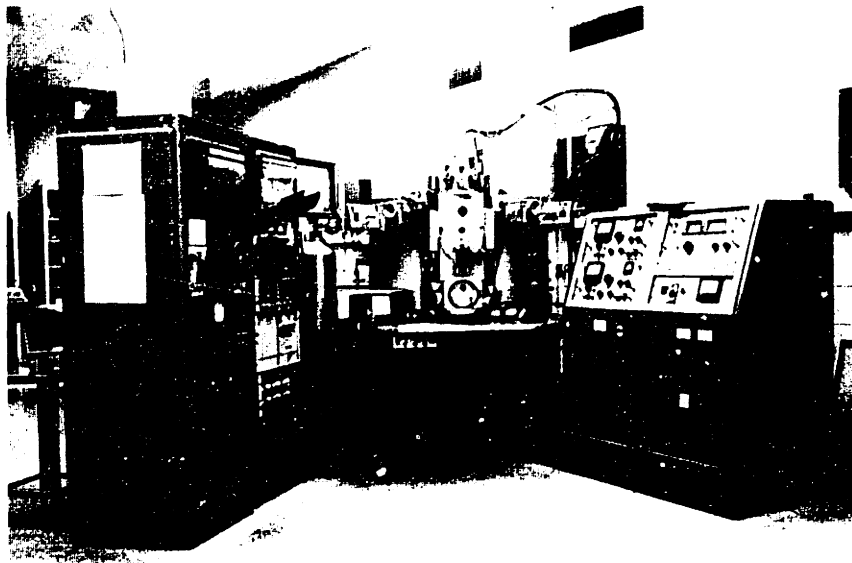
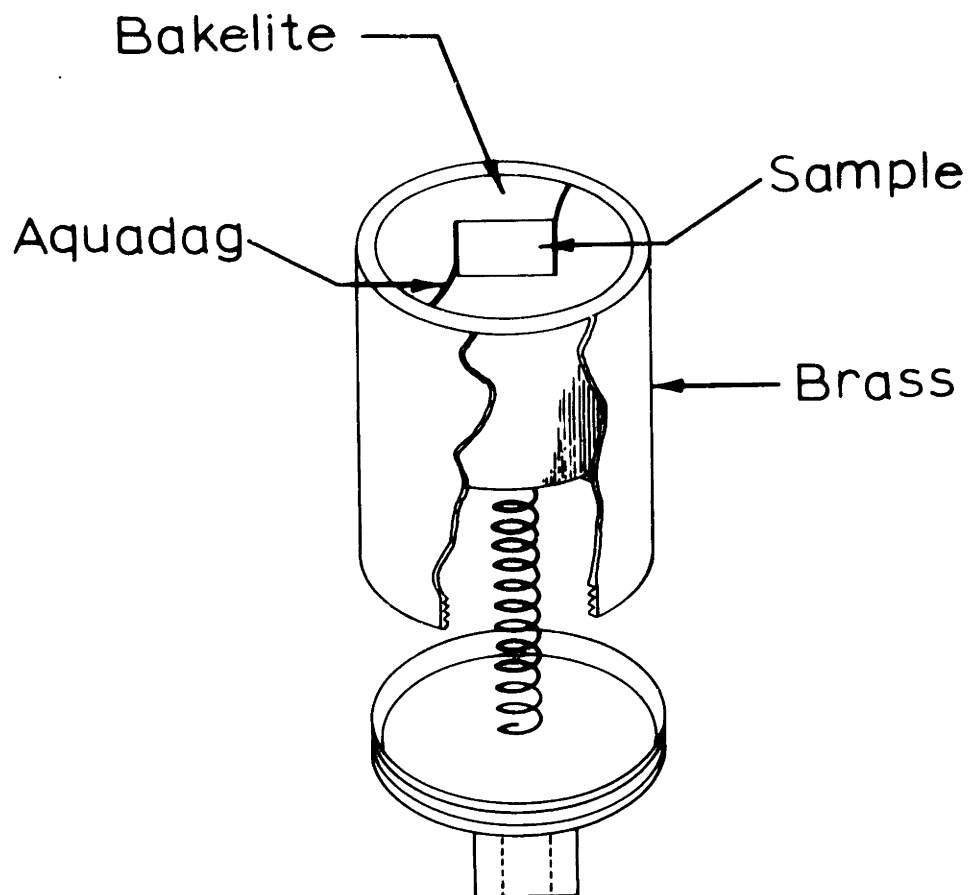


Figure 33 - Complete electron probe microanalyzer assembly.

These electrons excite the characteristic wavelengths of all the elements present whose thresholds lie below the accelerating voltage of the instrument. The X-rays then leave the sample and are Bragg reflected from a single crystal into a gas proportional counter (90 percent argon, 10 percent methane). The angle that the sample-to-detector-crystal axis makes with the plane of the sample is called the "take off" angle and is 52 1/2 degrees for the ARL probe. The pulses coming from the proportional counter are counted electronically. The time over which a count is to be taken depends on how small one wants to keep the fractional statistical variation $\frac{1}{\sqrt{N}}$, where N equals the total number of counts. The counting times in these experiments varied from forty seconds to two hundred seconds depending on the amount of thallium diffused into the crystal. Since a large number of counts have to be taken for volume diffusion runs and still more for grain boundary studies, a compromise had to be made between obtaining a significant concentration profile in a reasonable amount of time and minimizing fluctuation in count through long counting times. A large fraction of the experimental data was obtained with forty to fifty second counts.

The probe sample holder resembled a "lazy susan." It could accommodate eight one inch diameter brass cannisters (figure 34). Each one may be separately lifted from the lazy susan and brought into the electron beam. Once the sample has been lifted from the lazy susan, it may be brought into optical focus. By means of three external controls, it may be rotated about the axis of the cannister lifter rod, and driven in two mutually orthogonal directions (called the X and Y drive) in the focal plane by two external verniers calibrated in microns.

(A)



(B)

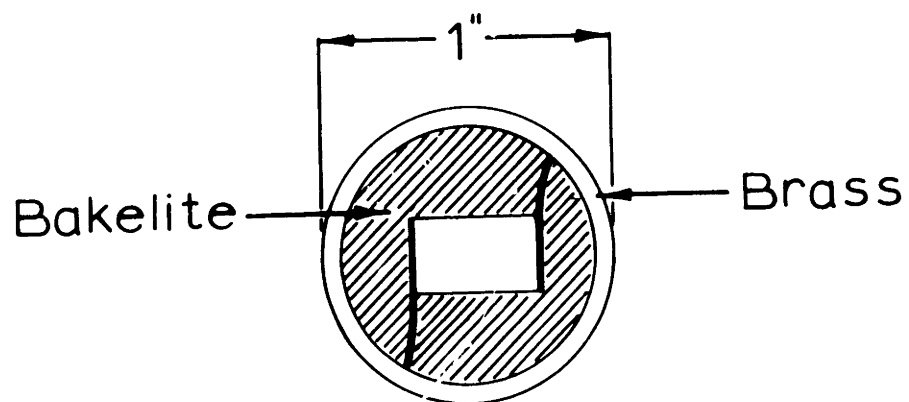


Figure 34 - (A) Side view of a brass cannister that holds sample mounted in bakelite and fits into the "lazy susan" in the probe. (B) Top view.

An essential requirement for reproducibility of counts at a given point on the sample is that the optical focus be at the same position as the electron beam focus. For this work, because potassium chloride fluoresces readily in the thirty kilovolt beam, the coincidence of the two focal planes was adjusted with the sample to be investigated and could be monitored continuously. However, as will be pointed out later, a very slight change in the focus of the sample can produce changes in counts that exceed any statistical fluctuations in the counting.

In order to scan the characteristic wavelengths of a wide range of elements and thus make the probe of significant practical value, three single crystals are mounted in the vacuum system, all intercepting the same take off angle, of fifty-two and one half degrees with respect to the sample face.

A quartz crystal covers the elements from silicon to rubidium. A lithium fluoride crystals covers the elements from potassium to indium, and an ammonium dihydrogen phosphate (ADP) crystal covers the range from magnesium to arsenic.

A probe similar in design to the ARL probe and constructed at MIT uses an epitaxially deposited lead stearate film on mica which allows the analysis of anions such as chlorine and oxygen. This will be referred to in section X.

These crystals can be rotated externally to bring them into the proper Bragg angle for the element to be analyzed. The rotation drive could be read directly to $\pm 0.0002^\circ$.

Thirty kilovolt electrons were used for this work, as this was the upper limit from a standpoint of stability of high voltage supply, exciting the K fluorescence (3.742 angstroms) of potassium and the L fluorescence of thallium (1.207 angstroms). The ADP crystal was used to detect potassium and the lithium fluoride was used for the thallium. Both crystals have their K and L edges well removed from these wavelengths. The continuum radiation peaks in the wavelength region centered around 1.207 angstroms (the actual position of this peak is hard to uniquely define because it will vary depending on the amount of thallium chloride and potassium chloride present in the sample) and so the signal to background ratio - ratio of the count from thallium chloride with the lithium fluoride crystal at the Bragg angle, to the count with the crystal suitably removed from the Bragg angle - was small, ranging from twenty-six to thirty-three.

Diffusion runs were done by incorporating a "step motor" which could step the X or Y drive in intervals ranging from one to ten microns depending on its setting. The counting electronics was so integrated with the step motor that discrete counts for a fixed time interval could be taken every one, two, three or more microns throughout the sample.

1. Standards

The standards were analyzed with the objective lens defocused in order to obtain a beams diameter that was large compared to the average grain size in the standards. Even with a spot size of one hundred and forty microns, however, the count varied considerably across the sample face. To improve this situation, an attempt was made at making a finer, more uniform powder mixture for the standards.

The powders from which the standards were made were separately stored overnight in a dry box in which was mounted an ultra sonically cleaned (motor operated) mortar and pestil. It was imperative to eliminate all moisture from this operation so that the reground powders would properly mix without sticking to container walls. Hence the reason for operating in a dry box. These powders were then ground for one half an hour and put in jars containing ultra sonically cleaned and outgassed porcelain balls. This jar was well sealed with electrical tape and put in a larger jar containing drierite. It was then completely surrounded by drierite, the top put on the larger jar, and the cap sealed with electrical tape. These were then taken out of the dry box and rolled from forty to forty-eight hours. The powders were pressed as before and polished

These standards were much more uniform and gave good translational uniformity with an eighty micron spot size (see figure 35).

Counts on the standards were taken at fifteen to thirty-five different positions and averaged. Counts were also taken on pure thallium chloride and pure potassium chloride with the lithium fluoride crystal set for bragg reflection of the thallium L line, and with the crystal turned off the L line (background). Counts were also taken on all the standards with the crystal turned off the "L" line. The difference between a count with the crystal placed at the "L" line and with the crystal placed off the "L" line was called a corrected count or $I_{\text{corrected}}$.

The ratio (labelled I_c in figure 36) of these latter counts to the corrected count for pure thallium chloride, when plotted as a func-

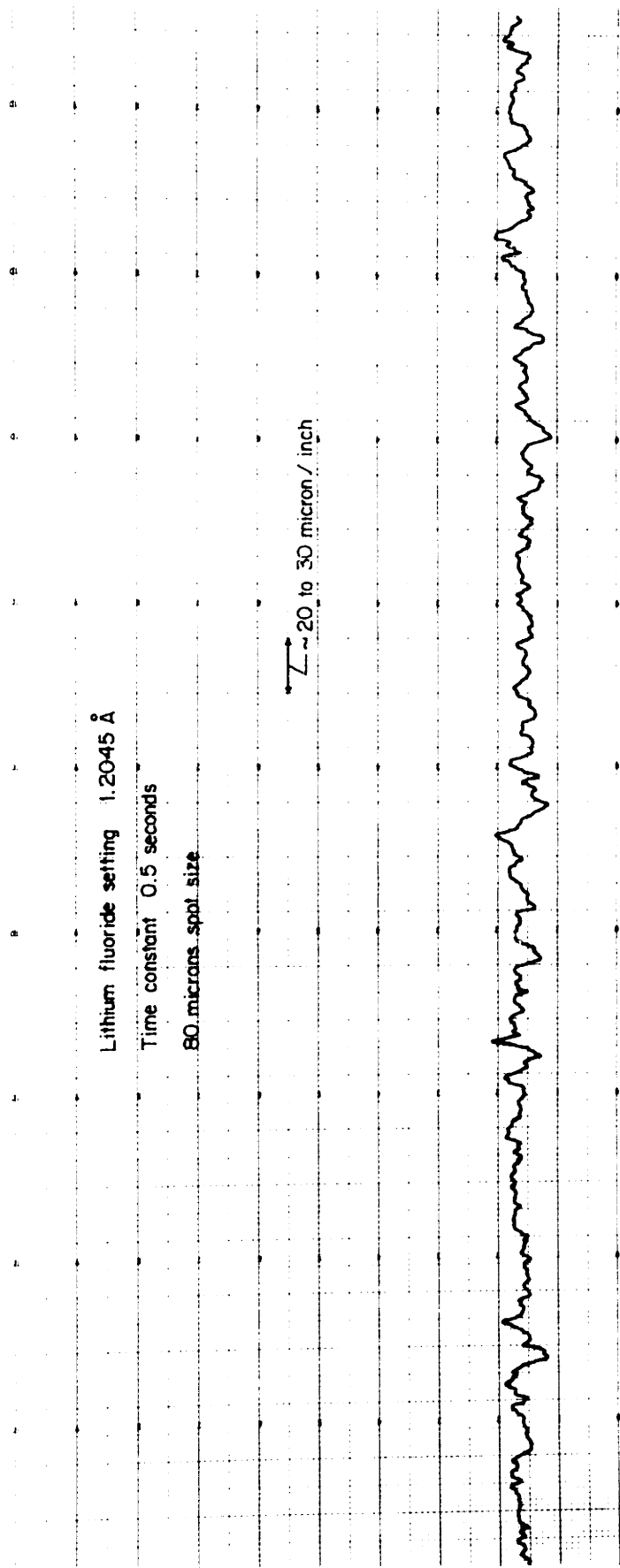


Figure 35 - Hand scan of a standard with 0.244 weight fraction of TlCl. Ordinate scale is detector current. Abscissa scale is direction along the surface of the standard.

tion of the known weight fraction of the standards, gave a satisfactory linear relationship of the form $A + Bw$ (see figure 36), where w is the weight fraction of $TlCl$ in the standard. The intercept A is the ratio of the corrected count for pure potassium chloride to the corrected count for pure thallium chloride.

The ratio of the background counts, taken at the $1.3000A^\circ$ setting of the lithium fluoride crystal, to the corrected count of pure thallium chloride were also plotted (as I_{B2}) versus the known weight fractions of the standards and it agreed well with the empirical background formula:⁶⁵

$$\frac{I_B}{I_{100}^{corr}} = w \frac{I_{B,Tl}^{100}}{I_{100}^{corr}} + (1 - w) \frac{I_{BK}^{100}}{I_{100}^{corr}} \equiv I_{B1} \quad (\text{figure 36}) \quad (49)$$

where $I_{B,Tl}^{100}$ is the background count from pure thallium chloride and I_{BK}^{100} is the count from pure potassium chloride with the lithium fluoride crystal set for Bragg reflection of the thallium "L" line.

Using the least square fit to I_c from figure 36, the definition of I_{corr} (i e., $I_{corr} = I - I_B$)

$$\frac{I_{corr}}{I_{100}^{corr}} = A + Bw = \frac{I}{I_{100}^{corr}} - \frac{I_B}{I_{100}^{corr}} \quad (50)$$

where I is the count recorded by the probe detector system with the lithium fluoride at the Bragg reflection angle for the thallium L line. Using equation (49), (50) then becomes

$$\frac{I_{corr}}{I_{100}^{corr}} = \frac{I}{I_{100}^{corr}} - w \frac{I_{B,Tl}^{100}}{I_{100}^{corr}} - (1-w) \frac{I_{BK}^{100}}{I_{100}^{corr}} \quad (51)$$

TABLE SIX

I_{corr}	$I_{\text{corr}}/I_{\text{corr}}^{100}$	w	$I_B(1.3000)/I_{\text{corr}}^{100}$	1-w	$\frac{I}{-B}$	Chemical Analysis
90	0.0027	0.003(A)	0.0192	0.997	0.0211	0.0032
232	0.0150	0.016(B)	0.0207	0.984	0.0220	
668	0.0231	0.039(B)	0.0218	0.961	0.0271	
1612	0.0485	0.060(A)	0.0202	0.940	0.0246	
2568	0.0772	0.088(A)	0.0225	0.912	0.0264	
1861	0.0642	0.114(B)	0.0236	0.886	0.0315	
4205	0.1264	0.139(A)	0.0278	0.861	0.0295	
3820	0.1148	0.162(A)	0.0245	0.238	0.0309	
3561	0.1229	0.184(B)	0.0281	0.816	0.0357	
4624	0.1390	0.205(A)	0.0273	0.795	0.0336	
4783	0.1438	0.225(A)	0.0274	0.775	0.0348	
5034	0.1737	0.244(B)	0.0303	0.756	0.0392	0.2640

Time of Counts 60 Seconds

(A) $I_{\text{BK}} = 581$

$I_{\text{BT1}} = 2741$

$I^{100} = 36,000$ (Pure TlCl with LiF on the Tl "L" Line)

$I_{\text{corr}}^{100} = 33260$

(B) $I_{\text{BK}} = 518$

$I_{\text{BT1}} = 1523$

$I^{100} = 25,599$

$I_{\text{corr}}^{100} = 24,076$

Table Six - Experimental data on the standards. Column headings are explained on pages 93 and 95. In the third column the "(A)" values were obtained on one day while the "(B)" values were obtained on another.

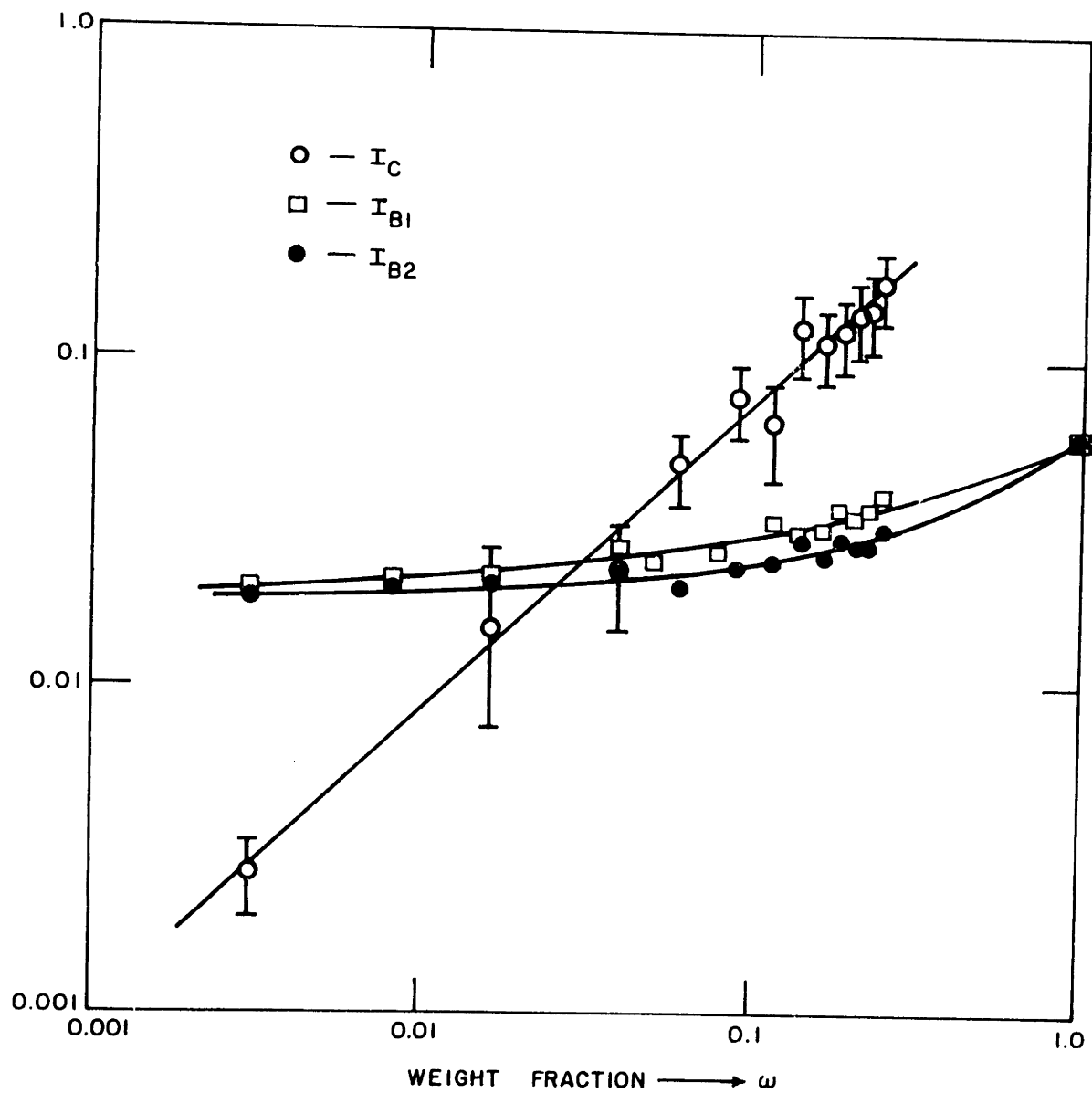


Figure 36 - Plot of $\text{Log } I_C$, $\text{Log } I_{B1}$ and $\text{Log } I_{B2}$ versus $\text{Log } w$.

This can then be solved for "w", giving:

$$w = \frac{\frac{I}{I_{\text{corr}}^{100}} - A - \frac{I_{\text{BK}}^{100}}{I_{\text{corr}}^{100}}}{B + \frac{I_{\text{BT1}}^{100}}{I_{\text{corr}}^{100}} - \frac{I_{\text{BK}}^{100}}{I_{\text{corr}}^{100}}} \quad (52)$$

In (52), all quantities can be obtained at the start of the day from a pure thallium chloride and pure potassium chloride standard. Following this the lithium fluoride crystal may merely be set at Bragg reflection of the "L" line and the diffusion analysis carried out. In practice, checks of I_{BT1}^{100} , I_{BK}^{100} , and I_{corr}^{100} were taken every three or four hours. The values inserted in (52) were an average between those values at the start of a period and those values at the end of a period. These fluctuations were never greater than four percent under proper operating conditions and, in most cases, were better than two percent.

Four to eight counts were taken on the pure standards for these calibrations and for all the diffusion runs. Each count was taken at a different position and at optimum focus. The setting for the background count was always 1.300 angstroms as this was sufficiently far removed from the peak to be truly in the background. Also, the count on the other side of the peak the same distance away, was within fifteen percent of the count at 1.3000A° indicating that the asymmetry was not excessive. The lithium fluoride crystal was always rotated into the thallium "L" reflection from the same direction since, because of the slack in the chain drive on the detector crystal, one specific direction of approach to the peak was the one that put the sample, detection crystal, and counter closest to the true focusing circle. In the earlier work,

the peak was determined by taking thirty second counts every 0.001 angstroms on pure thallium chloride through the peak but it was found that it was sufficient to slowly turn the detector crystal through the peak while watching the current meter for the lithium fluoride detector and setting the crystal where the peak occurred. Each time that the probe was used, one of these two methods was employed.

2. Single Crystals

In all of the volume and grain boundary diffusion analyses, "sample" currents for pure potassium chloride and pure thallium chloride were kept in the region of 0.024 microamps and 0.014 microamps respectively. The objective lens was always adjusted to give the best spot focus using pure potassium chloride as the calibrator and the condenser lens was always set to give about a one micron spot size. Two diffusion runs were taken on about half the samples, but it was found that reproducibility of diffusion data was better than a few percent while other factors were contributing much larger fluctuations. Therefore only single diffusion analyses were obtained for subsequent samples.

The single crystals were scanned perpendicular to the face exposed to the thallium chloride (see figure 29C) by means of a step motor. This motor was connected electronically with the counting apparatus so that after a count the motor would step the sample at a preset number of microns perpendicular to the $\eta = 0$ ($\eta = y/\sqrt{DT}$) face and then counting would resume. The amount of the step depended on the extent of the thallium penetration. The maximum jump was ten microns, whereas a typical jump for the low temperature diffusion runs was two microns.

The counts obtained as a function of penetration were converted to weight fraction of thallium chloride by means of equation (52).

The methods used to obtain D have been described in section III.A.

3. Polycrystalline Pellets and Harshaw Mosaic Crystals

The polycrystalline pellets and the mosaic crystals were scanned parallel to the face exposed to the thallium chloride, crossing several grain boundaries, to check for preferential diffusion. The steps (with the step motor) along an " $\eta = \text{constant}$ " line ($\eta = y/\sqrt{Dt}$) were four micron except in the region of a grain boundary where they were cut down to two micron steps. Figure 37 is a picture of the face perpendicular to the "exposed" face for a polycrystalline pellet subjected to a diffusion anneal.

4. Bicrystal

Figure 38A, B, and C are some typical micrographs of the faces cut perpendicular to the exposed face on three bicrystals subjected to diffusion anneals. For the bicrystals, step scans were taken along " $\eta = \text{constant}$ " lines, for various η values. As the grain boundary was approached, the steps were reduced to two micron so that the position of the peak count (moving on a "constant η " trajectory) could be localized to within two microns. This allows for more accurate estimates of $\left(\frac{\Delta\eta}{\Delta\xi}\right)_{\xi=0}$. The peak values were assumed to be the average grain boundary concentration. Actually this is not correct since, even with a one micron spot size, the width of the preferential diffusion region could be significantly smaller. It is, however, the only experimental means for obtaining this value.

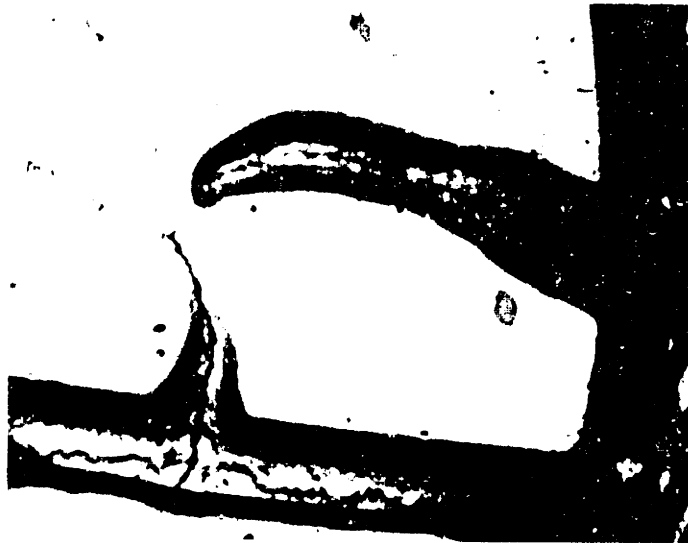


Figure 37 - Polycrystalline sample subjected to a diffusion anneal (vapor exchange couple). Face in photograph was exposed as indicated in figure 29A, B.



Figure 157

... ..



Figure 158

... ..



Figure 38A - Typical photomicrograph of a bicrystal subjected to a diffusion anneal.

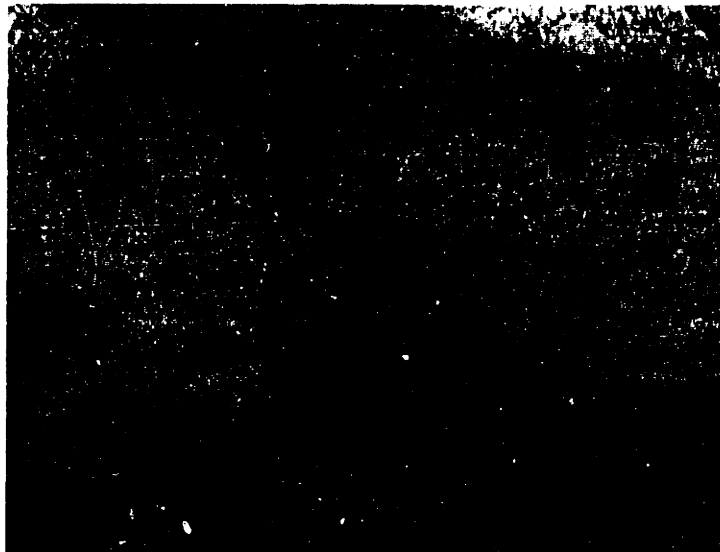


Figure 38B - Typical photomicrograph of a bicrystal subjected to a diffusion anneal.

INTENTIONAL DUPLICATE EXPOSURE

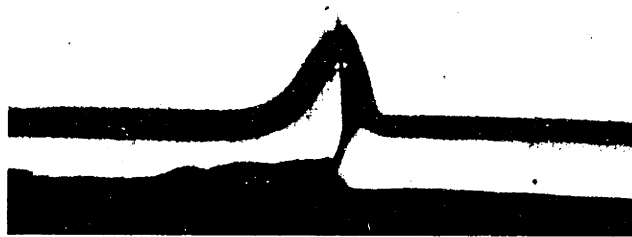


Figure 38C - Typical photomicrograph of a bicrystal subjected to a diffusion anneal.

VIII. RESULTS

A. Volume Diffusion Anneals

Some of the complementary error function plots displayed anomolous behavior due to the accumulation of thallium chloride and potassium chloride at the exposed surface. Figure 39 is a plot of weight fraction versus penetration for one of these cases. If the inverse complementary error function of C/C_0 is plotted versus penetration with C_0 being taken as the surface value of 0.51 weight to fraction, the curve of figure 40 results.

It is evident that the boundary condition for the error function solution was not maintained. The surface concentration slowly increased above its initial value to a steady state point indicated approximately by 0.51 weight fraction in figure 39. The positions close to the surface saw a surface concentration that was varying continuously. Each infinitesimal variation caused excess diffusion of thallium to these points thus making these points deviate from the straight line of figure 40. Positions well into the bulk, however, were not significantly affected by this "excess diffusant" that resulted from a continuously varying surface concentration. These points essentially saw a constant surface concentration at thirty-eight microns, this value being determined (see figure 40) by the intercept of the abscissa axis by the straight line slope. The straight line slope of figure 39 was therefore equated to $\frac{1}{2\sqrt{Dt}}$ and D was obtained in this fashion.

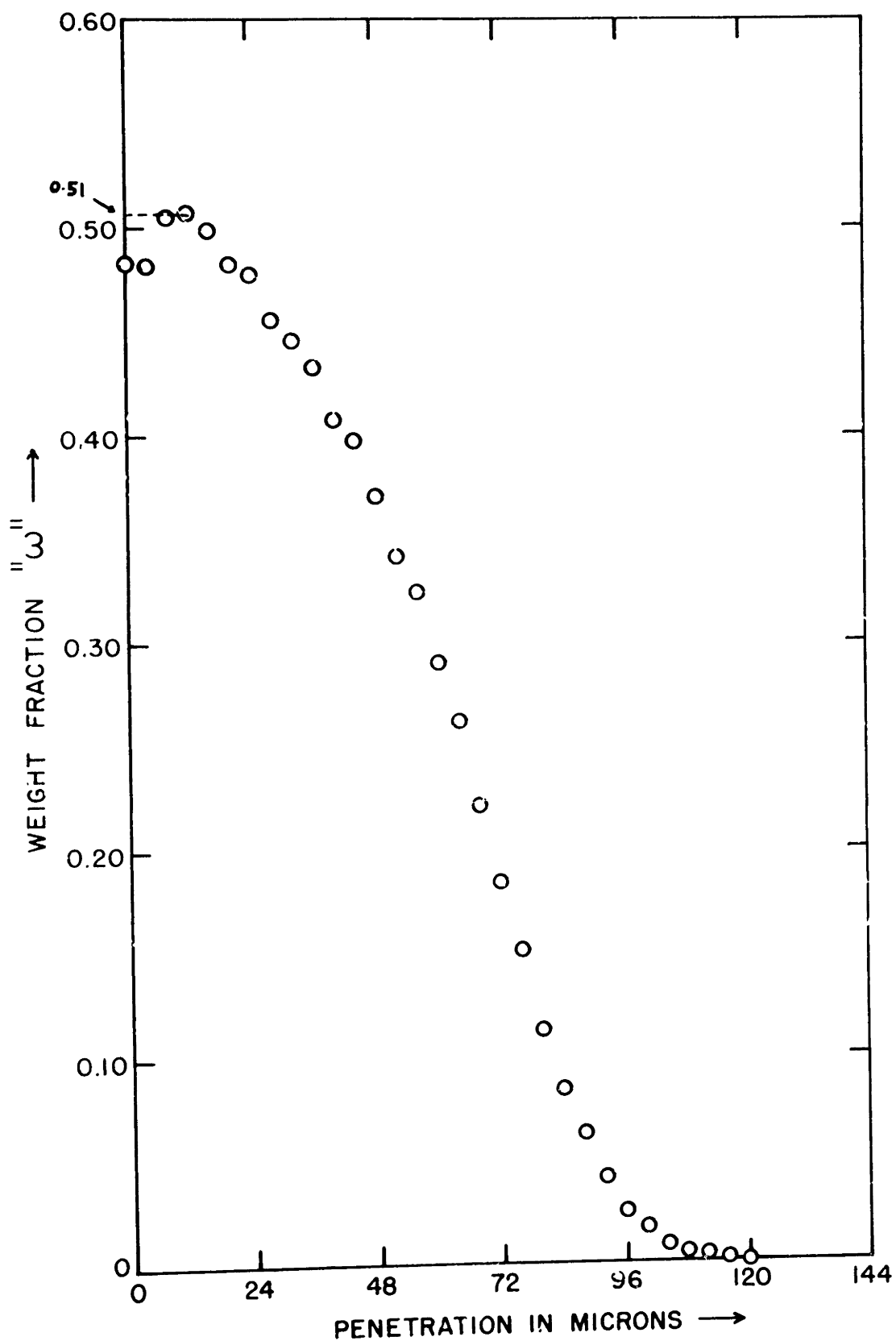


Figure 39 - Plot of weight fraction of thallium chloride versus penetration in microns for the case of anomolous behavior in the vicinity of the surface of a vapor exchange diffusion couple.

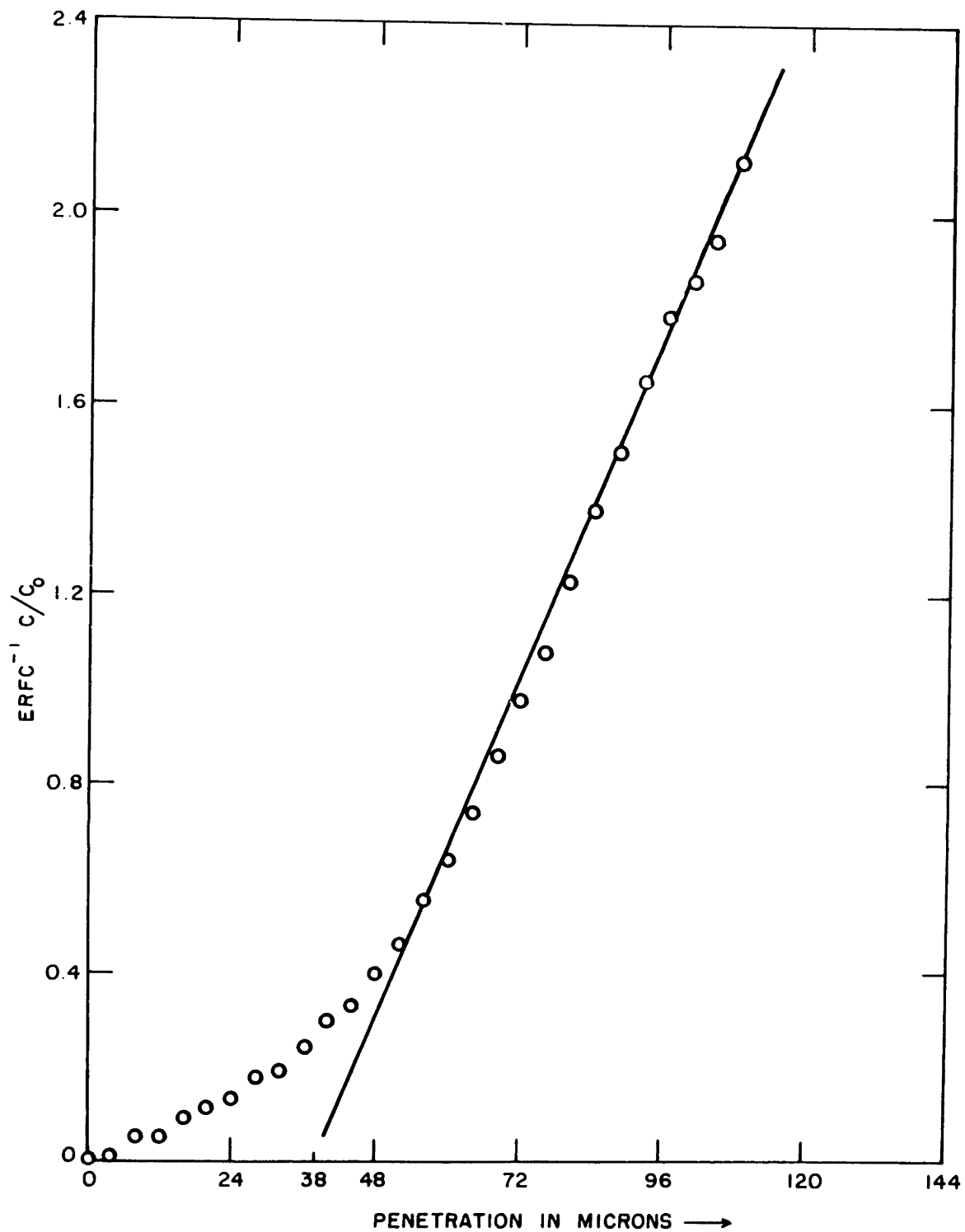


Figure 40 - Plot of the inverse complementary error function of C/C_0 versus penetration for the concentration-penetration curve of figure 39. C_0 is taken as the maximum value of C occurring in figure 39.

Another effect that occurred in the vapor exchange couples was that, on cooling, the thallium chloride vapor condensed on the exposed surface of the crystal. Because of this, as the probe measurements were performed near the surface, the count from the lithium fluoride detector rose in a manner not characteristic of error function behavior. To surmount this difficulty, the natural logarithm of concentration was plotted versus penetration. From figure 41 it may be seen that, near zero penetration, the slope of the natural logarithm of the complementary error function becomes linear. Therefore, by extrapolating the experimental curves to zero penetration, a true C_0 value may be obtained.

Figures 42 and 43 are more typical plots of concentration-penetration curves for the vapor exchange and sandwich couples respectively.

Reproducibility of a count at a given point, with best focus was within five percent, while fluctuations due to slight changes in focus amounted to ten to fifteen percent. This more than drowned out the fluctuations of counting statistics. Long count periods of up to five minutes were performed and fluctuations of ten to fifteen percent still prevailed.

In the low temperature region there were fewer data to establish concentration-penetration profiles because of the very low diffusion coefficients. The extrapolated C_0 value for vapor exchange couples was already close to the detectability limit of the probe in the low temperature region. Even the sandwich couples, subjected to a thirty-day diffusion anneal, had little data (for plotting LNC versus penetration squared) characteristic of thin film behavior.

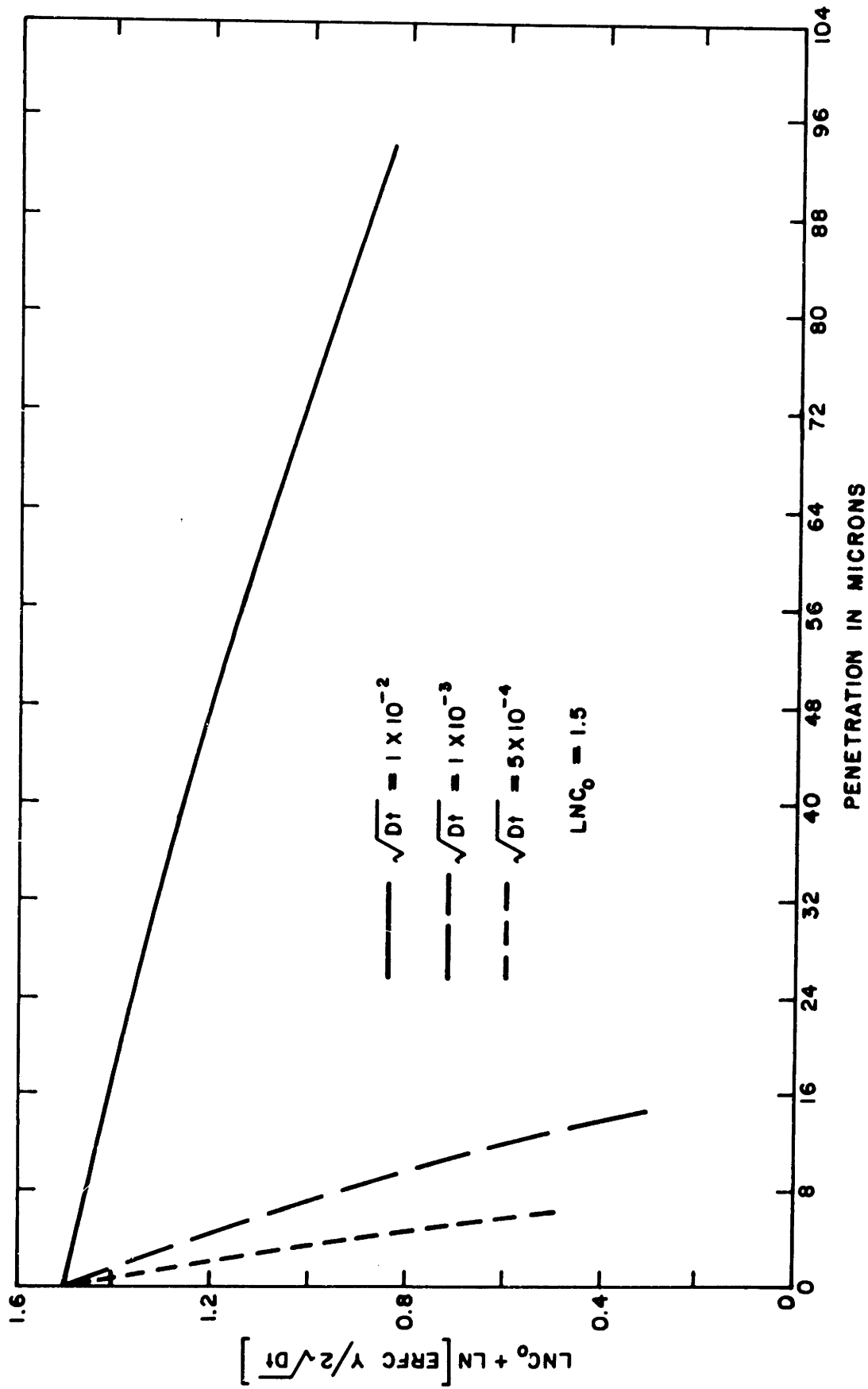


Figure 41 - Plot of the natural logarithm of the complementary error function versus penetration. C_0 is normalized so that $LNC_0 = 1.5$.

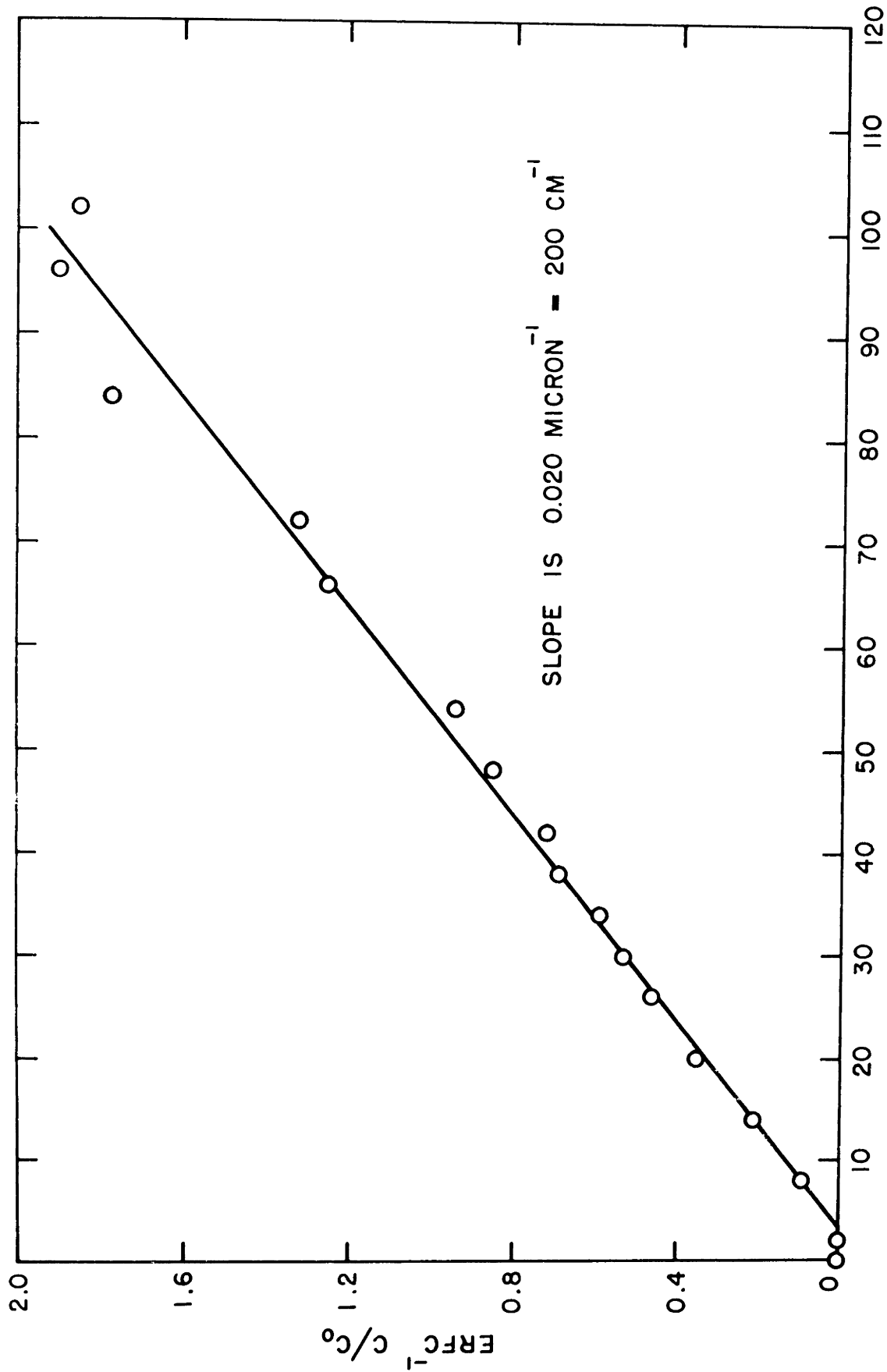


Figure 42 - A typical plot of the inverse complementary error function of C/C_0 versus penetration in microns. ($T = 688C^\circ$, $t = 2.58 \times 10^{-4}$ seconds) for a vapor exchange couple.

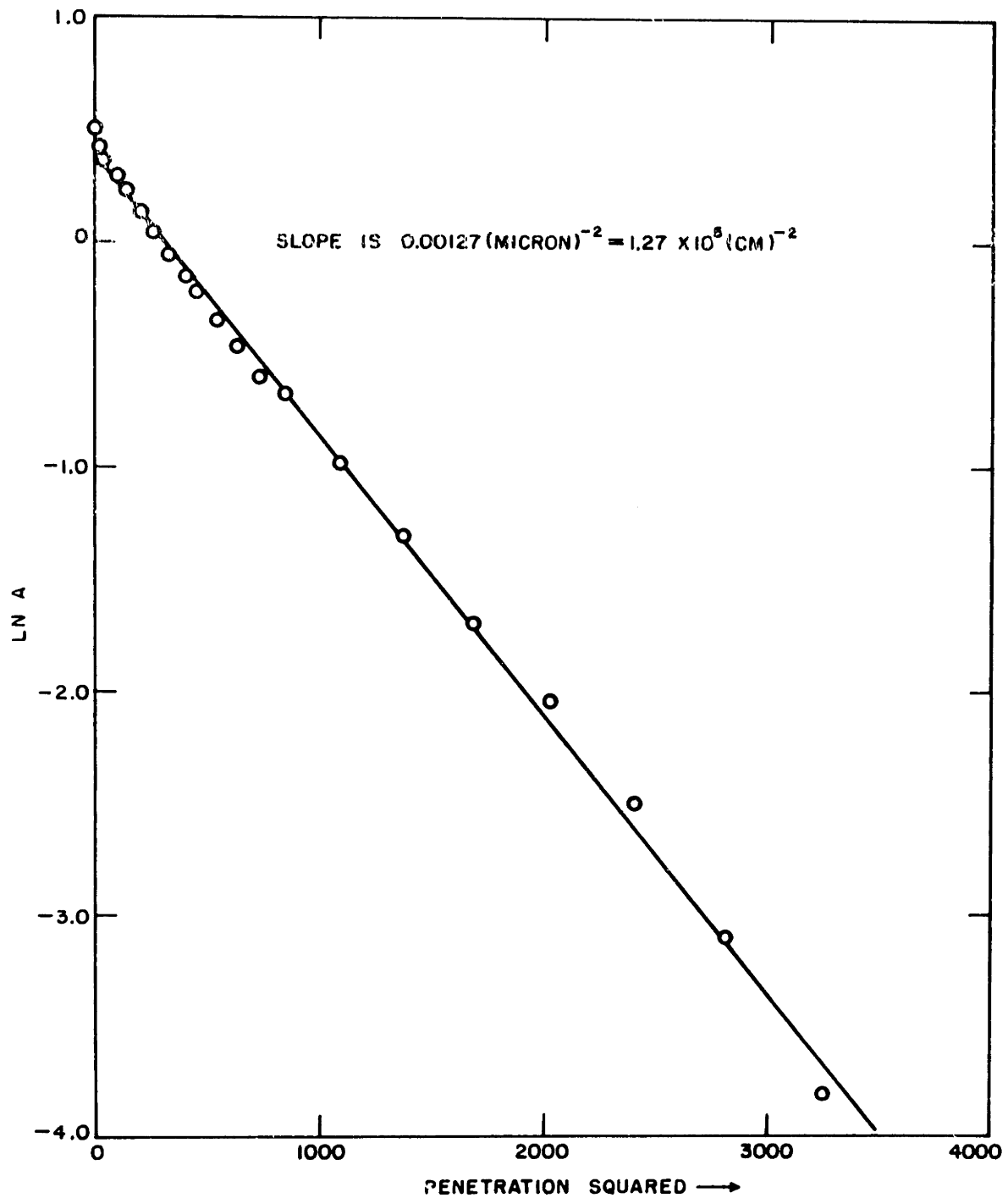


Figure 43 - A typical plot of the natural logarithm of the weight fraction of thallium chloride versus the square of the penetration for the sandwich couple. $T = 356^{\circ}$, $t = 7.84 \times 10^6$ seconds.

The cause of the scatter among the low temperature D values is differing amounts of divalent impurities from sample to sample. Also, dislocations, and/or sub mosaic grain boundaries could be making a significant contribution to mass transfer in this low temperature region below 480C° so that the effective D value derived from the data would depend on a previous sample treatment, temperature of diffusion anneal and time of diffusion anneal.

The diffusion measurements were conducted over a temperature range from 232C° to 727C°. The values of D obtained for the various temperatures are shown in table seven. A plot of $\ln D$ versus $1000/TK^\circ$ is shown in figure 44. The curve exhibited intrinsic and extrinsic behavior. The results in the intrinsic region may be described by an equation of the form $D = D_0 e^{-\Delta h/KT}$ cm²/sec., with D_0 equal to 6×10^{-3} cm²/sec. and Δh equals 1.42 electron volts/molecule. The results in the extrinsic region can be described by an equation of the form $D = D_0' e^{-\Delta h'/KT}$ cm²/sec., where D_0' equals 9×10^{-11} cm²/sec and $\Delta h'$ equals 0.25 electron volts/molecule.

The intrinsic temperature range was 727C° to 480C° and the extrinsic temperature range was 480C° to 232C°. Referring to table eight, the intrinsic Δh is lower than that of Dobrovinskaya and Podorozhanskaya by twenty-one percent which can be explained by the uncertainty in the D measurements of this work and theirs.

The $\Delta h'$ differs significantly from that of Dobrovinskaya, and Glassner and Reisfeld, and can't be explained by the uncertainty in D values alone. Glassner's value of 0.88 electron volts per molecule points toward an association mechanism for mass transfer in their samples.

TABLE SEVEN

$D \text{ cm}^2/\text{sec.}$	$\frac{10^3}{TK^\circ}$	$T \text{ C}^\circ$	$t \text{ sec.}$
4.0×10^{-10}	1.00	727	1.50×10^5
2.9×10^{-10}	1.00	727	2.88×10^4
2.25×10^{-10}	1.04	688	3.40×10^4
2.50×10^{-10}	1.04	688	2.58×10^4
1.17×10^{-10}	1.08	653	5.82×10^4
4.85×10^{-11}	1.10	636	1.47×10^5
5.05×10^{-11}	1.14	604	5.16×10^4
3.40×10^{-11}	1.15	596	7.14×10^4
1.65×10^{-11}	1.20	560	8.95×10^4
2.40×10^{-11}	1.22	546	3.49×10^5
9.20×10^{-12}	1.19	567	2.76×10^5
9.20×10^{-12}	1.25	527	5.22×10^4
3.00×10^{-12}	1.28	508	6.12×10^4
2.78×10^{-12}	1.30	496	5.8×10^5
2.55×10^{-12}	1.40	441	4.36×10^5
1.05×10^{-12}	1.50 TF	393	8.19×10^6
1.40×10^{-12}	1.52	385	5.80×10^6
8.05×10^{-13}	1.59 TF	355	3.04×10^6
1.30×10^{-13}	1.66 TF	330	1.08×10^5
3.70×10^{-13}	1.70 TF	315	3.03×10^6
4.0×10^{-13}	1.72 TF	308	9.68×10^6
4.56×10^{-13}	1.92 TF	248	3.03×10^6
3.8×10^{-13}	1.92 TF	248	6.05×10^5
6.26×10^{-13}	1.98 TF	232	4.17×10^5

Table Seven - Exact listing of the data points of figure 44, along with the times of the diffusion anneals.

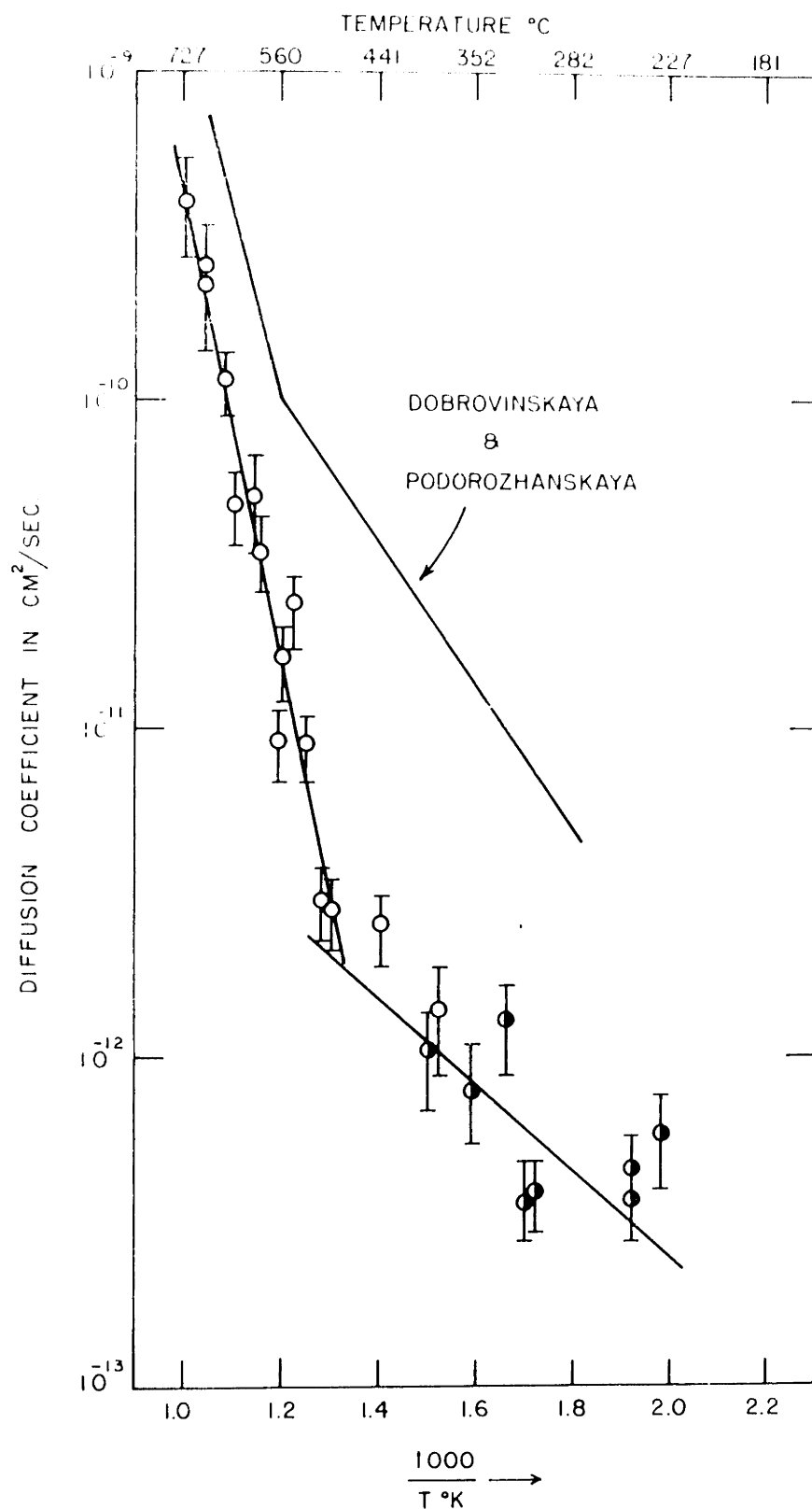


Figure 44 - Plot of the natural logarithm of the volume diffusion coefficients versus $1000/TK^\circ$. "o" were obtained from vapor exchange couples, "●" were obtained from sandwich (thin film) couples.

The value in this work of 0.25 electron volts per molecule is forty-two percent lower than Dobrovinskaya and Podorozhanskaya, indicating (if the latter's value of $\Delta h'$ is truly associated with the enthalpy of motion of dissociated vacancies) that in the extrinsic temperature range of this work, mass transfer was dominated by defects such as dislocations and/or grain boundaries. Yet, as will be seen in section VIII C. no preferential diffusion was observed at these defects.

Dienes'⁶⁹ theoretical derivation of the activation energy of motion for a jumping atom in KCl comes out to be 0.20 electron volt/molecule when the contribution to the polarization part of the activation energy from next-nearest neighbors is taken into account.

The large discrepancy in the Δh 's is a sufficient explanation for the discrepancies in the D_0 values also. An approximate divalent impurity concentration, obtained by dividing D_0' by D_0 is lower by two orders of magnitude than the value quoted by the Harshaw Chemical Company. If divalent impurity-cation vacancy complexes are contributing predominantly to mass transfer in this range then the small value of D_0/D_0' would be justified.

Assuming that the difference between the intrinsic and extrinsic activation energies for diffusion represents one half the energy of formation of Schottky pairs, the formation energy obtained is 2.34 electron volts/molecule. This agrees reasonably well with Dobrovinskaya's value of 2.54 electron volts/molecule and very well with Fuller's⁶⁸ result of 2.31 electron volts/molecule obtained from chlorine self diffusion studies. The theoretical^{66,67} values of 2.26

TABLE EIGHT

Δh_1 (eV)	Δh_2 (eV)	D_0 (cm ² /sec)	D'_0 (cm ² /sec)	N^{**}	Δh_f (eV)	Temp. Range	Ref.
1.47	0.25	6×10^{-3}	9×10^{-11}	2×10^{-8}	2.34	220-727C°	This
1.70	0.43	2.0	2×10^{-8}	-1×10^{-8}	2.54	525-727C°	29
---	0.88	---	1×10^{-3}	---	---	270-400C°	20
---	---	---	---	---	2.31	560-760C°	70
---	0.40A	---	---	---	---	---	69
---	0.20B	---	---	---	---	---	66
---	---	---	---	---	2.26	---	66
---	---	---	---	---	2.21	---	67

Table Eight: Listing of the quantities of physical interest derived from diffusion data of this work and that of others. First four rows are experimentally determined. The last three are taken from theory. In Dienes results, A is the value derived for Δh of motion in KCl, when only nearest neighbor polarization effects are included; B is the value derived for Δh of motion when the contribution of next nearest neighbors are included; Δh_1 is the slope in the intrinsic range; Δh_2 is the slope in the extrinsic range; N^{**} is the approximate divalent impurity concentration.

electron volt/molecule and 2.21 electron volt/molecule are also within seven percent of the value in this work.

B. Polycrystalline Diffusion Anneals

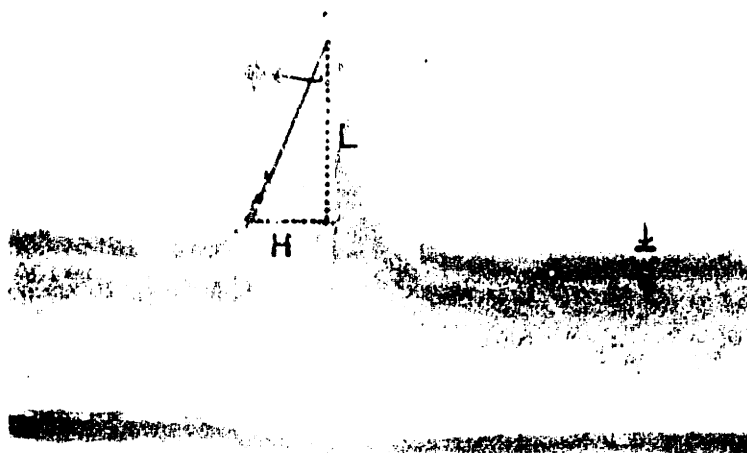
Polycrystalline samples exhibited noticeable preferential diffusion at many but not all grain boundaries. Separation of grains appeared to have occurred at some of the boundaries. In such instances, contours of constant concentration did not display the cusp-like behavior shown in figure 38 but rather a form similar to the one in figure 37.

Other boundaries did exhibit a true cusp-like form similar to that of figure 45. A reliable value of β , accurate to about thirty percent is obtained by making use of figure 12 of section III. B. and the experimental fact that the width of the dark regions that occur in all the volume and grain boundary work - and shown up most clearly in figure 38 - extends from 0.007 weight fraction to 0.015 weight fraction. This concentration span is designated by the "w" in figure 45. The inverse tangent of ϕ can easily be obtained with a rule. As may be seen from the curve of figure 12, the variation of β for a fixed ϕ is rather small in the 0.001 to 0.01 weight fraction range.

Boundaries with no preferential diffusion, as determined with the probe, had no noticeable cusp-like regions under optical observation and vice versa.

C. Harshaw Mosaics

The Harshaw samples with pronounced mosaic structure were carefully scanned with the electron beam along a line of constant η .



$$\phi = \tan^{-1} \left(\frac{H}{L} \right)$$

From above figure:

$$H = 12 \text{ mm. } L = 27 \text{ mm.}$$

$$\phi = \tan^{-1} 0.445 = 24^\circ$$

"w" in figure spans the weight fraction (of thallium chloride) range 0.007-0.015.

From figure 12:

$$\beta \cong 2.4 \quad \text{for } \phi = 24^\circ$$

Figure 45 - Preferential diffusion in one of the grain boundaries of a polycrystalline pellet (200x).

Several grain boundaries were crossed, but no preferential diffusion could be detected.

D. Bicrystals

Figure 46 is a typical family of curves obtained in traversing a grain boundary which displayed preferential diffusion. A horizontal line through the ordinate axis in this figure is a constant count or constant concentration line (since concentration of thallium and counts are linearly related). The points of intersection of this horizontal line with the families of curves determines " $\xi\eta$ " values that can be plotted on a two dimensional ξ - η diagram. The locus of these ξ, η values is a curve called an "isoconcentration contour." The results of drawing many horizontal lines through the ordinate of figure 46 is a family of isoconcentration contours (figure 47). The $\Delta\eta/\Delta\xi$ values at $\xi = 0$, and the angles that these contours make at the grain boundary are recorded in figure 47. The two values in the $(\Delta\eta/\Delta\xi)_{\xi=0}$ column are obtained from either side of the grain boundary, where the grain boundary in figure 47 is just the " η " axis. To get the values of β from figure 11, these $(\Delta\eta/\Delta\xi)_{\xi=0}$ values were averaged. The very next column to the right are the β values obtained by this method. The values of ϕ have already been averaged and the β 's in the last column to the right have been obtained by using figure 12. $\langle\beta\rangle_{K+W}$ is the average of the β 's obtained by the latter method.

In all the grain boundary analysis, the above technique was employed. The average β values (referred to as $\langle\beta\rangle$ above) were sometimes obtained by using figure 11 since in some cases, the actual

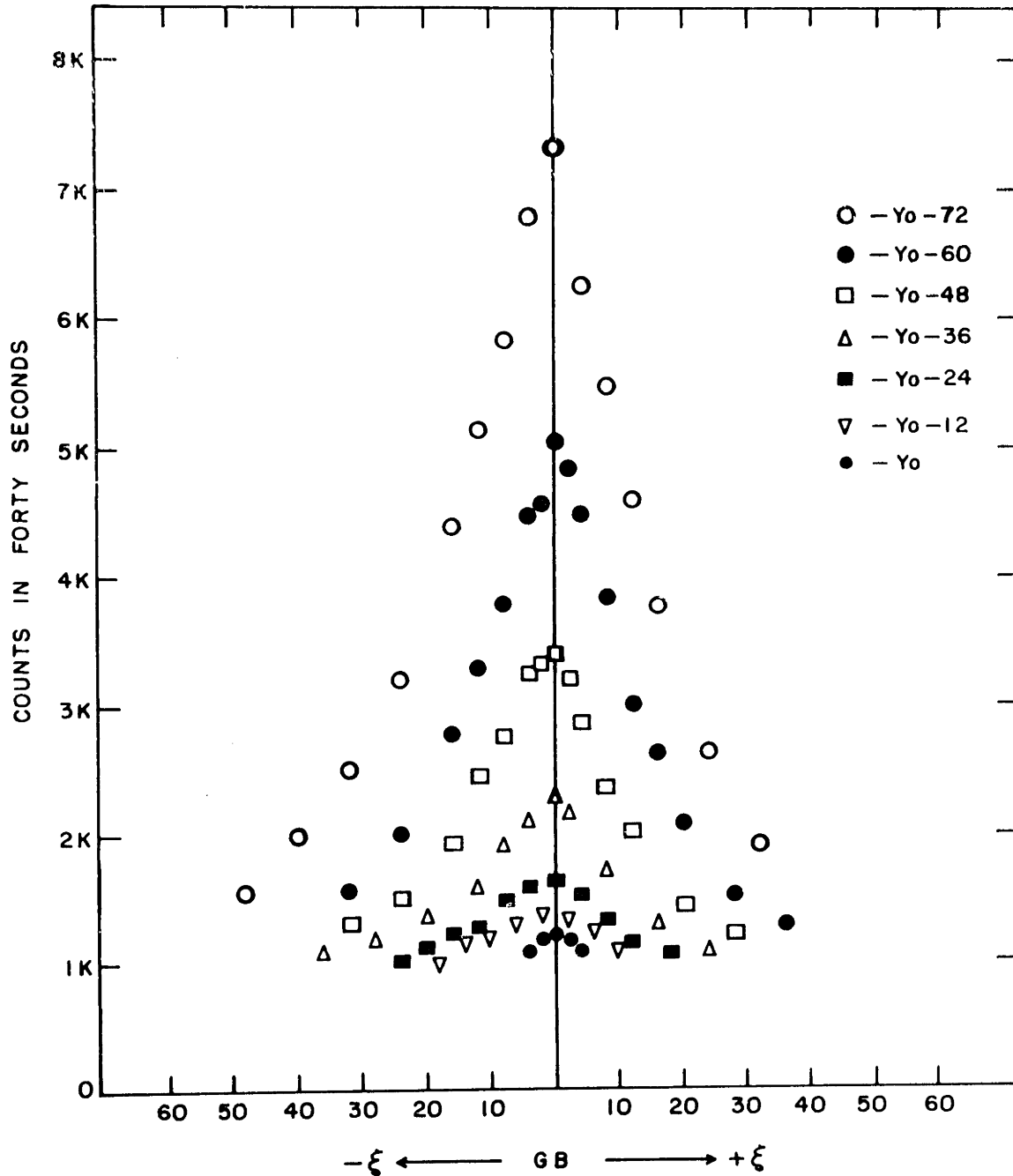


Figure 46 - Typical family of counts which occur when the bicrystal face orthogonal to the exposed face is scanned with the probe along a "constant η " trajectory. Each curve corresponds to a different value of $\eta = y/\sqrt{Dt}$. The " $\xi = 0$ " axis is the position of the grain boundary.

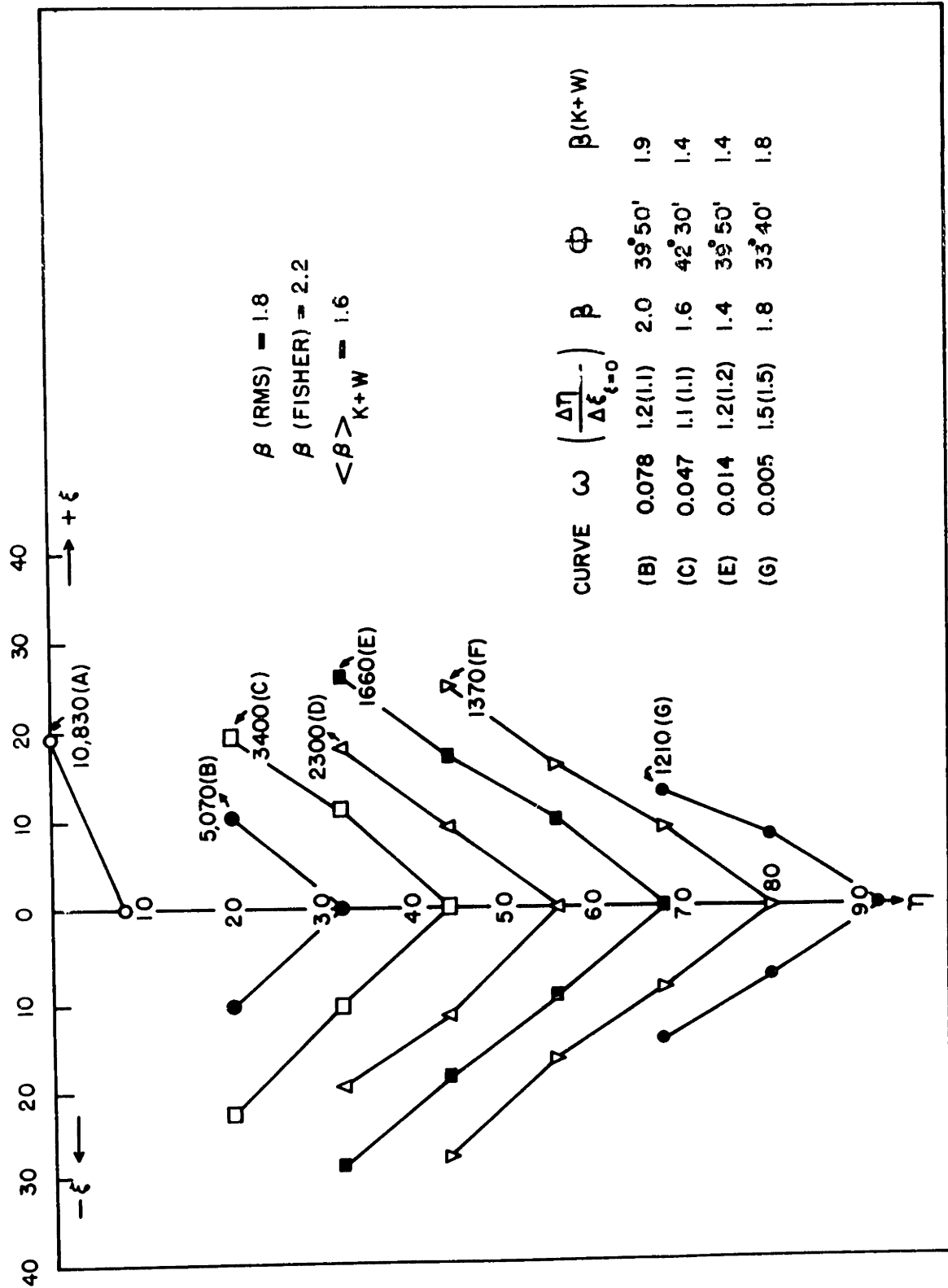


Figure 47 - Isoconcentration contours and tabulated parameters that lead to an evaluation of $\beta \equiv \frac{D_a}{D} \sqrt{Dt}$.

weight fractions of the isoconcentration contours corresponded more closely to those illustrated in this figure. Both methods give exactly the same result, so no error arose in comparing samples where β 's were obtained by different methods.

The natural logarithm of the average grain boundary concentration - taken to be the peak values in figure 46 - was also plotted versus γ for many of the samples. A typical plot is recorded in figure 48. The least square slope is related to β by means of figure 15. This is the β (RMS) value occurring in figure 47, and, in most cases it agreed quite well with the $\langle \beta \rangle$ obtained from the isoconcentration contours. The value of this slope can also be related to β by means of Fisher's equation (47). β (Fisher) in figure 47 is obtained by this method.

Table nine presents all of the data obtained for bicrystals. $(D' a)$ is the value obtained by analyzing the plane in figure 30B and $(D' a)_{\perp}$ is the value obtained by analyzing the plane in figure 30C.

Table ten compares β 's obtained by the Fisher analysis with those obtained using the exact analysis. With the exception of the data in the fifth row, the agreement is within eighty percent, although they do not seem to follow any sequence with respect to the β 's of column one (in the sense of being consistently greater than or less than these latter values).

The values of β in column two for the last two samples were derived from the least square slopes at large penetrations. This was done because of an anomalous change in slope that occurred in these samples; figure 49 shows the effect in Kyropoulos bicrystal number two.

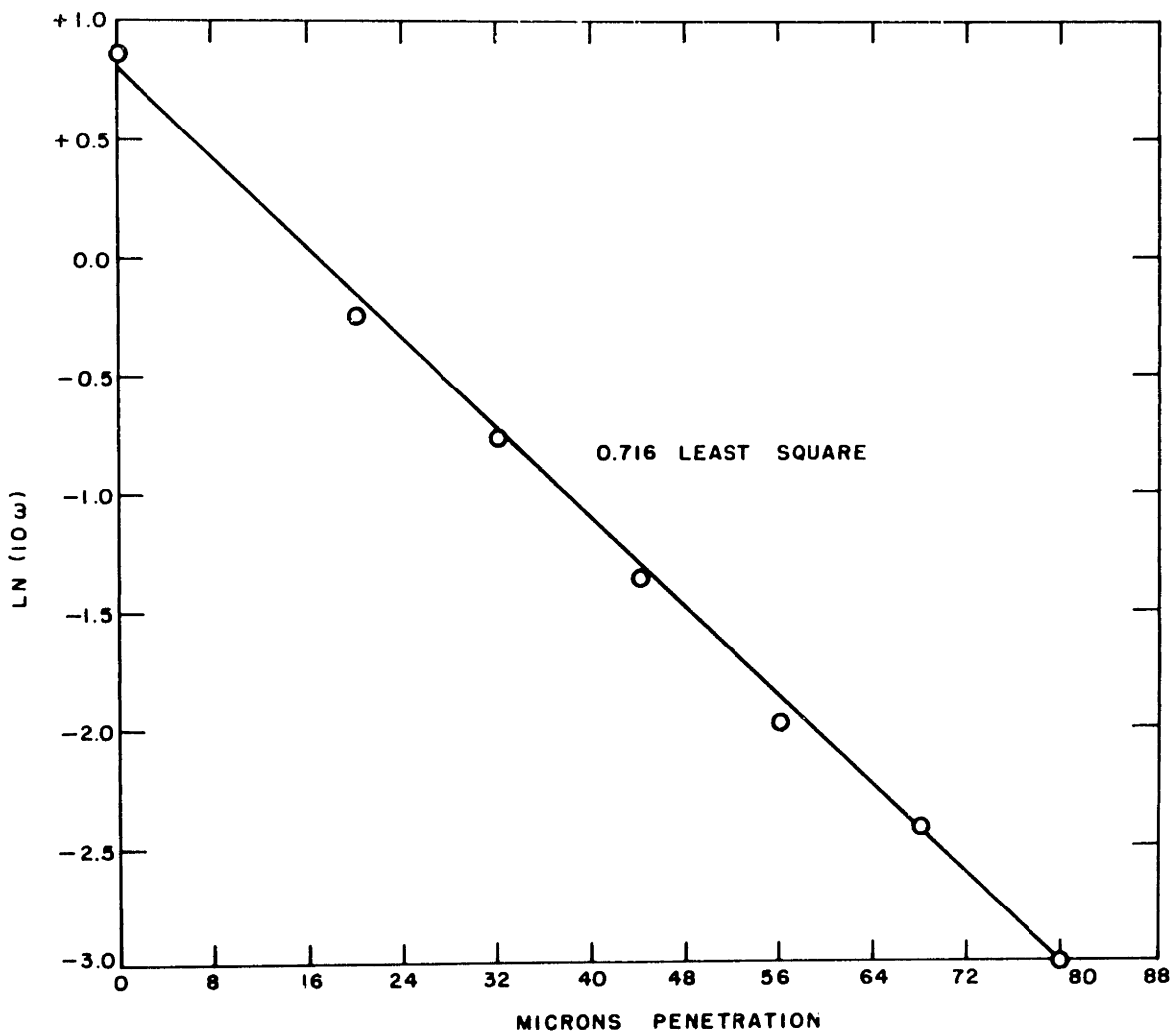


Figure 48 - Plot of the natural logarithm of the peak values in figure 46 versus penetration "y".

TABLE NINE

A. Harshaw Bicrystals

Sample	T C°	\sqrt{Dt}	$(D'a) \text{ cm}^3/\text{sec}$	$(D'a)_{\perp} \text{ cm}^3/\text{sec}$	Relative Grain Orientations
HB-8	550	3.8×10^{-3}	5.5×10^{-14}	----	9-5° about the [100] axis
HB-8	573	2.5×10^{-3}	3.1×10^{-14}	1.0×10^{-14}	
HB-8	604	4.7×10^{-3}	0	0	
HB-8	717	1.3×10^{-2}	0	0	
HB-9	717	8.8×10^{-3}	0	0	mosaic structure
HB-9	717	1.3×10^{-2}	0	0	no relative grain orientation was determined
HB-1	623	1.9×10^{-3}	0	0	~3°-4° mismatch mosaic structure
HB-3	623	1.9×10^{-3}	0	0	34° mismatch
HB-3	570	1.7×10^{-3}	4.0×10^{-14}	2.6×10^{-14}	
HB-4	623	1.9×10^{-3}	0	0	33° mismatch about the [100] axis
HB-4	570	1.7×10^{-3}	0	0	
HB-7	623	1.9×10^{-3}	0	0	
HB-7	570	1.7×10^{-3}	0	0	

Figure nine - Collected data on quantities of physical interest derived from preferential grain boundary diffusion analysis.

B. Pressure Sintered Bicrystals

Sample	T C°	\sqrt{Dt}	$(D'a) \text{ cm}^3/\text{sec}$	$(D'a)_\perp \text{ cm}^3/\text{sec}$	Relative Grain Orientation
B - 5	550	3.8×10^{-3}	0	2.1×10^{-14}	
B - 5	573	2.5×10^{-3}	0	0	100-111
B - 5	604	4.7×10^{-3}	0	0	
B - 5	633	2.3×10^{-3}	0	0	
B - 5	645	2.0×10^{-3}	0	0	
B - 5	685	2.6×10^{-3}	0	0	100-111
B - 5	717	1.3×10^{-2}	0	0	
B - 7	573	2.5×10^{-3}	0	2.5×10^{-14}	
B - 7	633	2.3×10^{-3}	0	0	111-6° from 100
B - 7	645	2.0×10^{-3}	0	0	
B - 7	685	2.4×10^{-3}	0	0	
B - 8	573	2.5×10^{-3}	0	0	
B - 8	633	2.3×10^{-3}	0	0	111-110
B - 8	645	2.0×10^{-3}	0	0	
B - 8	685	2.0×10^{-3}	0	0	

Table Nine - Collected data on quantities of physical interest derived from preferential grain boundary diffusion analysis.

C Kyropoulos Bicrystals

Sample	T C°	\sqrt{Dt}	$(D'a) \text{ cm}^3/\text{sec}$	$(D'a) \text{ cm}^3/\text{sec}$	Relative Grain Orientations
# 1	573	2.5×10^{-3}	9.5×10^{-14}	3.8×10^{-14}	
# 1	633	2.3×10^{-3}	19.0×10^{-14}	---	+14° about the [110] axis
# 1	645	1.9×10^{-3}	8.6×10^{-14}	---	
# 2	573	2.5×10^{-3}	7.9×10^{-14}	16.8×10^{-14}	
# 2	623	1.8×10^{-3}	16.1×10^{-14}	13.1×10^{-14}	+20° about the [100] axis
# 2	685	2.6×10^{-3}	26.0×10^{-14}		
# 3	573	2.5×10^{-3}	0	0	
# 3	633	2.5×10^{-3}	0	0	+8° about the [100] axis
# 3	645	1.9×10^{-3}	4.8×10^{-14}	0	
# 3	685	2.6×10^{-3}	0	0	
# 4	550	3.8×10^{-3}	6.7×10^{-14}	---	
# 4	604	4.7×10^{-3}	39.1×10^{-14}	---	111-8° from [100]
# 4	685	2.4×10^{-3}	0	0	

Table Nine - Collected data on quantities of physical interest derived from preferential grain boundary diffusion analysis.

TABLE TEN

<u>Sample</u>	<u>β from isoconc. contours</u>	<u>β from LNC versus n^p</u>	<u>β from Fisher</u>
B - 5	0.5	0.6	0.9
Kyropoulos #2	3.2	3.0	3.4
Kyropoulos #4	2.0	<1.0	1.2
HB - 8	1.1	<1.0	0.6
Kyropoulos #2	0.5	1.6	2.0
Kyropoulos #4	1.6	<1.0	0.9
B - 7	0.45	<1.0	0.17
Kyropoulos #1	1.1	1.0 (large n)	1.26 (large n)
Kyropoulos #2	1.3	1.2 (large n)	1.6 (large n)

Table Ten - Comparison of the β 's obtained by different methods.
The β 's in column one have been averaged over all the
isoconcentration contours.

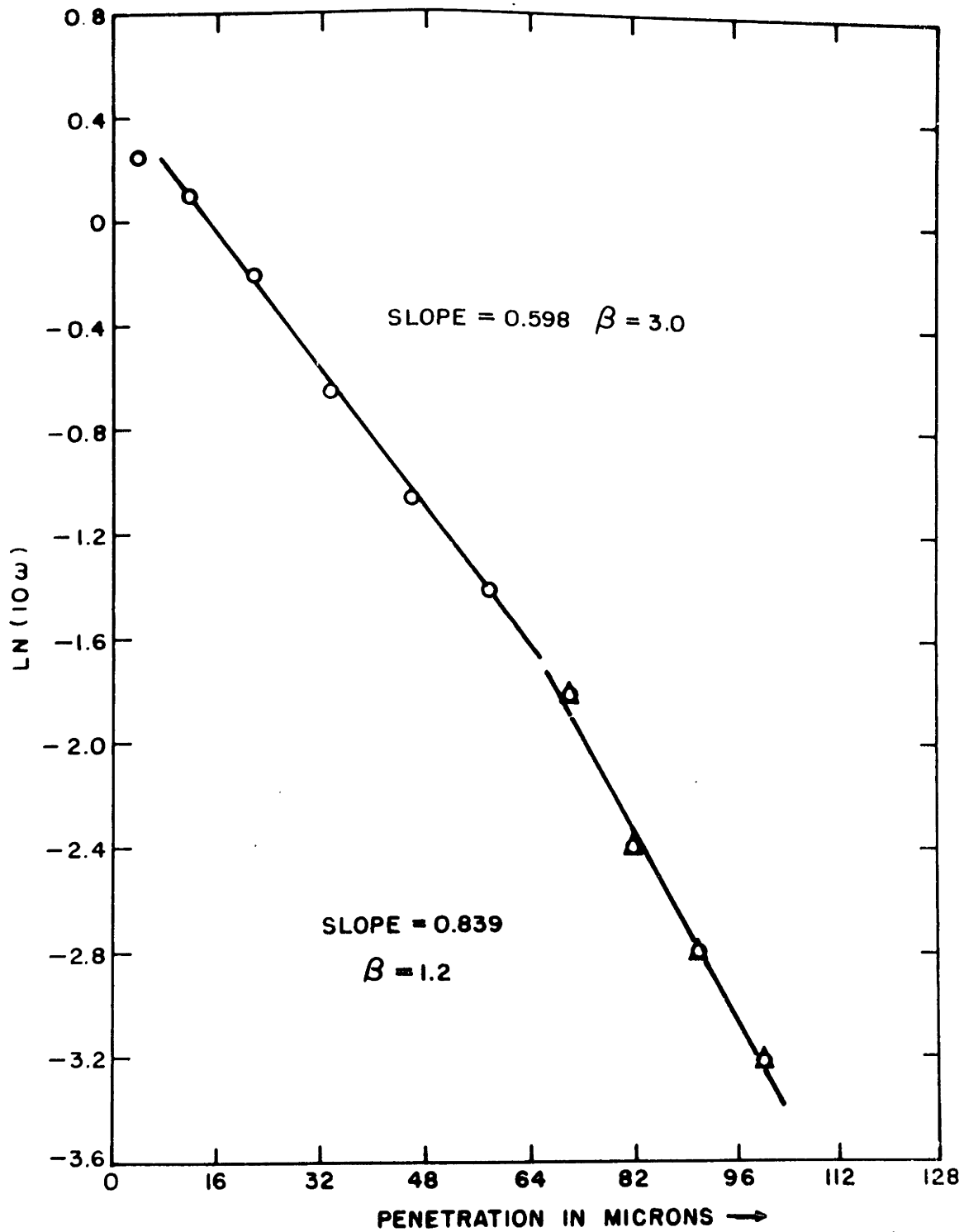


Figure 49 - Plot of the natural logarithm of the peak concentrations (similar to figure 48) versus penetration for Kyropoulos bicrystal number two; displaying a break in slope at large penetrations. The high temperature slope (0.839) was evaluated by least squares with the " Δ " points.

The low penetration slopes were always too small by a significant amount. The corresponding Fisher values in the third column were also derived from this high penetration slope.

Figure 50 is a plot of D' versus $\frac{1000}{T}$ from the data in table nine. This will be discussed in section IX.

The few polycrystals (greater than four millimeter grain size) obtained from the cooled down melt in the Kyropoulos apparatus showed no preferential diffusion.

In the case of the bicrystals, as with the polycrystals, no preferential diffusion could be detected with the probe when the dark cusp-like region could not be observed optically.

β 's were found to be (within experimental error) independent of concentration from 0.003 weight fraction to 0.090 weight fraction of thallium.

Because of fluctuations inherent in the electron micro probe, and poor signal to background values for thallium, the lower limit for values of β which could be evaluated was about 0.3. Therefore, "no preferential diffusion" meant that the β values were less than 0.3. Using the smallest spot size, the counts on a "constant η " path showed narrow peak widths, of the order of three to four micron wide in most cases. This indicates that the preferential diffusion region did not extend beyond a micron.

The values of β which were evaluated were accurate to better than forty percent.

Laue back reflections were taken on either side of the grain boundary plane for some of the bicrystals and the corresponding orienta-

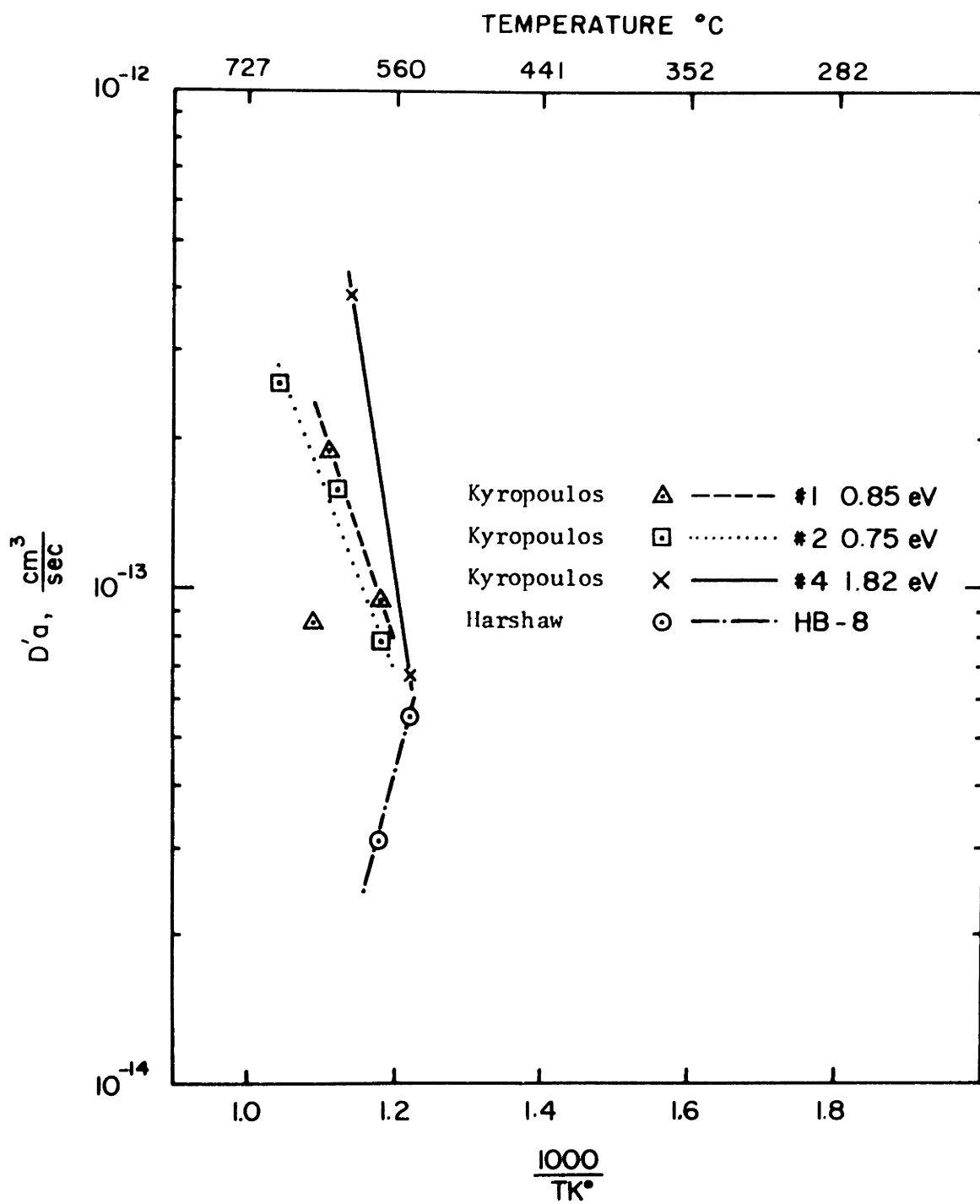


Figure 50 - Plot of the natural logarithm of $D'a$ (cm^3/sec) versus $\frac{1000}{T}$ for the bicrystals of table nine.

tions are noted in the last column of table nine. Laue back reflections of the pulled bicrystals and the pressure sintered bicrystals indicated significant polygonization and/or sub grains of very small size. Hence the quoted orientation for these is the orientation of the bicrystal seed used in fabrication of the bicrystals.

No areas of preferential diffusion were observed in these samples on which volume diffusion experiments were performed. Even the pressure sintered and Kyropoulos bicrystals on which volume diffusion runs were performed to confirm reproducibility of data, and which had a significant amount of sub mosaic type structure and/or polygonization showed no regions of excess thallium except in the vicinity of the main grain boundary. This seems to indicate that the value of Δh_m from this work is not associated with dislocations or sub mosaic type preferential diffusion. Of course, if the β 's for diffusion in these dislocation and grain boundary regions are small enough, it is possible that the diffusion anneal times of this work were not short enough to allow them to be measured with the probe.

IX. COMMENTS ON BICRYSTAL DIFFUSION RESULTS

The erratic results of table nine and figure 50 point toward an impurity hypothesis as the controlling factor in preferential grain boundary diffusion. Referring to figure 50, the Harshaw bicrystal HB-8 has positive slope in contradiction to the typical behavior of an $\text{LN}(D' a)$ versus $\frac{1}{T}$ plot. Kyropoulos bicrystal number four has a value of Δh_{gb} greater than either $\Delta h_{\text{intrinsic}}$ or $\Delta h_{\text{extrinsic}}$ of volume diffusion. Both of these effects could be attributed to segregation of a second phase at the grain boundary involving possibly $(\text{OH})^{-1}$. This could introduce a temperature dependence on a of the same form as D which could compensate for $e^{-\Delta h_{gb}/kT}$. It could also be that the segregation drastically affects the manner of mass transfer there, so that a plot of $\text{LN}(D' a)$ versus $\frac{1}{T}$ does not provide a result of physical significance.

Another proof of an extrinsic control on preferential grain boundary diffusion is Kyropoulos bicrystal number three (table nine) which shows preferential diffusion at 645C° but no preferential diffusion below this. One would expect, if preferential diffusion were truly intrinsically controlled, or controlled by the presence of excess vacancies at the boundary that β would increase with decreasing temperature since it would have a temperature dependence of the form: $\exp\left(\frac{3\Delta h - 2\Delta h'}{2kT}\right)$, where $\Delta h'$ is the grain boundary activation energy and Δh is the bulk activation energy. Also, the double values of $(D' a)_\perp$ for pressure sintered bicrystals B-5 and B-7 at 550C° and 573C° respectively, which arose from a check of two parallel planes containing the grain boundary, indicates that the cause could not be excess (grown-in)

divalent cation impurities at the grain boundary. There is no way of justifying excess divalent impurities at the grain boundary of pressure sintered bicrystals.

Ion size and/or ionic polarizability apparently plays an important role in impurity-controlled enhanced diffusion since preferential grain boundary diffusion in alkali halides has only been directly observed for cations with large ionic radius and large polarizability (i.e., cesium and thallium to date).

X. IMPURITY ANALYSIS OF GRAIN BOUNDARIES

Because the grain boundaries of the Kyropoulos bicrystals grew out of the boules rather quickly, very small samples had to be cut from them, and almost all samples were used up in the diffusion anneals. Attempts to remove these samples from the bakelite so that they could be broken at the grain boundaries were not successful. However one piece of Kyropoulos bicrystal number one and two were able to be broken at the grain boundaries. An optical photograph of number one is shown in figure 51A. This was taken around the perimeter of the grain boundary and shows small extrusions (their tips are in focus) of fairly high density. Figure 51B is a scanning electron microscope picture of the central region. A numerous amount of valleys exist which could allow for extensive "surface diffusion" of thallium chloride.

A grain boundary surface typical of Kyropoulos bicrystal number two, taken with the scanning electron microscope, is shown in figure 52. It appears to be extremely porous.

Figure 53 is two scanning electron microscope photographs of the grain boundary of Kyropoulos bicrystal number four. This picture seems to complement the others in that grain contacts similar to figures 51 and 52 appear to be present.

The ARL probe was employed in an attempt to detect excess calcium and silicon in the thallium poor and thallium rich regions of the grain boundaries of several of the diffusion annealed bicrystals. No excess was detected.



Figure 51A - Optical micrograph of the grain boundary surface of Kyropoulos bicrystal number one 500x.

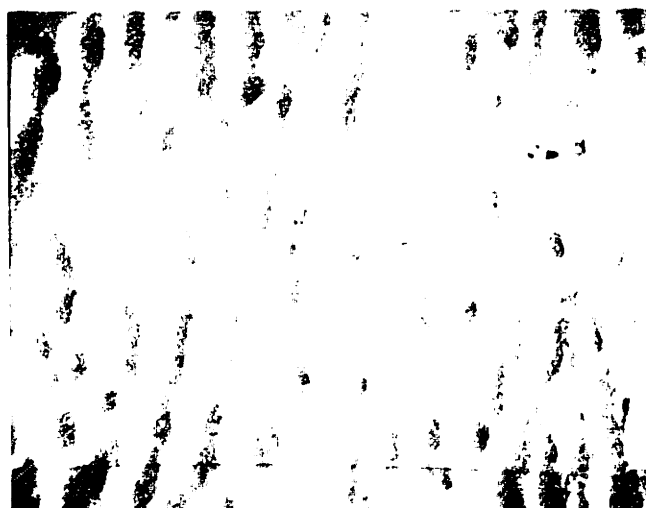


Figure 51B - Scanning electron micrograph of the central part of the same grain boundary surface 6500x.

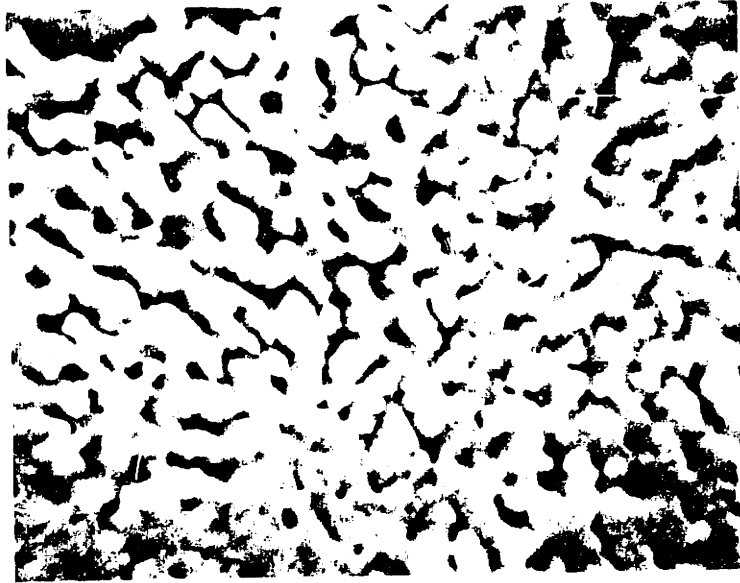


Figure 52 - Scanning electron micrograph of the grain boundary surface of Kyropoulos bicrystal number two 2600x.

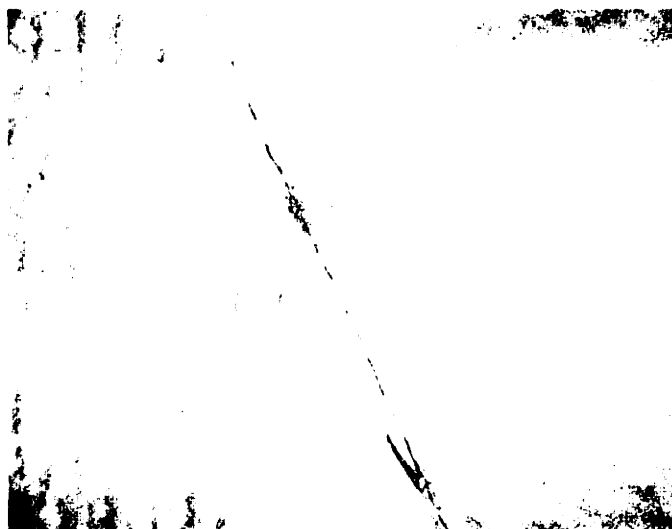


Figure 53A - Scanning electron micrographs of the grain boundary of Kyropoulos bicrystal number four 2400x.



Figure 53B - Scanning electron micrographs of the grain boundary of Kyropoulos bicrystal number four 24000x.

The MIT probe was used to examine possible oxygen segregation at the grain boundary of Kyropoulos bicrystal number two (used in a diffusion run at 623C° and displaying preferential diffusion). The crystal detector was lead stearate, spot size was about four microns (minimum spot size possible with this apparatus) and counting times were one hundred seconds. Contamination resulting from poor vacuum ($4-6 \times 10^{-4}$ torr) and high beam currents (0.3 microamps) caused appreciable variation in the counts at a given point. Sufficient time had to be allowed for the current meter to equilibrate before counts were recorded. Several counts were taken in bulk at thallium free sections of the grain boundary, and at thallium rich sections of the grain boundary. No excess grain boundary oxygen was detected.

Infrared absorption measurements were performed on the Kyropoulos and Harshaw samples to determine whether the OH vibrational mode could be excited. There were no significant peaks for any of the samples.

Ultra violet analysis was performed on four Kyropoulos and one Harshaw crystal with a Carey model fourteen spectrophotometer to determine the fraction of oxygen which was present (electronic excitation of oxygen occurs at about 2000A°) in the bulk of each. The procedure for obtaining the atomic fraction of oxygen was taken from that of Klein, et al,⁷¹ and the results are presented in table eleven. Table eleven also presents the divalent cation impurity concentrations in three of the crystals pulled by the Kyropoulos technique. These were obtained by putting the low temperature slope from figure 44 through the diffusion coefficients obtained for these crystals at the indicated temperatures. This was done at two temperatures for comparison purposes. Assuming that " $e^{\Delta G_f/2}$ " is about

TABLE ELEVEN

(a) Oxygen content of single crystal material used for bicrystals UV analysis (absorption line at 2000\AA).

Kyropoulos No. 1	4×10^{-7}
Kyropoulos No. 2	4×10^{-7}
Kyropoulos No. 3	6×10^{-7}
Harshaw	6×10^{-6}

(b) Divalent impurity concentrations of Kyropoulos material.

	T = 484C°	T = 432C°
Kyropoulos No. 2	2×10^{-8}	7×10^{-9}
Kyropoulos No. 3	2×10^{-8}	2×10^{-8}
Kyropoulos No. 4	3×10^{-8}	4×10^{-8}

Table Eleven - Impurity analysis of bulk crystals pulled from the melt.

one, and using the value for Δh_f from this work, the fraction of Schottky pairs at the temperature of the break in the curve of figure 44 is $\sim 2.4 \times 10^{-8}$. This is in the range of the values indicated in table nine B. There is thus not too much difference between the divalent impurity concentrations in the Kyropoulos and Harshaw bicrystals but an order of magnitude difference in the oxygen concentrations, the Harshaw material having the greater amount of oxygen.

The pressure sintered bicrystals exhibited no preferential diffusion, except for one case. It was therefore thought that by fabricating two identical pressure sintered bicrystals (i.e., same crystallographic faces forming the plane of the grain boundary), one under very water free conditions and one under very moist conditions, and then preparing low temperature diffusion specimens from these, that preferential diffusion would occur only for the latter ones.

The two single crystals for the "clean" run were cut, carefully water polished, rinsed well in ether, and dried in hot air. One had a (110) orientation and the other had an orientation a few degrees from the (100) direction. These were then put in an oven at about 350C° for two days. The die of the RF press was heated for an hour at about 440C° in dry nitrogen and then a small amount of two hundred mesh alumina powder, baked out at 300C° for two and one half days, was put in.

This was brought up to 700C° and held there for one and one half hours in flowing dry nitrogen, after which it was cooled to 380C°.

The crystal with (110) orientation was then inserted and the temperature of the assembly was brought up to 435C° for two and one half hours in flowing dry nitrogen. Then the other sample was put in, the

die filled with alumina, and the pressure increased to 924 psi. The press was continued for four hours in the temperature range of 450 to 500°C, and pressures ranging from 924 psi to 1500 psi. The pressure was then reduced to zero, and a one and one half hour cool down was employed.

For the "wet" bicrystal the pressing procedure was identical. The only difference in preparation was that at the start, the bottom crystal in the die (110 orientation) was subjected (at 200°C) to a two hour flow of nitrogen that was flowing through warm distilled-deionized water. The top part of the die was slightly moistened with water before pressing took place.

Both bicrystals were then annealed at about 700°C for thirty-five hours after which they were control cooled at 10°C/hour to 150°C.

The diffusion annealings were performed at 515°C, 545°C and 595°C, with corresponding \sqrt{Dt} 's of 1×10^{-3} , 1.5×10^{-3} and 2.8×10^{-3} cm. The results are shown in figures 54, 55, and 56. Clearly the "wet" bicrystals display pronounced preferential diffusion. The clean bicrystals display β 's that are so small as to be undetectable with the probe.

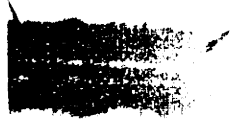


Figure 54A - Optical micrograph of the thallium diffusion contours in a pressure-sintered bicrystal. Diffusion temperature was 410°C.



Figure 54B - Optical micrograph of the thallium diffusion contours in a pressure-sintered bicrystal. Diffusion temperature was 410°C.

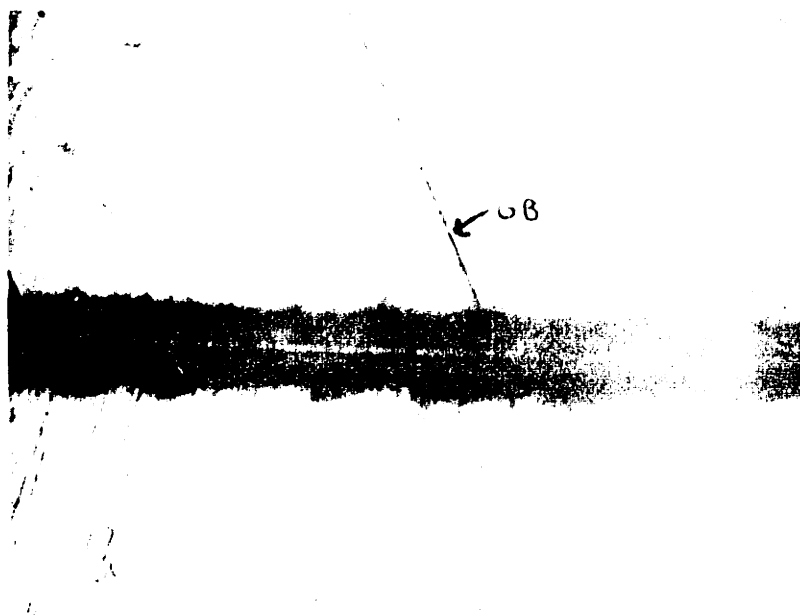
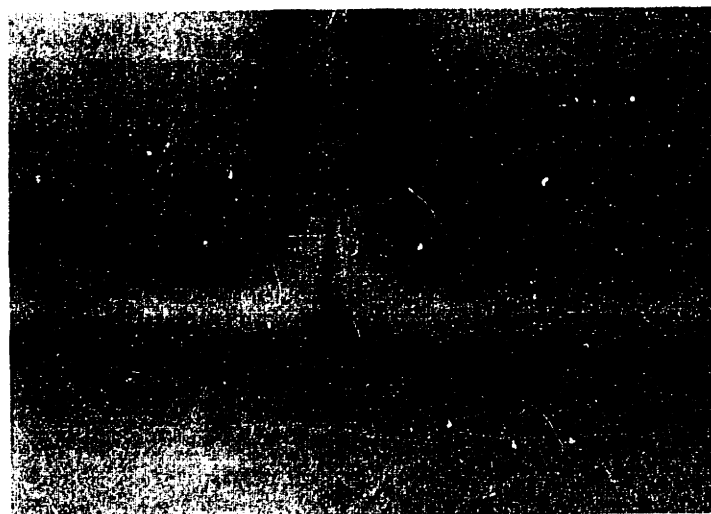


Figure 54A - Optical micrographs of the thallium diffusion contours in a "clean" (50x) pressure sintered bicrystal. Diffusion anneal was 515C°.



INTENTIONAL DUPLICATE EXPOSURE

Figure 54B - Optical micrographs of the thallium diffusion contours in a "wet" (100x) pressure sintered bicrystal. Diffusion anneal was 515C°.

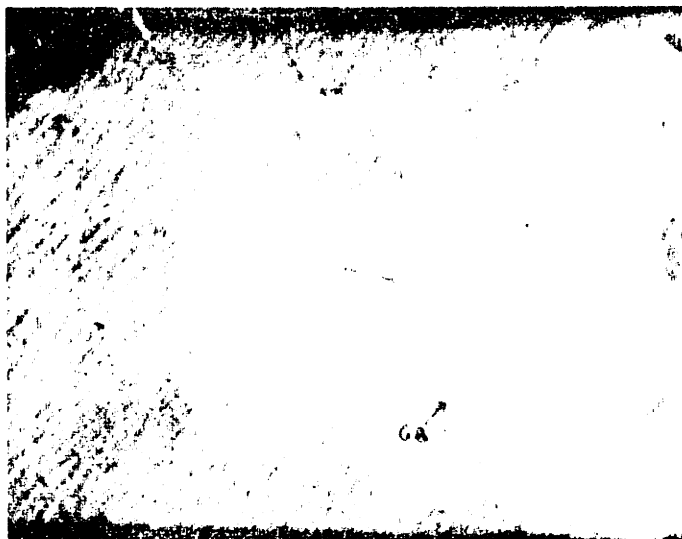


Figure 55A - Optical micrographs of the thallium diffusion contours in a "clean" (00x) pressure sintered bicrystal. Diffusion anneal was 5450° .



Figure 55B - Optical micrographs of the thallium diffusion contours in a "wet" (100x) pressure sintered bicrystal. Diffusion anneal was 5450° .

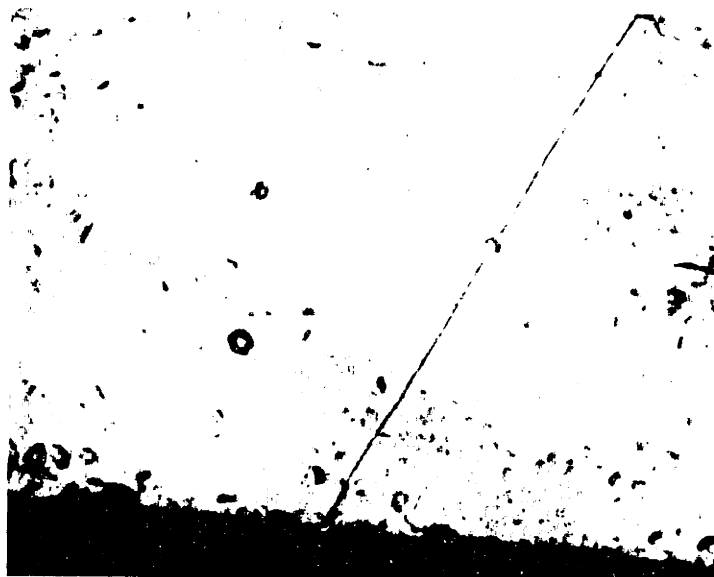


Figure 56A - Optical micrographs of the thallium diffusion contours in a "clean" (50x) pressure sintered bicrystal. Diffusion anneal was 595C° .



Figure 56B - Optical micrographs of the thallium diffusion contours in a "wet" (100x) pressure sintered bicrystal. Diffusion anneal was 595C° .

XI. CONCLUSIONS

A Volume Diffusion Work

Thallium moves by way of unassociated cation vacancies and its diffusion coefficient shows no dependence on concentration. The estimated values of Δh_f for Schottky pair formation is 2.34 eV and agrees well with previous theoretical and experimental work. $\Delta h'$ obtained from the low temperature slope differed significantly from the work of others but agreed well with the theoretical value of 0.20 electron volt/molecule in table eight. The solubility limit of Tl in the KCl structure at 250C° is experimentally determined as 0.06 weight fraction. The solubility is significantly higher at the higher temperatures. The degree of solid solubility made the analysis of Tl concentration distributions with the electron probe quite feasible.

B. Grain Boundary Diffusion Work

Sub mosaic, mosaic, and polygonization boundaries do not contribute sufficiently to mass transfer of thallium as to make their effect detectable with the electron probe for the diffusion times used in this work. The presence of impurities definitely exerts the controlling factor in preferential diffusion of thallium in potassium chloride bicrystals from 515C° to 700C°.

Scanning electron microscope pictures indicated that impurities might be influencing growth in the grain boundary region such that the grain boundary exhibits continuity from one grain to the next only in small "neck" regions.

D' values for thallium chloride diffusion in the grain boundaries of KCl crystals range from 2×10^{-14} to 40×10^{-14} cm^2/sec . The corresponding grain boundary half-width \underline{a} therefore, ranges from $10 \frac{D}{D'}$, microns to $100 \frac{D}{D'}$, microns. While a specific impurity could not be detected in the grain boundaries exhibiting enhanced diffusion, bicrystals in which the boundary had been intentionally exposed to H_2O exhibited an enormous enhancement in the degree of preferential diffusion.

XII. SUGGESTIONS FOR FUTURE WORK

Except for the work in section X, the grain boundary investigations have been limited to the temperature range from 550C° to 700C°. It would be of interest to analyze exceptionally clean grain boundaries free from segregates and with total continuity from one grain to the next to see if preferential diffusion may be intrinsically controlled in this range.

A check as to whether there might be precipitation in the grain boundaries of KCl would be to perform indentation hardness experiments across the grain boundary. This⁷² seems to be a technique that is very sensitive to even the smallest amount of precipitate.

The scanning electron microscope is an excellent tool for looking at the details of grain boundary structure because of its fine depth of field. It would be very informative to carry out a program of grain boundary analysis of all types of bicrystals and polycrystals to determine the finer details of grain boundary structure.

A careful diffusion program where very short times can be employed and yet errors due to warm up and cool down times be minimized could reveal $D'a$ values as low as 1×10^{-17} cm³/sec with the aid of the electron probe. In fact a diffusant other than thallium, with a higher signal to background ratio, could extend the probes sensitivity to even smaller values of β . It would therefore be possible, with very short diffusion times, to detect $D'a$ values smaller than 10^{-17} cm³/sec.

A UV analysis of a grain boundary with a very narrow slit whose long dimension coincides with the long dimension of the grain boundary plane and whose small dimension coincides with the narrow dimension of the grain boundary plane would yield quantitative information on oxygen concentrations at the grain boundary.

REFERENCES

1. W. D. Kingery, INTRODUCTION TO CERAMICS, John Wiley & Sons (1960), pp. 217-228.
2. P. G. Shewmon, DIFFUSION IN SOLIDS, McGraw Hill (1963), pp. 40-84; 1-40; 137-163; 164-187.
3. A. B. Lidiard, Handbuch Der Physik, 20, Springer-Verlag, Berlin (1957), pp. 246-349.
4. J. Crank, THE MATHEMATICS OF DIFFUSION, Oxford Press (1956), pp. 9-41; 148-149.
5. H. S. Carslaw and J. C. Jaeger, CONDUCTION OF HEAT IN SOLIDS, Oxford Press (1947), pp. 33-40; 239-260.
6. J. C. Fisher, J.A.P., 22 No. 1 (1951), pp. 74.
7. R. T. Whipple, Phil. Mag. Ser. 7, 45 (1954), pp. 1225.
8. C. C. Maneri and F. J. Milford, "A Discussion of Theories of Grain Boundary Diffusion," Battelle Memorial Institute (1961), ARL 48, Office of Aerospace Research U.S.A.F.; Contract No. AF 33(616)-6265; Project No. 7021; Task No. 70608.
9. A. E. Austin and F. J. Milford, J.A.P. 33 (12) (1962), p. 3574.
10. F. Karstensen, Zeit. Naturforsch. 14A, 1031 (1959).
11. D. Mapother, H. N. Crooks and R. Maurer, J. Chem. Phys., 18 No. 9, (Sept. 1950), pp. 1231-1236.
12. H. J. Arnikaar and M. Chemla, Comptes Rendus, 242 (1956), pp. 2132-2135.
13. J. F. Aschner, Thesis, University of Illinois (1954).
14. J. F. Laurent and J. Benard, J. Phys and Chem. Solids, 3 (1957), pp. 7-19.
15. D. K. Dawson and L. W. Barr, Phys. Rev. Letters, 19, No. 15 (1967), p. 844.
16. R. J. Friauf and V. C. Nelson, "Mass Transport In Oxides," U. S. Dept. of Commerce, NBS, Special Pub. No. 296, edited by J. B. Wachtman and A. D. Franklin (August 1968), p. 9.
17. G. Arai and J. G. Mullen, Phys Rev. 143, No. 2 (1966), pp. 663-665.
18. M. Chemla, Comptes Rendus 236 (February 1953), pp. 484-486.
19. M. Chemla, Comptes Rendus 238 (January 1954), pp. 82-84.

20. A. Glasner and R. Reisfeld, *J. Phys. Chem. Solids* 18, No. 4 (1961), pp. 345-355.
21. A. N. Murin, S. N. Banasevich and Yu S. Grushko, *Sov. Phys.-Solid State* 3, No. 8 (1962), 1762-1766.
22. B. G. Lur'e, A. N. Murin and R. F. Brigevich, *Sov. Phys.-Solid State* 4, No. 7 (1963), 1432-1433.
23. F. J. Keneshea and W. J. Fredericks, *J. Chem. Phys.* 38 (1963), p. 1952.
24. F. J. Keneshea and W. J. Fredericks, *J. Phys. Chem. Solids* 26 (1965), 501-508.
25. S. J. Rothman, L. W. Barr et al, *Phil. Mag.* 14 (1966), pp. 501-513.
26. C. A. Allen, D. T. Ireland and W. J. Fredericks, *J. Chem. Phys.* 46 (1967), p. 2000.
27. T. Tamai, *J. Phys. Soc. Japan* 16 (1961), p. 2459.
28. R. Illingworth, *J. Phys. Chem. Solids* 24 (1963), pp. 129-133.
29. E. R. Dobrovinskaya and N. M. Podorozhanskaya, *Ukr. Fiz. Zhorn.* 11 (1966), pp. 2, 227.
30. R. G. Fuller and M. H. Reilly, *Phys. Rev. Letters* 19 (3) (1967), pp. 113-115.
31. H. W. Etzel and R. J. Maurer, *J. Chem. Phys.* 18, No. 8 (1950), pp. 1003-1007.
32. T. E. Phipps and E. G. Partridge, *J. Am. Chem. Soc.* 51 (1929), pp. 1331-1344.
33. T. E. Phipps, W. D. Lansing and T. G. Cooke, *J. Am. Chem. Soc.* 48 (1926), pp. 112-125.
34. H. Grundig, *Zeit. Fur Physik* 158 (1960), to p. 594.
35. R. W. Dreyfus and A. S. Nowick, *Phys. Rev.* 126, No. 4 (1962), p. 1367.
36. J. Rolfe, *Can. J. Phys.* 42 (1964), pp. 2195-2216.
37. H. Kelting and H. Witt, *Zeit. Fur Physik*, 126 (1949), pp. 697-710.
38. R. W. Dreyfus and A. S. Nowick, *J.A.P.*, 33 (1962), p. 473.
39. R. G. Fuller, M. H. Reilly et al, *Phys. Rev. Letters*, 20, No. 13 (1968).

40. J. F. Laurent and J. Benard, *J. Phys. Chem. Solids* 3 (1957), p. 7.
41. J. F. Laurent and J. Benard, *J. Phys. Chem. Solids* 7 (1958), p. 218.
42. J. P. Roberts and C. Wheeler, *Trans. Far. Soc.* 56 (4) (1960), pp. 570-580.
43. R. Lindner, D. Campbell and A. Akerstrom, *Acta Chem. Scand.* 6 (4) (1952), pp. 457-467.
44. L. W. Barr and I. M. Hoodless, *Trans. Far. Soc.* 56 (1960), p. 697.
45. L. G. Harrison, *Trans. Far. Soc.* 57 (1961), p. 1191-1199.
46. Y. Oishi and W. D. Kingery, *J. Chem. Phys.* 33 (1960), p. 480.
47. J. Cabane and J. Beaumont, *Comptes Rendus* 252 (1961), pp. 113 and 266.
48. J. Cabane, *J. De Chimie Physique* 59 (1962), pp. 1123-1141.
49. B. J. Wuensch and T. Vasilos, *J. Am. Cer. Soc.* 47, No. 2 (1964).
50. B. J. Wuensch and T. Vasilos, *J. Am. Cer. Soc.* 49, No. 8 (1966), p. 433.
51. A. E. Paladino, L. G. Rubin et al, *J. Phys. Chem. Solids* 26 (1965), pp. 391-397.
52. Ya E. Geguzin and E. R. Dobrovinskaya, *Sov. Phys. Solid State* 7, No. 12 (1966), p. 2826.
53. E. W. Hart, *Acta Met.* 5 (1957), p. 597.
54. R. Smoluchowski, *Phys. Rev.* 87 (1952), p. 482.
55. Ya E. Geguzin and E. R. Dobrovinskaya, *Sov. Phys. Solid State* 11, No. 11 (1967), p. 626.
56. W. H. Rhodes and R. E. Carter, *J. Am. Ceramic Society* 49 (1966), pp. 244-249.
57. W. H. Rhodes and W. D. Kingery, *J. Am. Cer. Soc.* 49, No. 10 (1966), p. 521.
58. G. H. Frischat, *Zeit. Fur Angewandte Physik* 22, 4 (1967), pp. 281-287.
59. G. H. Frischat, *Berichte Der Deutschen Keramischen Gesellschaft* 44, 5 (1967), pp. 232-240.
60. G. Geschwind and E. Machlin, *J.A.P.* 38 (1967), p. 900.
61. J. H. Westbrook, "Impurity Effects at Grain Boundaries In Ceramics," *Soc. of Cer.* 3, *Brit. Cer. Soc.* (1967), pp. 623-684.

62. J. Tessman, A. Kahn, W. Shockley, *Phys. Rev.* 92 (1953), p. 890.
63. G. Padawar, ScD Thesis, M.I.T. (1966).
64. S. A. Long and T. D. McGee, *Am. Cer. Soc.* 46, No. 12 (1963), p. 583.
65. T. U. Ziebold and R. E. Ogilvie, Eds., "The Electron Microanalyzer and Its Applications," M.I.T. Summer Session (July 1966), pp. 21-23.
66. N. F. Mott and M. J. Littleton, *Trans. Far. Soc.* 34 (1938), p. 485.
67. P. Brauer, *Zeit. Naturforsch. A.* 7 (1952), p. 372.
68. M. Huggins and J. Mayer, *J. Chem. Phys.* 1 (1933), p. 643.
69. M. Born and J. Mayer, *Zeit. Physik* 75 (1932), p. 1.
70. G. J. Dienes, *J. Chem. Phys.* 16, No. 6 (1948), p. 620.
71. R. G. Fuller, *Phys. Rev.* 142, No. 2 (1966), pp. 524-529.
72. M. V. Klein, S. O. Kennedy et al, *Mat. Res. Bull.* 3 (1968), pp. 677-686.
73. P. J. Jorgensen and J. H. Westbrook, *Trans. A.I.M.E.* 233 (1965), p. 425.

AUTOBIOGRAPHICAL SKETCH

The author was born in Boston, Massachusetts in 1935. He attended grammar school in Everett, Mass., and high school in Dorchester, Mass. He obtained an A.B. in physics from Boston College, Chestnut Hill, Mass., and an M.S. in physics from the same school in 1959. His master's thesis was in the field of microwave spectroscopy and the title was, "The Dependence of Molecular Collision Diameters on Mix Ratios".

From 1959 to 1962 he worked at Naval Research Laboratories in Washington, D.C. as a solid state physicist, during which time he was involved with the measurement of minority carrier lifetimes in semiconducting materials, and with the investigation of the dependence of electrical and structural properties of germanium thin films on evaporation parameters. An NRL report (1960) was written up by him on the lifetime work, and the other work was published in Solid State Electronics Journal (1963).

From September 1962 to June 1963 he went to school at the University of Maryland, after which he took a summer job (June-November 1963) at the National Bureau of Standards as an atomic physicist. This work was centered around helium-neon gas lasers.

From November 1963 to September 1964 he worked at Sylvania on silicon thin film active devices and entered M.I.T. in the fall of 1964.

The author was a member of the American Institute of Physics at Boston College, the Sigma Pi Sigma at University of Maryland, and the Sigma Xi at M.I.T.